New Methods for Time-Domain Modelling of RF/Microwave Passive Structures and Active Devices

by

Shuiping Luo

Submitted in partial fulfillment of the requirements
for the degree of

DOCTOR OF PHILOSOPHY

Major Subject: Electrical and Computer Engineering

at

Dalhousie University
Halifax, Nova Scotia
January 2007

Your file Votre référence
ISBN: 978-0-494-27644-0
Our file Notre référence
ISBN: 978-0-494-27644-0

DALHOUSIE UNIVERSITY

To comply with the Canadian Privacy Act the National Library of Canada has requested that the following pages be removed from this copy of the thesis:

Preliminary Pages
- Examiners Signature Page
- Dalhousie Library Copyright Agreement

Appendices
- Copyright Releases (if applicable)

Table of Contents

List of Figures

List of Tables

List of Abbreviations

ABC	Absorbing Boundary Condition
CAD	Computer Aided Design
ADI	Alternating Direction Implicit
ADS	Advanced Design System
CFIE	Combined Field Integral Equation
CFL	Courant-Friedrich-Levy
CFS-PML	Complex Frequency Shifted Perfectly-Matched Layer
CPU	Central Processing Unit
EFIE	Electric Field Integral Equation
EM	Electromagnetic
FDTD	Finite-Difference Time-Domain
FDM	Finite Difference Method
FEM	Finite Element Method
FET	Field Effect Transistor
FFT	Fast Fourier Transform
IE	Integral Equation
MCD	Modified Central Difference
MFIE	Magnetic Field Integral Equation
MM	Moment Method
MoM	Method of Moment
MRTD	Multi-Resolution Time-Domain
PML	Perfectly Matched Layers
PSTD	Pseudo Spectral Time-Domain
RAM	Random Access Memory
RCS	Radar Cross Section
RF	Radio Frequency
TE	Transverse Electric
TLM	Transmission Line Method
TM	Transverse Magnetic

VF	Vector Fitting
1D	One Dimensional
2D	Two Dimensional
3D	Three Dimensional

Dedication

This work is dedicated to
my parents, my wife, and my son.

Acknowledgement

First and foremost, I would like to thank my supervisor, Dr. Zhizhang (David) Chen for his very valuable guidance and financial support throughout my research. I wish to thank as well the other members of the Guiding Committee for their help. I thank also my colleagues in the Microwave and Wireless Research Laboratory of Dalhousie University for their helpful discussion and support. Special thanks go to Mr. Yan Chen and Dr. Changning Ma for their help during my research. I extend my deepest thanks and appreciation to my wife Weijun Wu for her understanding and moral support during my Ph.D program.

Abstract

This thesis focuses on improving existing FDTD methods and time-domain modeling of active devices.

In this thesis, four methods are proposed to improve the efficiency of FDTD. First, a new compact two dimensional (2D) FDTD method is proposed to analyze the waveguide discontinuities along the direction of wave propagation, which is uniform in one of the transverse directions; it reduces the original three-dimensional (3D) problems to two-dimensional (2D) problems. Second, a compact one-dimensional (1D) FDTD formula is proposed for uniformly filled waveguide; it has the same numerical dispersion as the original 3D FDTD formula and can be used as an efficient incident wave generator and perfect absorbing boundary condition for the single mode. Then, a 1D modal Perfectly Matched Layers (PML) is developed by applying the proposed 1D FDTD to the traditional PML formula. Finally, a new 2D FDTD subgridding method is proposed that is not only very simple with controllable low reflections but also has been proven to be stable.

When the FDTD method is used to simulate RF/microwave circuits with active devices, the governing voltage-current equations of a device can be incorporated into the FDTD marching equations. However, the parameters of most electronic components are often given or measured in the frequency-domain and are band-limited. For instance, S-parameters of a field-effect transistor are usually given or obtained only in the frequency-domain and over a limited frequency range or band of interest.

Obtaining a causal time-domain model from the band-limited frequency-domain parameters is a challenge. In this thesis, three methods are proposed to solve this problem. The first two methods are iterative methods based on Fast Fourier Transform (FFT). One applies the FFT in combination with the error feedback principle and the second applies the Hilbert transform in conjunction with FFT. The third method uses the rational function fitting technique. The extracted time-domain parameters using the three methods not only are causal but also contain almost the same frequency-domain information as the original parameters over the given limited frequency range.

1 Introduction

Competition in science and technology today is intense, both between businesses and states. Industries and governments are dedicating more and more resources to research and development. New systems are becoming increasingly complex at the same time as the development period is becoming ever shorter. Because of the advance of computer technology, numerical simulation has become a very important and valuable tool in reducing the cost and time of prototyping and testing. In the fields of electromagnetic and microwave engineering, computational electromagnetics is very popular and provides a practical solution to large complex electromagnetic system problems. For example, the designers of high speed and very large scale integrated circuits and complex microwave integrated circuits must use numerical simulation tools for functional verification and signal integrity analysis before commitments are made to mass manufacture the products. Computational electromagnetics also provides a powerful tool for research in electromagnetic fields and microwave technology theory.

The success of computational electromagnetics depends on two factors. One is the advance of computer hardware; the other is the availability of good algorithms and computer software. Development of computer hardware is very rapid now, and is characterized by high performance and low prices. The hardware developed provides a powerful platform for software, and contributes to making the computational electromagnetics software practical and widespread. Low price and high performance hardware also enables more people to conduct their research on their personal computers. However, computer hardware, no matter how advanced, is inherently limited in its capability. Therefore, the availability of efficient software always plays a role in speeding up computations.

Maxwell's equations and the related boundary conditions are often used to solve electromagnetic problems directly. Computational electromagnetics use all kinds of numerical methods to approximate the differential or integral Maxwell's equations and the related boundary conditions. The electromagnetic problems can be described in frequency-domain or time-domain. The numerical methods to solve them are often called

frequency-domain methods and time-domain methods.

Frequency-domain formula states the electromagnetic problem for a given frequency. Numerical methods for frequency-domain problems do not suffer from stability problems and can use non-uniform meshes easily, so they are very efficient in solving large system problems with very fine structures and a narrow working frequency band. They are also very good at solving systems containing frequency-dependent materials.

However, if nonlinear elements are present in the systems being modeled or the working frequency band is very wide, then frequency-domain methods are not efficient. In these situations, time-domain methods provide better solutions because time-domain methods can include the nonlinear elements directly. If using a wideband exciting source, one simulation of a time-domain method can provide wideband frequency-domain results using the Fast Fourier transform (FFT).

Today, a number of efficient numerical methods for solving electromagnetic problems are available. Each method has its particular advantages and disadvantages, and is well-suited for a certain type of problems but not for others. In the following sections, the frequency-domain methods are discussed first, after which the time-domain methods are introduced.

1.1 Frequency-domain methods

Frequency-domain methods solve the electromagnetic problems in the frequency-domain and obtain the frequency-domain results directly. They can be based on differential Maxwell's equations or related integral equations. Many kinds of frequency-domain methods exist. The most popular methods are Method of Moments (MoM), Finite Element Methods (FEM), and Finite-Difference Methods (FDM).

1.1.1 Method of moments

Method of Moments (MoM) is a numerical procedure to solve a linear operator equation by transforming it into a system of simultaneous linear algebraic equations. The linear operator can be differential, integral, or integro-differential. This method can also be called Moment Method (MM). It solves the original operator equations by using weighted

residuals. Harrington has played an important role in popularizing this method in electromagnetic engineering, describing it in a detailed and systematic fashion [1]. As a powerful numerical method, the MoM has been used extensively for more than three decades. It is very suitable for radiating and scattering problems [1]-[19], for example, antenna analysis, waveguide discontinuity analysis, and Radar Cross Section (RCS) analysis.

The general procedure of the method of moments can be described as follows.

Assume that an electromagnetic problem can be modeled with the linear operator equation below.

$$L\bar{J} = \bar{F} \tag{1.1}$$

where L is the linear operator, $\bar{F}$ is the known force or source function, and $\bar{J}$ is the unknown quantities need to be solved.

The first step is to expand $\bar{J}$ as a finite sum of basis functions:

$$\bar{J} = \sum_{i=1}^{M} J_i \bar{b}_i \tag{1.2}$$

where J_i are the expansion coefficients that need to be determined and $\bar{b}_i$ are the known basis functions pre-selected by a user.

By substituting (1.2) into (1.1), the following equation is obtained:

$$\bar{F} = L\sum_{i=1}^{M} J_i \bar{b}_i = \sum_{i=1}^{M} J_i L\bar{b}_i \tag{1.3}$$

The second step is to test the error of the above equation with another pre-selected M linear independent weighting functions $\bar{w}_j$ (j=1,2,...M). More specifically, the following equations are obtained by taking the inner product of each weighting function on both sides of equation (1.3).

$$< \bar{w}_j, \bar{F} > = < \bar{w}_j, \sum_{i=1}^{M} J_i L\bar{b}_i >= \sum_{i=1}^{M} J_i < \bar{w}_j, L\bar{b}_i > \qquad j = 1,2,...,M \tag{1.4}$$

The above equations can be used to find the unknown coefficient J_i.

Equation (1.4) can be rewritten in a matrix form as:

$$[V]=[Z][I] \tag{1.5}$$

where:

$$Z_{ji} =< \bar{w}_j, L\bar{b}_i > \tag{1.6}$$

$$V_j =< \bar{w}_j, \bar{F} > \tag{1.7}$$

$$I_i = J_i \tag{1.8}$$

1.1.2 Finite element method

In general, MoM is very good for analyzing unbounded radiation problems of perfect electric conductor configurations and homogeneous dielectrics. For problems with complicated geometries and many arbitrarily shaped dielectric regions, however, MoM is not very efficient due to the possible fast change of the medium properties. The finite element method (FEM), by contrast, is good at modeling inhomogeneous dielectric bodies as it requires the entire volume of the solution domain to be meshed. Therefore each mesh element may have completely different material properties from those of neighboring elements and this makes FEM excellent at modeling complex inhomogeneous configurations. However, FEM may not model unbounded radiation problems as effectively as MoM because of the potential errors due to the absorbing boundaries introduced.

The FEM has become one of the most popular frequency-domain methods in computational electromagnetics [20]-[30]. One way to construct the FEM formulation is to use variational techniques and work by minimizing or maximizing an expression that is known to be stationary about the true solution. For example, solutions of Maxwell's equations always require that the energy within a structure is minimized; the finite element method can solve for the unknown field quantities by minimizing the energy functional.

The finite element method involves the subdivision of the problem region into subdomains or finite elements and approximation of the field in each element in terms of the linear combinations of basis functions. The basis functions usually are simple

functions (often linear) defined over each element. The element model contains information about the geometry, material properties, excitations and boundary constraints. For a three-dimensional time-harmonic problem, the energy functional can be written as:

$$F = \int_v (\frac{\mu | \bar{H} |^2}{2} + \frac{\varepsilon | \bar{E} |^2}{2} - \frac{\sigma | \bar{E} |^2}{2\omega}) dv \tag{1.9}$$

The first two terms in the integrand are the energy stored in the magnetic and electric fields, and the third term is the energy dissipated due to conductivity.

Expressing $\bar{H}$ in terms of $\bar{E}$, the functional F becomes a function of $\bar{E}$. The field region is then divided into a number of small homogeneous element areas. The elements can be small in regions with geometric details and much larger in uniform regions. The electric field $\bar{E}$ can be expanded as a linear combination of known basis functions with unknown coefficients. F then becomes a functional about these unknown coefficients. Setting the derivative of this functional with respect to unknown coefficients to zero, a system of equations with all the unknown coefficients is obtained:

$$\begin{bmatrix} J_1 \\ J_2 \\ \cdot \\ \cdot \\ J_n \end{bmatrix} = \begin{bmatrix} y_{11} & y_{12} & \cdot & \cdot & \cdot \\ y_{21} & y_{22} & \cdot & \cdot & \cdot \\ \cdot & \cdot & \cdot & \cdot & \cdot \\ \cdot & \cdot & \cdot & \cdot & \cdot \\ \cdot & \cdot & \cdot & \cdot & y_{nn} \end{bmatrix} \begin{bmatrix} E_1 \\ E_2 \\ \cdot \\ \cdot \\ E_n \end{bmatrix} \tag{1.10}$$

where J_i (i=1,2,..,n) are the sources term, E_i (i=1,2,..,n) are the unknown coefficients, and y_{ij} (i=1,2,..,n; j=1,2,…,n) are functions of the target geometry, material properties, and boundary constrains.

After solving equation (1.10), the field distribution is known and other physical quantities of interest can be computed from the known field distribution.

The major advantage of FEM over other numerical methods is that the geometric and material properties of each element can be defined independently and flexibly. This makes FEM competitive in modeling problems with complicated geometries and many arbitrarily shaped dielectric regions, since FEM can use small elements in regions of complex geometry and big elements in large uniform regions.

1.1.3 Finite difference method

Finite difference method was one of the first numerical methods to be used in computational electromagnetics because of its simplicity in concept [31]-[34]. Similar to the FEM, the finite difference method is based on the differential equations of the electromagnetic problems. The finite difference method uses the difference operator to approximate the original differential operator and convert the original differential equations into a system of algebraic equations. With the advance of computer technology, the finite difference method developed extensively, and has become one of the numerical methods used currently [35]-[39]. However, it is not as popular as the finite element method for frequency-domain problems. This may result from the fact that finite element method attracted much attention in civil and mechanical engineering.

The general procedure of finite difference method consists of three steps:

a) Divide the problem domain into grids and use the node values of fields as unknowns.

b) Replace the differential equation by the approximate difference equations, which relate the field value in a node to the field values at neighboring nodes. This converts the original differential equation into a system of linear algebra equations in the unknown field values at the discretized nodes.

c) Solve the system of linear algebraic equations with the known boundary conditions.

1.2 Time-domain methods

The frequency-domain formulae are not good at handling nonlinear elements and materials; they can obtain the result about one frequency point for each simulation and are efficient only for narrow band applications. Time-domain methods, however, can obtain the results of wide band frequencies with only one simulation and handle the nonlinear elements and materials easily. Today, wideband applications are very popular. Time-domain methods are very good options to obtain the wideband results efficiently, and they are becoming more and more competitive. Usually, each frequency-domain method has a time-domain counterpart. For example, there are time-domain FEM [40] and MoM [41] associated with the frequency-domain FEM and MoM. However, the most popular time-domain methods are finite-difference time-domain method (FDTD) and

transmission line method (TLM). In the FDTD and TLM, the simple and explicit updating formulations make the FDTD and TLM relatively easy to program. However, the explicit time-domain updating methods can experience numerical stability problems. To ensure the time-domain computation to be stable, the time step has to be smaller than an upper limit which is related to spatial steps. For fine structures that require small spatial steps, the time step has to be small. This will reduce the efficiency of the explicit time-domain marching methods.

1.2.1 FDTD

The FDTD is one of the most popular time-domain methods. It was proposed by K. S. Yee [42] in 1966. Like the FEM, it uses the partial differential equations which describe the target electromagnetic system. Unlike the FEM, the FDTD method does not use variational concepts or weighted residuals; instead, it directly approximates the time and space derivatives in the time dependent Maxwell curl equations by simple 2^{nd} order central differences. FDTD uses a staggered grid in time and space, and the electric and magnetic fields are computed on the staggered grid with a marching-on-in-time technique. It provides a direct solution of Maxwell's curl equations and is very flexible at solving complicated electromagnetic problems.

Although the FDTD method was proposed in 1966 [42], it began to garner public attention only after the 1980s. The early FDTD methods needed to discretize the whole problem domain by uniform grids. For complex practical problems, this required a huge amount of computer memory and CPU power, more than computers could provide at the time. From the 1980s on, two factors pushed forward the development of FDTD. One was the swift advance in computer performance, including CPU speed and computer memory, which provided the enabling technology and hardware base. The other factor was application requirements. Practical electromagnetic engineering problems methods became more and more complicated; take, for example, the electromagnetic compatibility analysis of complex electronic systems and the signal integrity analysis of large-scale integrated circuits. These complex electromagnetic problems require flexible and powerful electromagnetic simulation tools. As a direct solution to Maxwell's curl equations, using a simple and explicit updating formula, the FDTD method became one

of the most popular numerical methods [43]-[54]. After Berenger proposed the perfectly matched layer absorbing boundary conditions [50], the method could be made accurate on smaller meshes.

When using the FDTD method, there are two constraints [55]: one is the Courant-Friedich-Levy (CFL) limit that guarantees stability; the other is to sufficiently resolve the problem to reduce the numerical dispersion resulting from the discretization. The first limit can be removed by the unconditionally stable alternating direction implicit finite-difference time-domain (ADI-FDTD) method [56][57]; the second limit can be removed by the application of high-order schemes such as the Multi-Resolution Time-Domain (MRTD) method [58] and the Pseudo-Spectral Time-Domain (PSTD) method [59].

1.2.2 TLM

The transmission line method (TLM) is another popular time-domain method proposed by Johns [60]. TLM is a numerical technique for solving field problems using circuit equivalent. It employs the analogy between the Maxwell's equations for electric fields and magnetic fields and the equations for voltages and currents on a mesh of continuous transmission lines [61]. By computing the voltage and current in the networks, the electric and magnetic fields can be solved. The symmetrical condensed node formula introduced by Johns [62] has become the standard for 3D TLM methods.

Like other numerical methods, the TLM method solves the electromagnetic problem by approximating the original continuous problem using a discretized system. However, the transmission line matrix method uses a physical discretization process; the other numerical methods, such as the finite difference method and the finite element method use the mathematical discretization process. Because of the simplicity in formula and programming, the TLM method obtained much attention in many applications and became one of the most popular time-domain methods [63]-[69].

The general procedure of TLM methods includes two basic steps:

a) Replace the field region by an equivalent transmission line network and derive the equivalence between the field and the network quantities.
b) Solve the equivalent transmission line system through the repeated scattering and transmission of voltage waves.

TLM shares both the major advantages and disadvantages of FDTD. On one hand, they both used explicit update formula and easily can handle complex structures and nonlinear elements and materials; on the other hand, they both suffer from the numerical dispersion problem [70] and a tight time-step constraint.

1.3 Motivation and contributions

Although the FDTD method is simple in concept and programming as well as robust and flexible in applications, it still requires intensive computer resources, especially for complex and electrically large structures. Therefore, efforts in improving computational efficiency and accuracy continue unabated. There are many techniques to achieve high computational efficiency [55]; for example, semi-analytical methods were applied to reduce the problem dimensions, incident wave generator and absorbing boundary conditions were developed with high performance and efficiency, and subgridding method were formulated for complex structures with fine geometric details.

For waveguide structure, a semi-analytical method, called compact 2D FDTD, was proposed [71][72]. It can obtain the propagation characteristics of waveguide structure by reducing a 3D FDTD problem to a 2D FDTD problem, but it cannot be used to analyze the discontinuity along the direction of wave propagation. To solve the issue, a new compact 2D FDTD method is proposed in the third chapter of this thesis; it can be used to analyze the discontinuity along the direction of wave propagation.

During the application of waveguide structures, an incident wave as the source and absorbing boundary condition as the matching load are often required in order to obtain the S-parameters [73]. Usually, the incident wave is obtained by simulating a long uniform waveguide and it needs a large amount of computer memory and long run time. There are many kinds of absorbing boundary conditions in waveguide applications [50][74]-[86]; however, they can not provide good absorption for frequencies around the

cut-off frequency. To solve the issue, a compact 1D FDTD formula is proposed in the fourth chapter, which can provide very good absorption performance for the full frequency spectrum including the cut-off frequency. When applied to the Complex Frequency Shifted Perfectly-Matched Layer (CFS-PML) methods [83][84], an efficient modal based PML is produced in the fifth chapter.

In order to solve complex problems with fine geometric details, many FDTD subgridding methods have been proposed [87]-[98]. However, these subgridding schemes have suffered the problems of late-time instability or uncontrollable reflections from the interfaces. To overcome the problem, a new subgridding formula is proposed in the sixth chapter, which is robust and has controllable low reflection.

When the FDTD method is used to simulate RF/microwave circuits with active devices, it is necessary to consider how to combine the FDTD with active devices. One approach is to use the time-domain lump-element circuit model of the active device directly [99][101]; another approach is to use the frequency-domain parameters of the active device [102][103]. The time-domain lump-element circuit model of an active device is not available often and only the frequency-domain parameters are available. In such a case, the frequency-domain parameters should be converted into causal time-domain parameters.

However, the frequency-domain parameters of many electronic components are often given or measured in a band-limited frequency range. Direct application of the inverse Fourier transform to the band-limited frequency-domain parameters usually leads to non-causal parameters in the time-domain. Such non-causal time-domain parameters are neither physical nor compatible with, or capable of, being incorporated into a simulator based on a causal mathematical model such as the FDTD method. To obtain a causal time-domain model from the band limited frequency-domain parameters, three methods have been used in this thesis.

First, two iterative methods based on the Fast Fourier Transform (FFT) are presented in the seventh chapter: one applies the FFT in combination with the error feedback principle; the other applies the Hilbert transform in conjunction with the FFT. These methods are conceptually simple and easy to implement. The extracted time-domain

parameters are not only causal but also contain almost the same frequency-domain information as the original parameters over the given limited frequency range in both magnitude and phase.

However, the time-domain parameters extracted using the iterative methods are only in numerical form and are computationally time consuming when a convolution is performed with them in a time-domain simulation. To solve this problem, a rational function fitting technique is introduced in the eighth chapter, which extracts the causal time-domain parameters of an active device from their known band-limited frequency-domain counterparts. One of the major advantages of this technique is that the resulting time-domain parameters can be expressed in the form of exponential functions. The convolution with these exponential functions can then be performed in a recursive fashion without requiring a complete past history of the time-domain parameters, and the CPU time for each time-marching step is constant. The total CPU time and memory of a convolution will increase linearly with the time steps. Therefore, computational efficiency is improved significantly, especially for a simulation with a large number of iterations.

Finally, it is worth to mention that the most work of the thesis has been published in [104]-[112].

2 Concept of FDTD

2.1 Introduction of classical FDTD

The FDTD method is a direct approximation of Maxwell's curl equations in the time-domain. It discretizes the differential form of Maxwell's equations directly by using 2nd order central finite difference approximation. In the FDTD, the electric field E-grid is offset both spatially and temporally from the magnetic field H-grid. The resulting update formulae for the $\bar{E}$ and $\bar{H}$ fields are known as the leap-frog scheme.

2.1.1 Yee's grid and FDTD formula

In a linear and isotropic medium, Maxwell's curl equations can be written as:

$$\mu \frac{\partial \bar{H}}{\partial t} = -\nabla \times \bar{E} - \rho' \bar{H} \tag{2.1}$$

$$\varepsilon \frac{\partial \bar{E}}{\partial t} = \nabla \times \bar{H} - \sigma \bar{E} \tag{2.2}$$

where ε is the electrical permittivity, μ is the magnetic permeability, σ is the conductivity, and ρ' is the magnetic conductivity respectively.

In Cartesian coordinates, (2.1) and (2.2) can be rewritten as the following six scalar equations:

$$\frac{\partial H_x}{\partial t} = \frac{1}{\mu}\left(\frac{\partial E_y}{\partial z} - \frac{\partial E_z}{\partial y} - \rho' H_x\right) \tag{2.3}$$

$$\frac{\partial H_y}{\partial t} = \frac{1}{\mu}\left(\frac{\partial E_z}{\partial x} - \frac{\partial E_x}{\partial z} - \rho' H_y\right) \tag{2.4}$$

$$\frac{\partial H_z}{\partial t} = \frac{1}{\mu}\left(\frac{\partial E_x}{\partial y} - \frac{\partial E_y}{\partial x} - \rho' H_z\right) \tag{2.5}$$

$$\frac{\partial E_x}{\partial t} = \frac{1}{\varepsilon}\left(\frac{\partial H_z}{\partial y} - \frac{\partial H_y}{\partial z} - \sigma E_x\right) \tag{2.6}$$

$$\frac{\partial E_y}{\partial t} = \frac{1}{\varepsilon}\left(\frac{\partial H_x}{\partial z} - \frac{\partial H_z}{\partial x} - \sigma E_y\right) \tag{2.7}$$

$$\frac{\partial E_z}{\partial t} = \frac{1}{\varepsilon}\left(\frac{\partial H_y}{\partial x} - \frac{\partial H_x}{\partial y} - \sigma E_z\right) \tag{2.8}$$

Using 2nd order central finite difference to approximate the spatial and temporal derivatives in (2.3) - (2.8), Yee's FDTD formulae can be obtained as follows [55]:

$$H_x\Big|_{i,j+\frac{1}{2},k+\frac{1}{2}}^{n+\frac{1}{2}} = \frac{1-\dfrac{\rho'_{i,j+\frac{1}{2},k+\frac{1}{2}}\Delta t}{2\mu_{i,j+\frac{1}{2},k+\frac{1}{2}}}}{1+\dfrac{\rho'_{i,j+\frac{1}{2},k+\frac{1}{2}}\Delta t}{2\mu_{i,j+\frac{1}{2},k+\frac{1}{2}}}} H_x\Big|_{i,j+\frac{1}{2},k+\frac{1}{2}}^{n-\frac{1}{2}} + \frac{\dfrac{\Delta t}{\mu_{i,j+\frac{1}{2},k+\frac{1}{2}}}}{1+\dfrac{\rho'_{i,j+\frac{1}{2},k+\frac{1}{2}}\Delta t}{2\mu_{i,j+\frac{1}{2},k+\frac{1}{2}}}}\left(\frac{E_y\Big|_{i,j+\frac{1}{2},k+1}^{n} - E_y\Big|_{i,j+\frac{1}{2},k}^{n}}{\Delta z} - \frac{E_z\Big|_{i,j+1,k+\frac{1}{2}}^{n} - E_z\Big|_{i,j,k+\frac{1}{2}}^{n}}{\Delta y}\right) \tag{2.9}$$

$$H_y\Big|_{i+\frac{1}{2},j,k+\frac{1}{2}}^{n+\frac{1}{2}} = \frac{1-\dfrac{\rho'_{i+\frac{1}{2},j,k+\frac{1}{2}}\Delta t}{2\mu_{i+\frac{1}{2},j,k+\frac{1}{2}}}}{1+\dfrac{\rho'_{i+\frac{1}{2},j,k+\frac{1}{2}}\Delta t}{2\mu_{i+\frac{1}{2},j,k+\frac{1}{2}}}} H_y\Big|_{i+\frac{1}{2},j,k+\frac{1}{2}}^{n-\frac{1}{2}} + \frac{\dfrac{\Delta t}{\mu_{i+\frac{1}{2},j,k+\frac{1}{2}}}}{1+\dfrac{\rho'_{i+\frac{1}{2},j,k+\frac{1}{2}}\Delta t}{2\mu_{i+\frac{1}{2},j,k+\frac{1}{2}}}}\left(\frac{E_z\Big|_{i+1,j,k+\frac{1}{2}}^{n} - E_z\Big|_{i,j,k+\frac{1}{2}}^{n}}{\Delta x} - \frac{E_x\Big|_{i+\frac{1}{2},j,k+1}^{n} - E_x\Big|_{i+\frac{1}{2},j,k}^{n}}{\Delta z}\right) \tag{2.10}$$

$$H_z\Big|_{i+\frac{1}{2},j+\frac{1}{2},k}^{n+\frac{1}{2}} = \frac{1-\dfrac{\rho'_{i+\frac{1}{2},j+\frac{1}{2},k}\Delta t}{2\mu_{i+\frac{1}{2},j+\frac{1}{2},k}}}{1+\dfrac{\rho'_{i+\frac{1}{2},j+\frac{1}{2},k}\Delta t}{2\mu_{i+\frac{1}{2},j+\frac{1}{2},k}}} H_z\Big|_{i+\frac{1}{2},j+\frac{1}{2},k}^{n-\frac{1}{2}} + \frac{\dfrac{\Delta t}{\mu_{i+\frac{1}{2},j+\frac{1}{2},k}}}{1+\dfrac{\rho'_{i+\frac{1}{2},j+\frac{1}{2},k}\Delta t}{2\mu_{i+\frac{1}{2},j+\frac{1}{2},k}}}\left(\frac{E_x\Big|_{i+\frac{1}{2},j+1,k}^{n} - E_x\Big|_{i+\frac{1}{2},j,k}^{n}}{\Delta y} - \frac{E_y\Big|_{i+1,j+\frac{1}{2},k}^{n} - E_y\Big|_{i,j+\frac{1}{2},k}^{n}}{\Delta x}\right) \tag{2.11}$$

$$E_x\Big|_{i+\frac{1}{2},j,k}^{n+1} = \frac{1-\dfrac{\sigma_{i+\frac{1}{2},j,k}\Delta t}{2\varepsilon_{i+\frac{1}{2},j,k}}}{1+\dfrac{\sigma_{i+\frac{1}{2},j,k}\Delta t}{2\varepsilon_{i+\frac{1}{2},j,k}}} E_x\Big|_{i+\frac{1}{2},j,k}^{n} + \frac{\dfrac{\Delta t}{\varepsilon_{i+\frac{1}{2},j,k}}}{1+\dfrac{\sigma_{i+\frac{1}{2},j,k}\Delta t}{2\varepsilon_{i+\frac{1}{2},j,k}}} \left(\frac{H_z\Big|_{i+\frac{1}{2},j+\frac{1}{2},k}^{n+1/2} - H_z\Big|_{i+\frac{1}{2},j-\frac{1}{2},k}^{n+1/2}}{\Delta y} - \frac{H_y\Big|_{i+\frac{1}{2},j,k+\frac{1}{2}}^{n+1/2} - H_y\Big|_{i+\frac{1}{2},j,k-\frac{1}{2}}^{n+1/2}}{\Delta z} \right) \tag{2.12}$$

$$E_y\Big|_{i,j+\frac{1}{2},k}^{n+1} = \frac{1-\dfrac{\sigma_{i,j+\frac{1}{2},k}\Delta t}{2\varepsilon_{i,j+\frac{1}{2},k}}}{1+\dfrac{\sigma_{i,j+\frac{1}{2},k}\Delta t}{2\varepsilon_{i,j+\frac{1}{2},k}}} E_y\Big|_{i,j+\frac{1}{2},k}^{n} + \frac{\dfrac{\Delta t}{\varepsilon_{i,j+\frac{1}{2},k}}}{1+\dfrac{\sigma_{i,j+\frac{1}{2},k}\Delta t}{2\varepsilon_{i,j+\frac{1}{2},k}}} \left(\frac{H_x\Big|_{i,j+\frac{1}{2},k+\frac{1}{2}}^{n+1/2} - H_x\Big|_{i,j+\frac{1}{2},k-\frac{1}{2}}^{n+1/2}}{\Delta z} - \frac{H_z\Big|_{i+\frac{1}{2},j+\frac{1}{2},k}^{n+1/2} - H_z\Big|_{i-\frac{1}{2},j+\frac{1}{2},k}^{n+1/2}}{\Delta x} \right) \tag{2.13}$$

$$E_z\Big|_{i,j,k+\frac{1}{2}}^{n+1} = \frac{1-\dfrac{\sigma_{i,j,k+\frac{1}{2}}\Delta t}{2\varepsilon_{i,j,k+\frac{1}{2}}}}{1+\dfrac{\sigma_{i,j,k+\frac{1}{2}}\Delta t}{2\varepsilon_{i,j,k+\frac{1}{2}}}} E_z\Big|_{i,j,k+\frac{1}{2}}^{n} + \frac{\dfrac{\Delta t}{\varepsilon_{i,j,k+\frac{1}{2}}}}{1+\dfrac{\sigma_{i,j,k+\frac{1}{2}}\Delta t}{2\varepsilon_{i,j,k+\frac{1}{2}}}} \left(\frac{H_y\Big|_{i+\frac{1}{2},j,k+\frac{1}{2}}^{n+1/2} - H_y\Big|_{i-\frac{1}{2},j,k+\frac{1}{2}}^{n+1/2}}{\Delta x} - \frac{H_x\Big|_{i,j+\frac{1}{2},k+\frac{1}{2}}^{n+1/2} - H_x\Big|_{i,j-\frac{1}{2},k+\frac{1}{2}}^{n+1/2}}{\Delta y} \right) \tag{2.14}$$

where $U\Big|_{i,j,k}^{n} = U(i\Delta x, j\Delta y, k\Delta z, n\Delta t)$ represents the value of $U(x,y,z,t)$ at the point $(x,y,z) = (i\Delta x, j\Delta y, k\Delta z)$ at time $t = n\Delta t$. Δx, Δy, Δz and Δt are the spatial and temporal increments respectively.

The corresponding field components in the Yee's grids are shown in Fig. 2.1.

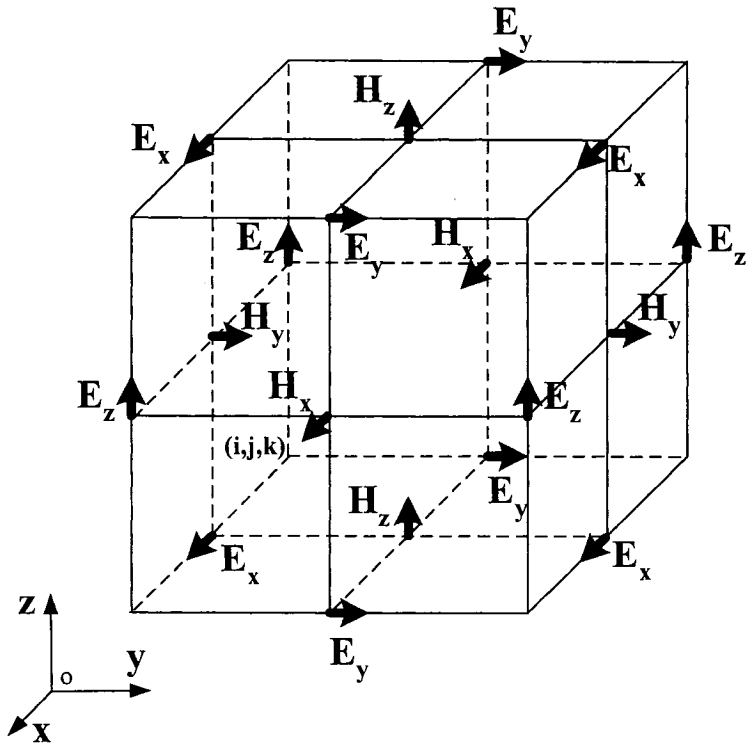

Figure 2.1 Positions of the field components in Yee's grids.

It can be seen from equations (2.9) - (2.14) and Figure 2.1 that the components of electric and magnetic fields are interlaced within the FDTD grid and computed at alternate half time steps. Given the initial values and boundary values of electric and magnetic fields, equations (2.9) - (2.14) can be updated explicitly. It is, therefore, an explicit time-domain method. There is no need to solve systems of linear algebraic equation, each field component value can be evaluated directly from the neighboring field components and its own value in the last time step. The simplicity of concept and ease of programming makes FDTD one of the most popular electromagnetic numerical methods.

2.1.2 Numerical stability

FDTD is an explicit update formula in the time-domain. Usually, explicit update formulae have stability problems. For the given spatial increments Δx, Δy, and Δz, in

order to keep the simulation stable, the time step size Δt must satisfy the following stability condition [55]:

$$\Delta t \leq \frac{1}{\frac{1}{\sqrt{\mu\varepsilon}}\sqrt{\frac{1}{\Delta x^2}+\frac{1}{\Delta y^2}+\frac{1}{\Delta z^2}}} \tag{2.15}$$

This stability condition is called CFL stability condition because the analysis method was presented by Courant, Friedrich, and Levy (CFL).

2.1.3 Numerical dispersion

When using FDTD to simulate electromagnetic wave propagation, the numerical phase velocity of the simulated wave mode in the FDTD lattice can differ from the actual wave velocity c; this phenomenon is called numerical dispersion of FDTD [55]. The numerical dispersion causes the numerical phase velocity to differ from the actual wave velocity, and it will reduce the accuracy of computed results. Hence it is desirable to understand numerical dispersion's operation and its effect on accuracy, especially for electrically large structures.

Considering a plane monochromatic traveling wave in a uniform lossless medium, Taflove derived the following numerical dispersion relationship for FDTD [55]:

$$\left[\frac{1}{c\Delta t}\sin(\frac{\omega\Delta t}{2})\right]^2=\left[\frac{1}{\Delta x}\sin(\frac{\tilde{k}_x\Delta x}{2})\right]^2+\left[\frac{1}{\Delta y}\sin(\frac{\tilde{k}_y\Delta y}{2})\right]^2+\left[\frac{1}{\Delta z}\sin(\frac{\tilde{k}_z\Delta z}{2})\right]^2 \tag{2.16}$$

where $\tilde{k}_x$, $\tilde{k}_y$, and $\tilde{k}_z$ are, respectively, the x, y, and z components of the numerical wavevector, and ω is the wave angular frequency.

In contrast to the numerical dispersion relationship of FDTD, the analytical dispersion relationship of plane wave in uniform lossless medium is much simpler [122]:

$$\frac{\omega^2}{c^2}=k_x^2+k_y^2+k_z^2 \tag{2.17}$$

where k_x, k_y, and k_z are, respectively, the x, y, and z components of the analytical wavevector.

It can be seen from equations (2.16) and (2.17) that the numerical dispersion is different from the analytical dispersion. In contrast to the numerical dispersion relationship of FDTD, the analytical dispersion relationship of plane wave in a uniform lossless medium is much simpler. In order to have an acceptably small error from numerical dispersion, the spatial increments Δx, Δy, Δz should be less than one tenth of the smallest wavelength [55].

2.2 Lumped Elements in FDTD

When the FDTD is used to analyze structures including lumped circuit elements, one way to account for the lumped circuit element is to add a lumped electric current density term in the Maxwell's equations. The process can be described as follows.

Maxwell's curl equations applied to the cells that contain the device are:

$$\varepsilon \frac{\partial \overline{E}}{\partial t} = \nabla \times \overline{H} - \overline{J}_d \tag{2.18}$$

$$\mu \frac{\partial \overline{H}}{\partial t} = -\nabla \times \overline{E} \tag{2.19}$$

where $\overline{J}_d$ is the additional current density term resulting from the lump-element device.

To compute $\overline{J}_d$, for simplicity, consider an one-port lump-element device that is oriented in the z-direction as shown in Figure 2.2. Suppose that the current flowing through the device is i_d. Then the current density $\overline{J}_d$ can be obtained as

$$J_d = \frac{i_d}{\Delta x \Delta y} \tag{2.20}$$

where Δx and Δy are the space increments of the FDTD mesh that covers the cross section of the device.

i_d can be determined through the known device I-V relationship,

$$i_d = f(v_d) \tag{2.21}$$

where v_d is the device voltage oriented in the z-direction. For instance, for a resistor of resistance R, $i_d = v_d / R$.

The device voltage v_d can be obtained from its relations to the electric field:

$$v_d = E_z \Delta z \tag{2.22}$$

Combination of (2.20)-(2.22) reads

$$J_d = \frac{f(E_z \Delta z)}{\Delta x \Delta y} \tag{2.23}$$

The above equation can be substituted into (2.18), forming the Maxwell's equations that include the lump device model for FDTD computations. The unknowns are the field quantities to be solved.

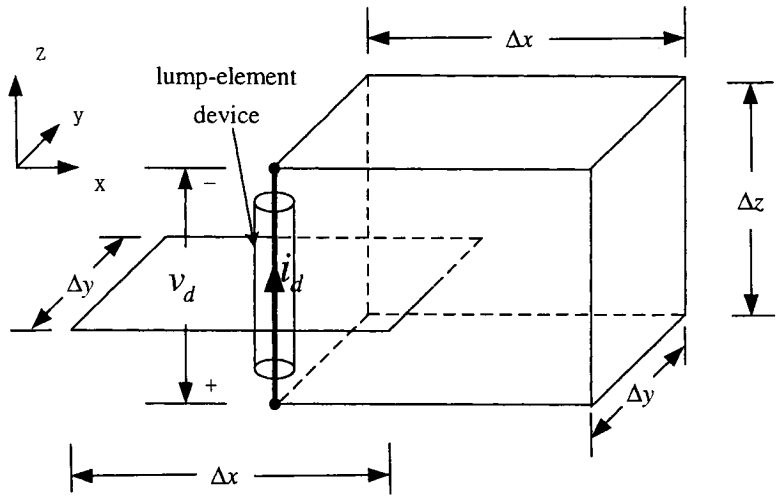

Figure 2.2 The position of a one-port lump-element device in the FDTD grid.

The above concept can be extended to multi-port device models. Figure 2.3 shows a two-port transistor in the FDTD grid and Figure 2.4 presents the extracted two-port network representation of the device.

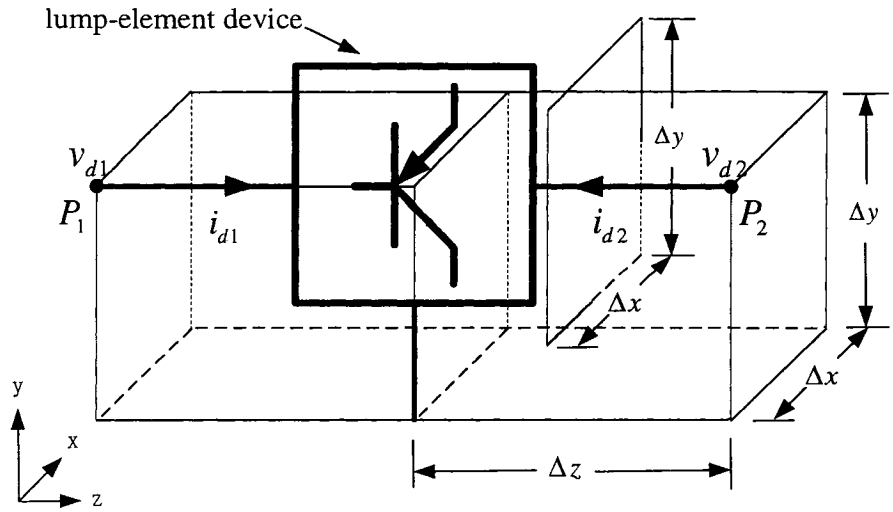

Figure 2.3 A two-port lump-element device (transistor) in the FDTD grid.

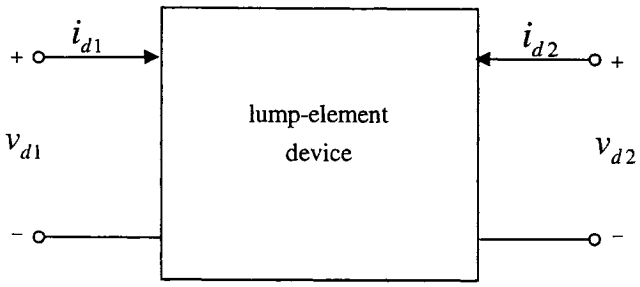

Figure 2.4 The equivalent two-port network of an active device.

$v_{d1}(t)$ and $v_{d2}(t)$, and $i_{d1}(t)$ and $i_{d2}(t)$ are the voltages and currents at the two ports of the network. They can be related by the known device admittance parameters (Y-parameters):

$$\begin{bmatrix} i_{d1}(t) \\ i_{d2}(t) \end{bmatrix} = \begin{bmatrix} y_{11}(t) \otimes v_{d1}(t) + y_{12}(t) \otimes v_{d2}(t) \\ y_{21}(t) \otimes v_{d1}(t) + y_{22}(t) \otimes v_{d2}(t) \end{bmatrix} \tag{2.24}$$

where $\otimes$ represents time-domain convolution, and $y_{11}(t)$, $y_{12}(t)$, $y_{21}(t)$ and $y_{22}(t)$ are the time-domain Y-parameters.

$v_{d1}(t)$ and $v_{d2}(t)$, and $i_{d1}(t)$ and $i_{d2}(t)$ are also related to electric fields and current densities in a way similar to that described before for the case of one-port device. For instance, voltages v_{d1} and v_{d2} are related to electric fields as shown below:

$$v_{di} = -\int_{P_0}^{P_i} \bar{E} \cdot d\bar{l} \qquad i = 1,2 \tag{2.25}$$

where P_0 is the voltage reference point (for example, the grounded via) and P_i is the point need to be computed. $i_{d1}(t)$ and $i_{d2}(t)$ are related to the current densities through (2.20), or more specifically,

$$J_{di} = \frac{i_{di}}{\Delta x \Delta y} \qquad i = 1,2 \tag{2.26}$$

Combination of (2.24)-(2.26) reads:

$$J_{di} = f_i(\bar{E}, y_{i1}, y_{i2}) \qquad i = 1,2 \tag{2.27}$$

Substitution of the above equation into (2.18) forms the Maxwell's equations that include the lump device model for FDTD computations. Again, the unknowns are the field quantities to be solved.

Once the Maxwell's equations including lump-element devices are formed, they can be solved with details described in [55][99]-[103].

2.3 Conclusion

This chapter has reviewed the basic concepts and formulas associated with FDTD and introduced briefly the stability condition and numerical dispersion of FDTD. Finally, the method incorporating the governing voltage-current equations of a device into the FDTD frame was discussed.

3 New Compact 2D FDTD Method for 3D Waveguide Structures

3.1 Introduction

Computational efficiency still remains a challenge with the FDTD method. For a three-dimensional guided-wave structure, three-dimensional numerical FDTD grids are generally needed. To reduce the memory and CPU time requirements, two-dimensional compact FDTD methods have been developed [71][72] where field variations along the propagation (or longitudinal) direction are assumed to be complex exponential functions. The methods are very useful and effective in analyzing the dispersion characteristics of guided-wave structures, such as microstrip lines or coplanar waveguides.

However, the compact 2D FDTD methods developed so far assume the structure uniformity along the propagation direction and cannot be used for computing geometric or material discontinuities in the propagation direction. Therefore, an efficient method is desired that can account for waveguide structure discontinuities. Among many waveguide structures, structure uniformity does exist in one of the transverse directions. For example, many rectangular waveguide connectors and filters popular in industry [113]-[115] have such a feature. Navarro et al. studied these types of structures partially [116], but only considered the TE10 mode in the H-plane waveguides. Field variations in one of the transverse directions (for example, the y direction in this case) are assumed to be non-existent. Such an assumption is not suitable for many applications where higher-order modes exist. Therefore, a more general compact 2D FDTD method is needed. Since the structures are uniform in one transverse direction, field distributions in this direction can be expanded with sine or cosine functions in space. Based on this, we propose a new compact 2D FDTD method.

First, we can classify the traveling modes based on the number of periods of field variations in this uniform direction; then, we can use this fact to reduce the 3D waveguide problems to a 2D problems and solve them with the new 2D compact FDTD formulation. In contrast to the 2D compact FDTD methods reported before [71][72], the proposed

method can be applied to discontinuity problems in the longitudinal direction.

This chapter is organized in the following way. First, the derivations of the proposed 2D compact formulae are given. Two numerical examples are then presented to demonstrate the validity and effectiveness of the proposed technique. Finally, discussion and conclusions are presented.

3.2 Formula of the New Compact 2D FDTD

Without losing generality, we assume that the geometry of the waveguide structures under study are uniform in the y direction. We also assume that the modes under consideration have n standing waves in the y direction; we can call them T_n modes for simplicity.

Since the perfect conductors are placed at the end walls of the y-direction, the normal magnetic field component H_y and tangent electric field components E_x and E_z have to be zero at y=0 and b. As a result, variations of the field components along y-direction can be expanded in terms of $\sin(\pi y/b)$ or $\cos(\pi y/b)$. More specifically, the six field components can be expressed as:

$$
\begin{aligned}
E_x(x,y,z,t) &= \tilde{E}_x(x,z,t)\sin(\frac{n\pi y}{b}) \\
E_y(x,y,z,t) &= \tilde{E}_y(x,z,t)\cos(\frac{n\pi y}{b}) \\
E_z(x,y,z,t) &= \tilde{E}_z(x,z,t)\sin(\frac{n\pi y}{b}) \\
H_x(x,y,z,t) &= \tilde{H}_x(x,z,t)\cos(\frac{n\pi y}{b}) \\
H_y(x,y,z,t) &= \tilde{H}_y(x,z,t)\sin(\frac{n\pi y}{b}) \\
H_z(x,y,z,t) &= \tilde{H}_z(x,z,t)\cos(\frac{n\pi y}{b})
\end{aligned}
\tag{3.1}
$$

where b is the width of the waveguide in the y direction, $\tilde{E}_x$ - $\tilde{H}_z$ represent the remaining part of each field value function after the term including the variations along the y direction is extracted.

By inserting (3.1) into Maxwell's equations in the Cartesian coordinates, the following equations are obtained:

$$
\begin{aligned}
&\frac{\partial \tilde{E}_x}{\partial t}\sin(\frac{n\pi y}{b}) = -\frac{1}{\varepsilon}(\frac{n\pi}{b}\tilde{H}_z + \frac{\partial \tilde{H}_y}{\partial z})\sin(\frac{n\pi y}{b}) \\
&\frac{\partial \tilde{E}_y}{\partial t}\cos(\frac{n\pi y}{b}) = \frac{1}{\varepsilon}(\frac{\partial \tilde{H}_x}{\partial z} - \frac{\partial \tilde{H}_z}{\partial x})\cos(\frac{n\pi y}{b}) \\
&\frac{\partial \tilde{E}_z}{\partial t}\sin(\frac{n\pi y}{b}) = \frac{1}{\varepsilon}(\frac{\partial \tilde{H}_y}{\partial x} + \frac{n\pi}{b}\tilde{H}_x)\sin(\frac{n\pi y}{b}) \\
&\frac{\partial \tilde{H}_x}{\partial t}\cos(\frac{n\pi y}{b}) = -\frac{1}{\mu}(\frac{n\pi}{b}\tilde{E}_z - \frac{\partial \tilde{E}_y}{\partial z})\cos(\frac{n\pi y}{b}) \\
&\frac{\partial \tilde{H}_y}{\partial t}\sin(\frac{n\pi y}{b}) = -\frac{1}{\mu}(\frac{\partial \tilde{E}_x}{\partial z} - \frac{\partial \tilde{E}_z}{\partial x})\sin(\frac{n\pi y}{b}) \\
&\frac{\partial \tilde{H}_z}{\partial t}\cos(\frac{n\pi y}{b}) = -\frac{1}{\mu}(\frac{\partial \tilde{E}_y}{\partial x} - \frac{n\pi}{b}\tilde{E}_x)\cos(\frac{n\pi y}{b})
\end{aligned}
\tag{3.2}
$$

Removing the common terms on both sides of (3.2), we can reduce (3.2) to 2D Maxwell's equations:

$$
\begin{aligned}
&\frac{\partial \tilde{E}_x(x,z,t)}{\partial t} = -\frac{1}{\varepsilon}(\frac{n\pi}{b}\tilde{H}_z(x,z,t) + \frac{\partial \tilde{H}_y(x,z,t)}{\partial z}) \\
&\frac{\partial \tilde{E}_y(x,z,t)}{\partial t} = \frac{1}{\varepsilon}(\frac{\partial \tilde{H}_x(x,z,t)}{\partial z} - \frac{\partial \tilde{H}_z(x,z,t)}{\partial x}) \\
&\frac{\partial \tilde{E}_z(x,z,t)}{\partial t} = \frac{1}{\varepsilon}(\frac{\partial \tilde{H}_y(x,z,t)}{\partial x} + \frac{n\pi}{b}\tilde{H}_x(x,z,t)) \\
&\frac{\partial \tilde{H}_x(x,z,t)}{\partial t} = -\frac{1}{\mu}(\frac{n\pi}{b}\tilde{E}_z(x,z,t) - \frac{\partial \tilde{E}_y(x,z,t)}{\partial z}) \\
&\frac{\partial \tilde{H}_y(x,z,t)}{\partial t} = -\frac{1}{\mu}(\frac{\partial \tilde{E}_x(x,z,t)}{\partial z} - \frac{\partial \tilde{E}_z(x,z,t)}{\partial x}) \\
&\frac{\partial \tilde{H}_z(x,z,t)}{\partial t} = -\frac{1}{\mu}(\frac{\partial \tilde{E}_y(x,z,t)}{\partial x} - \frac{n\pi}{b}\tilde{E}_x(x,z,t))
\end{aligned}
\tag{3.3}
$$

By replacing the derivatives with their 2nd order central finite-difference counterparts, the discretized equations shown in (3.4) - (3.9) are obtained:

$$
\begin{aligned}
\tilde{E}_x^{n+1}(i+\tfrac{1}{2},k) = \tilde{E}_x^{n}(i+\tfrac{1}{2},k) &- \frac{\Delta t}{\varepsilon}\frac{n\pi}{b}\tilde{H}_z^{n+\frac{1}{2}}(i+\tfrac{1}{2},k) \\
&- \frac{\Delta t}{\varepsilon}\frac{\tilde{H}_y^{n+\frac{1}{2}}(i+\frac{1}{2},k+\frac{1}{2}) - \tilde{H}_y^{n+\frac{1}{2}}(i+\frac{1}{2},k-\frac{1}{2})}{\Delta z}
\end{aligned}
\tag{3.4}
$$

$$
\begin{aligned}
\tilde{E}_y^{n+1}(i,k) = \tilde{E}_y^{n}(i,k) &+ \frac{\Delta t}{\varepsilon}\frac{\tilde{H}_x^{n+\frac{1}{2}}(i,k+\frac{1}{2}) - \tilde{H}_x^{n+\frac{1}{2}}(i,k-\frac{1}{2})}{\Delta z} \\
&- \frac{\Delta t}{\varepsilon}\frac{\tilde{H}_z^{n+\frac{1}{2}}(i+\frac{1}{2},k) - \tilde{H}_z^{n+\frac{1}{2}}(i-\frac{1}{2},k)}{\Delta x}
\end{aligned}
\tag{3.5}
$$

$$\tilde{E}_z^{n+1}(i,k+\tfrac{1}{2}) = \tilde{E}_z^{n}(i,k+\tfrac{1}{2}) + \frac{\Delta t}{\varepsilon}\frac{n\pi}{b}\tilde{H}_x^{n+\frac{1}{2}}(i,k+\tfrac{1}{2}) + \frac{\Delta t}{\varepsilon}\frac{\tilde{H}_y^{n+\frac{1}{2}}(i+\frac{1}{2},k+\frac{1}{2}) - \tilde{H}_y^{n+\frac{1}{2}}(i-\frac{1}{2},k+\frac{1}{2})}{\Delta x} \tag{3.6}$$

$$\tilde{H}_x^{n+\frac{1}{2}}(i,k+\tfrac{1}{2}) = \tilde{H}_x^{n-\frac{1}{2}}(i,k+\tfrac{1}{2}) - \frac{\Delta t}{\mu}\frac{n\pi}{b}\tilde{E}_z^{n}(i,k+\tfrac{1}{2}) + \frac{\Delta t}{\mu}\frac{\tilde{E}_y^{n}(i,k+1) - \tilde{E}_y^{n}(i,k+1)}{\Delta z} \tag{3.7}$$

$$\tilde{H}_y^{n+\frac{1}{2}}(i+\tfrac{1}{2},k+\tfrac{1}{2}) = \tilde{H}_y^{n-\frac{1}{2}}(i+\tfrac{1}{2},z) - \frac{\Delta t}{\mu}\frac{\tilde{E}_x^{n}(i+\frac{1}{2},k+1) - \tilde{E}_x^{n}(i+\frac{1}{2},k)}{\Delta z} + \frac{\Delta t}{\mu}\frac{\tilde{E}_z^{n}(i+1,k+\frac{1}{2}) - \tilde{E}_z^{n}(i,k+\frac{1}{2})}{\Delta x} \tag{3.8}$$

$$\tilde{H}_z^{n+\frac{1}{2}}(i+\tfrac{1}{2},k) = \tilde{H}_z^{n-\frac{1}{2}}(i+\tfrac{1}{2},k) + \frac{\Delta t}{\mu}\frac{n\pi}{b}\tilde{E}_x^{n}(i+\tfrac{1}{2},k) - \frac{\Delta t}{\mu}\frac{\tilde{E}_y^{n}(i+1,k) - \tilde{E}_y^{n}(i,k)}{\Delta x} \tag{3.9}$$

The grid positions and field components for the 2D FDTD method is shown in Figure 3.1.

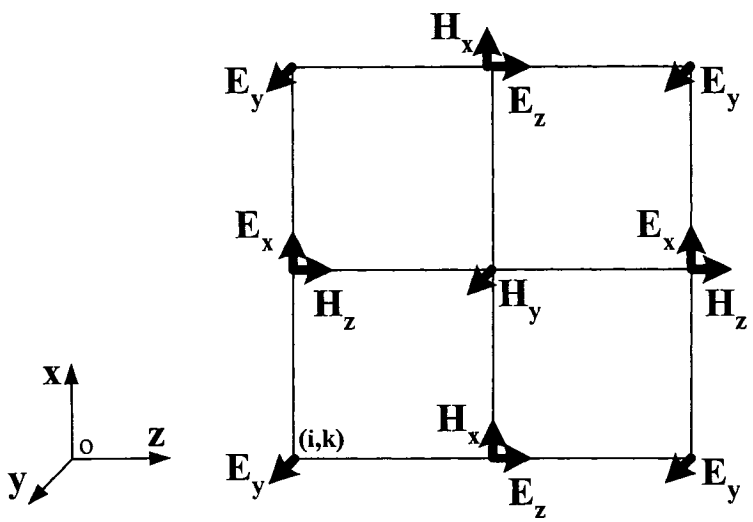

Figure 3.1 The electric and magnetic fields positions in a unit cell of the compact 2D FDTD grid.

Equations (3.4) - (3.9) are two-dimensional and easy to program. In the following sections, two numerical examples are given to show the efficiency of this new method.

3.3 Numerical Validation

To validate the proposed method, we first apply it to a rectangular waveguide cavity with length d=0.04m in the z direction, width a=0.03m in the x direction, and height b=0.02m in the y direction (which is assumed to be the geometry uniform direction). The analytical resonant frequencies were documented in [117]. The cavity structure is shown in Figure 3.2 and the numerical grid plane is in the x-z plane.

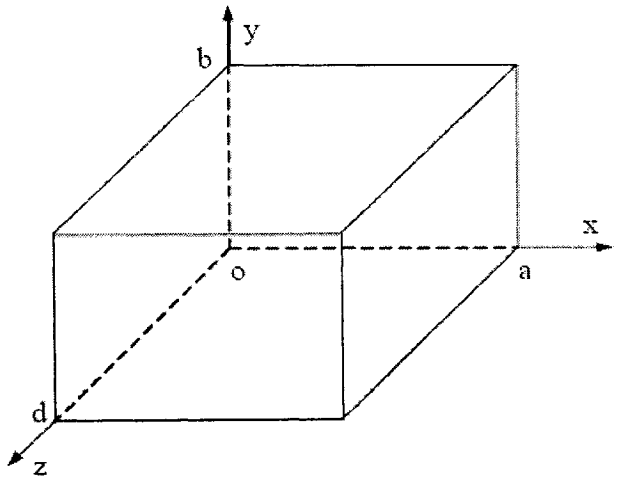

Figure 3.2 The rectangular waveguide cavity of length d=0.04m in the z direction, width a=0.03m in the x direction, and height b=0.02m in the y direction.

In order to facilitate the comparisons, a reference 3D FDTD simulation is also run for the same cavity structure. The mesh sizes with both the proposed method and the reference method are taken to be the same: Δx=0.001m, Δy=0.001m, and Δz=0.001m. The time step size is $\Delta t=\Delta t_{CFL}=1.9245\times10^{-12}s$, and the Δt_{CFL} is the CFL time step limit computed for the conventional 3D FDTD. The total number of iterations taken is 8192. The source for 2D FDTD is a point source with E_z and H_z. The source for 3D FDTD is a line source with E_z that varies as $\sin(\pi y/b)$ along y direction (for TM_z mode), and with H_z that varies as $\cos(\pi y/b)$ along the y direction (for TE_z mode). The source in the time-domain is two pulses, which are equal to 1 at time step 1 and equal to -1 at time step 2. There are two

reasons to select this kind of source: one is that it is easy to be implemented, the other is that it includes all the possible frequencies needed. H_y and E_y are recorded and Fourier-transformed to obtain the resonant frequencies by identifying the amplitude peak points.

Table 3-1 shows the analytical resonant frequency of the first five modes of T_1 and the relative errors of numerical results computed with the proposed 2D FDTD and the reference 3D FDTD methods.

Table 3-1 The comparison between numerically computed and analytical resonant frequencies

The resonant modes	Analytical results	errors with the proposed method	errors with the reference FDTD
TE_{011}	8.3853GHz	-0.15%	-0.15%
TM_{110}	9.0139GHz	-0.08%	-0.08%
TE_{111}/TM_{111}	9.7628GHz	0.06%	0.06%
TE_{012}	10.607GHz	-0.13%	-0.13%
TE_{112}/TM_{112}	11.726GHz	0.07%	0.07%

Table 3-2 shows the respective memory and CPU time used with the 2D FDTD and the 3D FDTD for the first example. The running platform is the Matlab on a laptop Pentium-IV PC with 1.8-GHz CPU and 512-MB RAM.

Table 3-2 The memory and CPU time needed for the 2D FDTD and 3D FDTD corresponding to the first example

	The reference 3D FDTD	The Proposed Method
Memory	1507KB	316KB
CPU time	399s	9s

It can be seen from Table 3-1 that the proposed method yields almost the same results as those with the reference 3D FDTD method. However, the proposed 2D FDTD method uses about 1/44 of the CPU time (including FFT) of the reference 3D FDTD and about 1/5 of the memory (including FFT) of the reference 3D FDTD.

The second example is to validate the discontinuity in a waveguide structure. It is a rectangular waveguide cavity of the same size as the previous example but with a groove in the middle of the z direction as shown in Figure 3.3. The width of the groove is 0.006m and the depth is 0.01m.

The mesh size, the time step size, and the source are the same as in the first example. The total number of iterations is 16384. H_y and E_y are again recorded and Fourier

transformed to obtain the resonant frequencies by identifying the amplitude peak points. Table 3-3 shows the values of resonant frequency of the first five modes of T_1 computed by the proposed 2D FDTD and the reference 3D FDTD methods. Table 3-4 shows the computation resources used with the two methods.

Once again, it can be seen from Table 3-3 that the proposed method gives almost the same results as the reference 3D FDTD. However, the proposed 2D FDTD method uses about 1/42 of the CPU time (including FFT) of the reference 3D FDTD and about 1/3 of the memory (including FFT) of the reference 3D FDTD.

Table 3-3 The comparison of resonant frequencies obtained by 2D FDTD and the 3D FDTD in the second example

	The reference 3D FDTD	The Proposed Method
Mode 1	8.0873GHz	8.0873GHz
Mode 2	9.0387GHz	9.0387GHz
Mode 3	9.4827GHz	9.4827GHz
Mode 4	10.720GHz	10.720GHz
Mode 5	11.988GHz	11.988GHz

Table 3-4 The memory and CPU time needed for the 2D FDTD and 3D FDTD in the second example

	The reference 3D FDTD	The Proposed Method
Memory	1763KB	572KB
CPU time	786.5s	18.8s

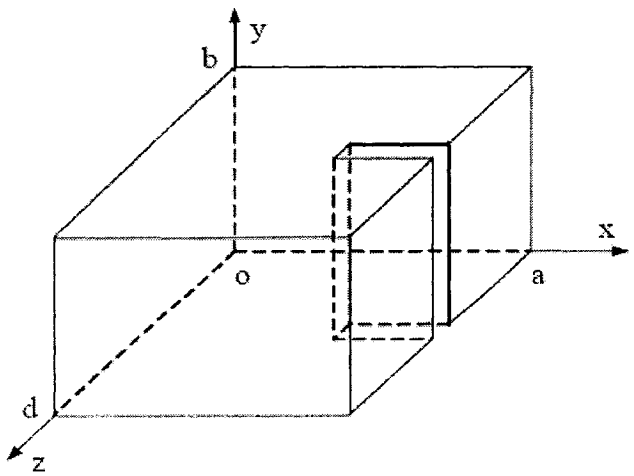

Figure 3.3 The rectangular waveguide cavity with a groove in the middle of the z direction.

3.4 Discussion and Conclusion

In this chapter, a new compact 2D FDTD method for 3D waveguide problems has been proposed. Numerical examples presented in this chapter show that this method has the same accuracy as the traditional 3D FDTD method, but with much less memory requirements and CPU time. Nevertheless, it should be noted that the numerical analysis is not a theoretical one; more comprehensive analytical studies are needed on the exact stability condition and numerical dispersion relationship of the proposed compact 2D FDTD. In addition, further applications to complicated waveguide structures are needed. These will be left for future work.

4 Compact 1D FDTD Method for Waveguide Structures

4.1 Introduction

When using the FDTD method to compute waveguide structures, two things are often needed: a known incident wave for calculating electrical parameters (e.g., scattering parameters) and effective absorbing boundary conditions for terminating open structures. To obtain an incident wave, a separate simulation of a long waveguide structure is usually run [73]. However, for a three-dimensional (3D) structure, such a simulation is often inefficient because it requires a large amount of memory and CPU time. In order to solve the problems as well as to develop efficient absorbing boundary conditions, many one-dimensional (1D) methods have been proposed [74]-[81]. Most of them use analytically or semi-analytically generated Green's functions. However, these analytical continuous Green's functions often have characteristics quite different from those of the 3D FDTD formulations of a discrete domain, for instance, at the cut-off frequencies. Consequently, they do not offer highly accurate results, for instance, near or below the cut-off frequency of a waveguide mode.

To solve the problem, we propose a new simple 1D FDTD method in this chapter. Unlike other methods developed so far, this method is derived directly from the FDTD formulae; therefore, it has the same numerical characteristics as that of the 3D FDTD method with which it interfaces. As a result, it not only allows efficient computation of an incident wave due to its 1D nature, but it also enables an extremely high absorption of numerical incident waves (e.g. better than -200dB even at or below a cut-off frequency).

This chapter is organized as follows. Section 4.2 presents the derivation of the proposed 1D method, while Section 4.3 illustrates the dispersion analysis of the proposed method. Section, 4.4 describes the two applications of the proposed method: generation of the incident wave and absorption of waves. Section 4.5 sets forth the numerical results that demonstrate the validity and effectiveness of the proposed technique. Further discussion and conclusions relating to the proposed method follow in Section 4.6.

4.2 Formula of the Proposed 1D FDTD Method

For linear and lossless medium, the conventional 3D FDTD formulae can be written as:

$$\begin{aligned} E_x\big|_{i-\frac{1}{2},j,k}^{n+1} &= E_x\big|_{i-\frac{1}{2},j,k}^{n} \\ &+\frac{\Delta t}{\varepsilon\Delta y}\left(H_z\big|_{i-\frac{1}{2},j+\frac{1}{2},k}^{n+\frac{1}{2}} - H_z\big|_{i-\frac{1}{2},j-\frac{1}{2},k}^{n+\frac{1}{2}}\right) \\ &-\frac{\Delta t}{\varepsilon\Delta z}\left(H_y\big|_{i-\frac{1}{2},j,k+\frac{1}{2}}^{n+\frac{1}{2}} - H_y\big|_{i-\frac{1}{2},j,k-\frac{1}{2}}^{n+\frac{1}{2}}\right) \end{aligned} \tag{4.1}$$

$$\begin{aligned} H_y\big|_{i-\frac{1}{2},j,k-\frac{1}{2}}^{n+\frac{1}{2}} &= H_y\big|_{i-\frac{1}{2},j,k-\frac{1}{2}}^{n-\frac{1}{2}} \\ &+\frac{\Delta t}{\mu\Delta x}\left(E_z\big|_{i,j,k-\frac{1}{2}}^{n} - E_z''\big|_{i-1,j,k-\frac{1}{2}}^{n}\right) \\ &-\frac{\Delta t}{\mu\Delta z}\left(E_x''\big|_{i-\frac{1}{2},j,k}^{n} - E_x''\big|_{i-\frac{1}{2},j,k-1}^{n}\right) \end{aligned} \tag{4.2}$$

The equations for the other field components can be expressed similarly.

For a homogeneously filled waveguide, field distribution pattern of a given mode on a cross-section do not change with time or frequency or with the longitudinal coordinate. They can be found analytically or numerically (e.g. [71][72]). Supposing that the mode is traveling in the z-direction and Yee's grid is applied as shown in Figure 4.1, the discretized form of equations (4.1) - (4.2) can then be rewritten as:

$$\begin{aligned} E_x\big|_{i-\frac{1}{2},j,k}^{n+1} &= E_x\big|_{i-\frac{1}{2},j,k}^{n} \\ &+\frac{\Delta t}{\varepsilon\Delta y}\left(\alpha_{zy}\big|_{i-\frac{1}{2},j-\frac{1}{2}} - 1\right)H_z\big|_{i-\frac{1}{2},j-\frac{1}{2},k}^{n+\frac{1}{2}} \\ &-\frac{\Delta t}{\varepsilon\Delta z}\left(H_y\big|_{i-\frac{1}{2},j,k+\frac{1}{2}}^{n+\frac{1}{2}} - H_y\big|_{i-\frac{1}{2},j,k-\frac{1}{2}}^{n+\frac{1}{2}}\right) \end{aligned} \tag{4.3}$$

$$\begin{aligned} H_y\big|_{i-\frac{1}{2},j,k-\frac{1}{2}}^{n+\frac{1}{2}} &= H_y\big|_{i-\frac{1}{2},j-\frac{1}{2},k-\frac{1}{2}}^{n-\frac{1}{2}} \\ &+\frac{\Delta t}{\mu\Delta x}\left(1-\beta_{zx}\big|_{i,j}\right)E_z\big|_{i,j,k-\frac{1}{2}}^{n} \\ &-\frac{\Delta t}{\mu\Delta z}\left(E_x\big|_{i-\frac{1}{2},j,k}^{n} - E_x\big|_{i-\frac{1}{2},j,k-1}^{n}\right) \end{aligned} \tag{4.4}$$

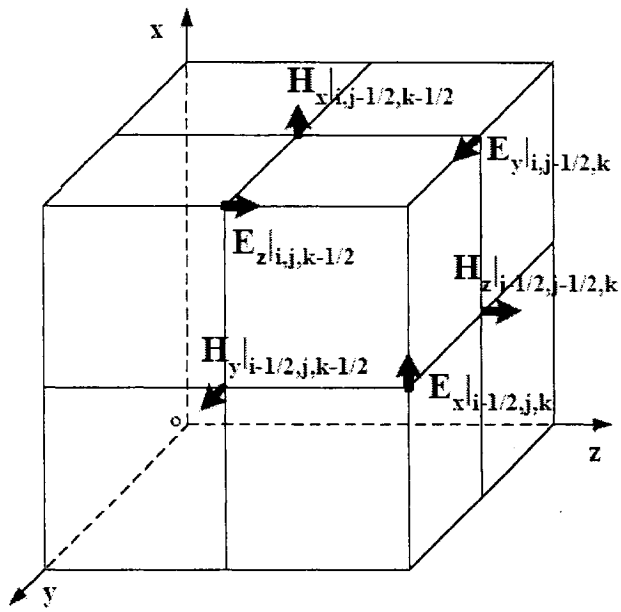

Figure 4.1 The electric and magnetic field positions in Yee's lattice for a waveguide structure, with Z the wave propagation direction.

The equations for other field components can be written similarly as follows:

$$E_y\Big|_{i,j-\frac{1}{2},k}^{n+1} = E_y\Big|_{i,j-\frac{1}{2},k}^{n} + \frac{\Delta t}{\varepsilon \Delta z}\left(H_x\Big|_{i,j-\frac{1}{2},k+\frac{1}{2}}^{n+\frac{1}{2}} - H_x\Big|_{i,j-\frac{1}{2},k-\frac{1}{2}}^{n+\frac{1}{2}}\right) - \frac{\Delta t}{\varepsilon \Delta x}\left(\alpha_{zx}\Big|_{i-\frac{1}{2},j-\frac{1}{2}} - 1\right) H_z\Big|_{i-\frac{1}{2},j-\frac{1}{2},k}^{n+\frac{1}{2}} \tag{4.5}$$

$$E_z\Big|_{i,j,k-\frac{1}{2}}^{n+1} = E_z\Big|_{i,j\frac{1}{2},k-\frac{1}{2}}^{n} + \frac{\Delta t}{\varepsilon \Delta x}\left(\alpha_{yx}\Big|_{i-\frac{1}{2},j} - 1\right) H_y\Big|_{i-\frac{1}{2},j,k-\frac{1}{2}}^{n+\frac{1}{2}} - \frac{\Delta t}{\varepsilon \Delta y}\left(\alpha_{xy}\Big|_{i,j-\frac{1}{2}} - 1\right) H_x\Big|_{i,j-\frac{1}{2},k-\frac{1}{2}}^{n+\frac{1}{2}} \tag{4.6}$$

$$H_x\Big|_{i,j-\frac{1}{2},k-\frac{1}{2}}^{n+\frac{1}{2}} = H_x\Big|_{i,j-\frac{1}{2},k-\frac{1}{2}}^{n-\frac{1}{2}} + \frac{\Delta t}{\mu \Delta z}\left(E_y\Big|_{i,j-\frac{1}{2},k}^{n} - E_y\Big|_{i,j-\frac{1}{2},k-1}^{n}\right) - \frac{\Delta t}{\mu \Delta y}\left(1 - \beta_{zy}\Big|_{i,j}\right) E_z\Big|_{i,j,k-\frac{1}{2}}^{n} \tag{4.7}$$

$$H_z\Big|_{i-\frac{1}{2},j-\frac{1}{2},k}^{n+\frac{1}{2}} = H_z\Big|_{i-\frac{1}{2},j-\frac{1}{2},k}^{n-\frac{1}{2}} + \frac{\Delta t}{\mu\Delta y}(1-\beta_{xy}\Big|_{i-\frac{1}{2},j})E_x\Big|_{i-\frac{1}{2},j,k}^{n} - \frac{\Delta t}{\mu\Delta x}(1-\beta_{yx}\Big|_{i,j-\frac{1}{2}})E_y\Big|_{i,j-\frac{1}{2},k}^{n} \tag{4.8}$$

where

$$\alpha_{zy}\Big|_{i-\frac{1}{2},j-\frac{1}{2}} = \frac{H_z\Big|_{i-\frac{1}{2},j+\frac{1}{2},k}^{n+\frac{1}{2}}}{H_z\Big|_{i-\frac{1}{2},j-\frac{1}{2},k}^{n+\frac{1}{2}}} \tag{4.9}$$

$$\alpha_{zx}\Big|_{i-\frac{1}{2},j-\frac{1}{2}} = \frac{H_z\Big|_{i+\frac{1}{2},j-\frac{1}{2},k}^{n+\frac{1}{2}}}{H_z\Big|_{i-\frac{1}{2},j-\frac{1}{2},k}^{n+\frac{1}{2}}} \tag{4.10}$$

$$\alpha_{yx}\Big|_{i-\frac{1}{2},j} = \frac{H_y\Big|_{i+\frac{1}{2},j,k-\frac{1}{2}}^{n+\frac{1}{2}}}{H_y\Big|_{i-\frac{1}{2},j,k-\frac{1}{2}}^{n+\frac{1}{2}}} \tag{4.11}$$

$$\alpha_{xy}\Big|_{i,j-\frac{1}{2}} = \frac{H_x\Big|_{i,j+\frac{1}{2},k-\frac{1}{2}}^{n+\frac{1}{2}}}{H_x\Big|_{i,j-\frac{1}{2},k-\frac{1}{2}}^{n+\frac{1}{2}}} \tag{4.12}$$

$$\beta_{zy}\Big|_{i,j} = \frac{E_z\Big|_{i,j-1,k-\frac{1}{2}}^{n}}{E_z\Big|_{i,j,k-\frac{1}{2}}^{n}} \tag{4.13}$$

$$\beta_{zx}\Big|_{i,j} = \frac{E_z\Big|_{i-1,j,k-\frac{1}{2}}^{n}}{E_z\Big|_{i,j,k-\frac{1}{2}}^{n}} \tag{4.14}$$

$$\beta_{xy}\Big|_{i-\frac{1}{2},j} = \frac{E_x\Big|_{i-\frac{1}{2},j-1,k}^{n}}{E_x\Big|_{i-\frac{1}{2},j,k}^{n}} \tag{4.15}$$

$$\beta_{yx}\Big|_{i,j-\frac{1}{2}} = \frac{E_y\Big|_{i-1,j-\frac{1}{2},k}^{n}}{E_y\Big|_{i,j-\frac{1}{2},k}^{n}} \tag{4.16}$$

Coefficients α and β are ratios of field quantities on the nodes of a cross section of the waveguide. They are constant and can be found from the known unchanged field distributions of a given mode. Each mode has its own set of coefficients α and β . Note that in computing α and β , one should choose non-zero field points for the denominators in equations (4.9) - (4.16) for a given mode.

Careful examination of the equations reveals that equations (4.3) - (4.8) are essentially 1D FDTD recursive formulae. Computations need to be carried out only along the z-direction (or the k-direction) with the specified i and j for each mode. At any other i and j, the field quantities can be obtained from the known field distributions on the same cross section.

4.3 Numerical Dispersion of the Proposed Method

In order to compare the numerical dispersion of the proposed method with the conventional FDTD method, we consider the TE_{mn} mode in a rectangular waveguide as an example. For the TM_{mn} mode, a similar analysis can be made and similar conclusions reached.

Suppose the rectangular waveguide has width a in x direction and height b in y direction. The field components for the TE_{mn} mode along z-direction can be written as:

$$\begin{aligned}
E_x &= E_{x0}\cos(k_x x)\sin(k_y y)e^{j(k_z z-\omega t)} \\
E_y &= E_{y0}\sin(k_x x)\cos(k_y y)e^{j(k_z z-\omega t)} \\
E_z &= 0 \\
H_x &= H_{x0}\sin(k_x x)\cos(k_y y)e^{j(k_z z-\omega t)} \\
H_y &= H_{y0}\cos(k_x x)\sin(k_y y)e^{j(k_z z-\omega t)} \\
H_z &= H_{z0}\cos(k_x x)\cos(k_y y)e^{j(k_z z-\omega t)}
\end{aligned} \tag{4.17}$$

where $k_x = \frac{m\pi}{a}$, $k_y = \frac{n\pi}{b}$, k_z is the spatial frequency in the z direction, and ω is the temporal angular frequency.

Substituting (4.17) into (4.3) - (4.8), we obtain:

$$\begin{aligned}
&\frac{j}{\Delta t}\sin(\frac{\omega\Delta t}{2})E_{x0} - \frac{1}{\varepsilon\Delta y}\sin(\frac{k_y\Delta y}{2})H_{z0} \\
&\qquad - \frac{j}{\varepsilon\Delta z}\sin(\frac{k_z\Delta z}{2})H_{y0} = 0
\end{aligned} \tag{4.18}$$

$$\begin{aligned}
&\frac{j}{\Delta t}\sin(\frac{\omega\Delta t}{2})E_{y0} + \frac{j}{\varepsilon\Delta z}\sin(\frac{k_z\Delta z}{2})H_{x0} \\
&\qquad + \frac{1}{\varepsilon\Delta x}\sin(\frac{k_x\Delta x}{2})H_{z0} = 0
\end{aligned} \tag{4.19}$$

$$\frac{1}{\mu\Delta z}\sin(\frac{k_z\Delta z}{2})E_{y0}+\frac{1}{\Delta t}\sin(\frac{\omega\Delta t}{2})H_{x0}=0 \tag{4.20}$$

$$\frac{1}{\mu\Delta z}\sin(\frac{k_z\Delta z}{2})E_{x0}-\frac{1}{\Delta t}\sin(\frac{\omega\Delta t}{2})H_{y0}=0 \tag{4.21}$$

$$\frac{1}{\mu\Delta y}\sin(\frac{k_y\Delta y}{2})E_{x0}-\frac{1}{\mu\Delta x}\sin(\frac{k_x\Delta x}{2})E_{y0}+\frac{j}{\Delta t}\sin(\frac{\omega\Delta t}{2})H_{z0}=0 \tag{4.22}$$

The above equations form a system of five homogeneous equations with unknowns E_{x0}, E_{y0}, H_{x0}, H_{y0}, and H_{z0}. Because the solutions of the system must be nontrivial, the determinant of its coefficient matrix should be equal to zero. This leads to:

$$\sin(\frac{\omega\Delta t}{2})=0 \tag{4.23}$$

$$\frac{\sin^2(\frac{k_z\Delta z}{2})}{\Delta z^2}=\frac{\mu\varepsilon\sin^2(\frac{\omega\Delta t}{2})}{\Delta t^2} \tag{4.24}$$

$$\frac{\sin^2(\frac{k_x\Delta x}{2})}{\Delta x^2}+\frac{\sin^2(\frac{k_y\Delta y}{2})}{\Delta y^2}+\frac{\sin^2(\frac{k_z\Delta z}{2})}{\Delta z^2}=\frac{\mu\varepsilon\sin^2(\frac{\omega\Delta t}{2})}{\Delta t^2} \tag{4.25}$$

where $k_x=\frac{m\pi}{a}$ and $k_y=\frac{n\pi}{b}$.

Equation (4.23) corresponds to $\omega=0$, and represents the static solution. Equation (4.24) will lead to $H_{z0}=0$, which does not agree with the assumption of TE modes. Therefore, the remaining equation (4.25) is the numerical dispersion relationship of the TE modes. More details on the numerical dispersion relationship can be found in Appendix A.

It is obvious that equation (4.25) is the same as the numerical dispersion relationship of the 3D FDTD method [55] for TE_{mn} mode with $k_x=\frac{m\pi}{a}$ and $k_y=\frac{n\pi}{b}$.

To verify the above claim numerically, we considered a rectangular waveguide with width a=0.02m in x direction, height b=0.01m in y direction and z was the wave traveling direction. The mesh size was Δx=0.001m, Δy=0.001m, and Δz=0.001m for the 3D FDTD mesh that discretizes the waveguide. The time step size was taken as $\Delta t=\Delta t_{max}$ where

Δt_{max} is the CFL time step limit of the 3D FDTD formulae. TE_{10} mode was excited with a modulated Gaussian pulse $\sin(2\pi f_0 t)e^{-(t-t_0)^2/T^2}$ in the center of the structure. Parameter T equaled $20\Delta t$, t_0 equaled $60\Delta t$, f_0 equaled 60.465GHz and the corresponding wavelength λ_g in the waveguide was about $5\Delta z = 0.005m$. The recording point was $300\Delta z$ or $60\lambda_g$ away from the source plane. Such a long distance between the source and the field recording point allows us to observe effects of the numerical dispersion on the field solutions. Figure 4.2 shows the E_ys computed with the 3D FDTD and the proposed 1D FDTD. The difference of the two E_ys computed with the 3D FDTD and the proposed 1D FDTD is shown in Figure 4.3.

As can be seen, two E_ys overlap completely. The maximum difference between the two E_ys is less than 2×10^{-15}(V/m), whereas the maximum field value is around 0.5 (V/m). Such small differences suggest that they are due to computer rounding-off errors. Note that the selection of the specified *i* and *j* in equations (4.3) - (4.8) has very little effect on the error level. These verify experimentally the claim we had before: the numerical dispersion relationship of the proposed 1D FDTD is the same as that of the original 3D FDTD.

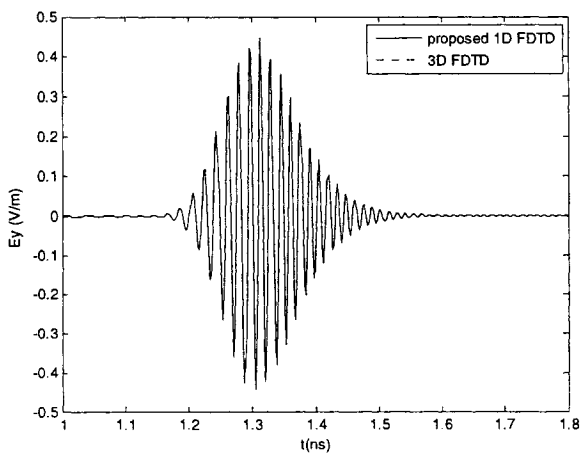

Figure 4.2 The E_y recorded at a point $300\Delta z$ or $60\lambda_g$ away from the source plane.

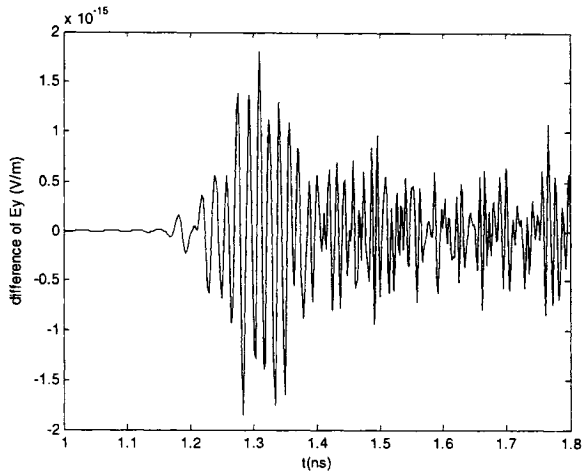

Figure 4.3 The difference between the two E_ys produced by the 1D FDTD and the reference 3D FDTD.

4.4 Applications of the Proposed Method

The proposed method as represented by equations (4.3) - (4.8) have two major applications in simulating a waveguide structure: to efficiently generate numerical incident waves that are required for computing electrical parameters such as scattering parameters and to serve as a wideband absorbing boundary that is computed only in one dimension.

Efficient generation of an incident wave

Because of its 1D nature, the proposed method can be used to obtain an incident wave by computing a long waveguide structure; the waveguide is long enough that the wave reflected by any imperfect termination at the ends cannot return to the measurement point and contaminate the incident wave [73]. In the numerical example presented in Section 4.5, the incident wave obtained with the proposed method is found to be fundamentally the same as that obtained using the conventional 3D FDTD method; the differences was less than -200dB. In other words, the proposed method can produce an incident wave for all intents and purposes identical to that obtained with the conventional 3D FDTD. This stems from the fact that the proposed 1D method is derived from the 3D FDTD method and therefore has the same numerical characteristics as that of the 3D FDTD method, as proven before.

Absorbing boundary condition

Since the proposed method can easily simulate a long waveguide structure, it can also be used to terminate a waveguide structure as illustrated in Figure 4.4. In Figure 4.4, a waveguide is connected to a discontinuity where both of them are modeled using the conventional 3D FDTD grid. The waveguide is then terminated with the absorbing boundary that is modeled using the proposed 1D FDTD method. Field components $E_x|_{i-\frac{1}{2},j,k-1}$ and $E_y|_{i,j-\frac{1}{2},k-1}$ are used to pass the field values from the 3D FDTD grid into the proposed 1D FDTD grid, while field components $E_y|_{i,j-\frac{1}{2},k}$ and $E_x|_{i-\frac{1}{2},j,k}$ are used to pass the field values in the proposed 1D FDTD grid into the 3D FDTD grid.

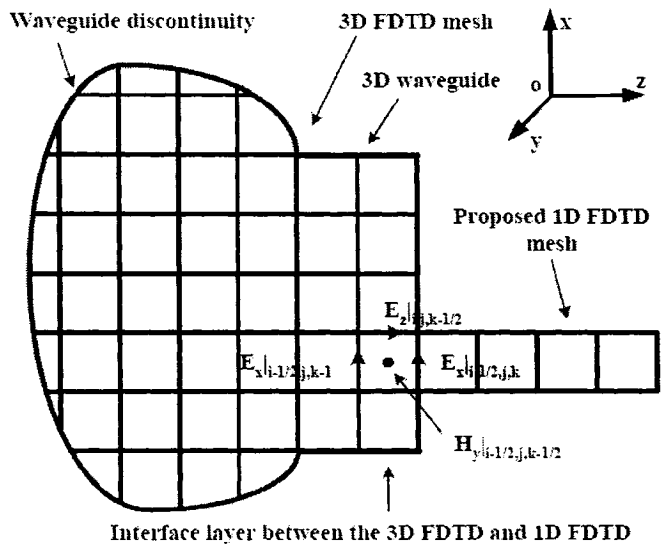

Figure 4.4 The proposed absorbing termination using the 1D FDTD mesh [76][77].

Multi-modes generally exist in the waveguide. However, equations (4.3) - (4.8) are valid only for a single mode. To solve the problem, each mode has to be extracted at the interface between the 3D FDTD mesh and the proposed 1D FDTD mesh. The mode extraction can be performed using the orthogonality of modes as described in [76][77]. Figure 4.5 illustrates such extraction operations. For the computation of the total field value in the 3D FDTD from the known mode field values obtained by the 1D FDTD, it just needs to add the field values of different mode together. The 3D field values of each

mode can be obtained by the 1D FDTD field values and the field distribution pattern of this mode.

In Figure 4.5, each mode corresponds to an independent 1D FDTD mesh line. The positioning of the 1D FDTD mesh lines, i.e. the specific values of i and j in (4.3) - (4.8), can be the same or can be different. The requirement for the positioning of each 1D FDTD mesh line is that it should not be at the null field points of the mode it simulates.

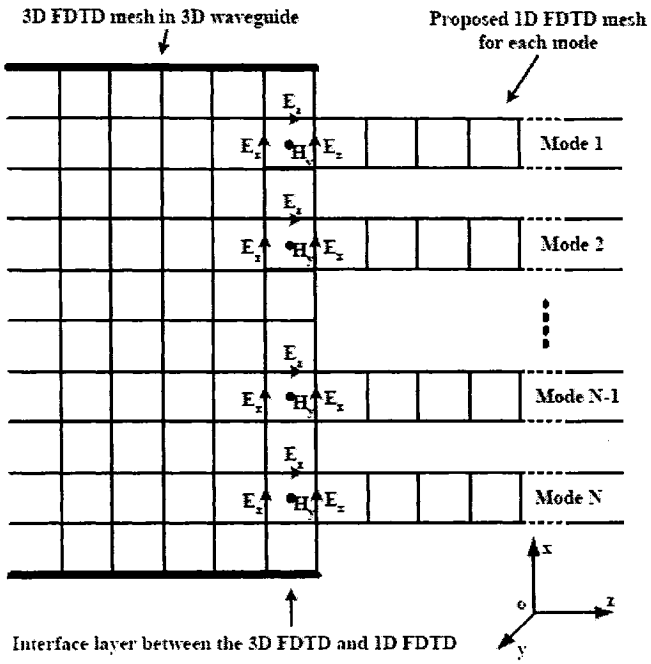

Figure 4.5 The mode extraction and combination diagram at the interface between the waveguide and the 1D FDTD absorbing termination [76][77].

In the numerical example presented in Section 4.5, it is shown that the proposed termination provides an absorption of better than -200dB even at or below the cut-off frequencies in both the single and multi mode case.

4.5 Numerical Examples

We considered again the same waveguide as that used in Section 4.3: a rectangular waveguide with width a=0.02m in x direction, height b=0.01m in the y direction and z as

the wave propagating direction. The mesh size is Δx=0.001m, Δy=0.001m, and Δz=0.001m. The time step size is taken as $\Delta t=\Delta t_{max}$. The total number of the iterations is 4096 (which amounts to 7.8808ns of the real time). The source used in the FDTD simulation is the Dirac impulse function $\delta(n)$. Matlab was used to program the methods and the simulations were run on a laptop Pentium-IV PC with 1.8-GHz CPU and 512-MB RAM.

For the first application, we computed the incident waves for TE_{11} mode. The waveguide is long enough to ensure there is no reflection from the far end to the recording points. The time-domain signatures of E_y, obtained with a reference full-wave 3D FDTD simulation and the proposed 1D FDTD simulation, were recorded at a point $1\Delta z$ away from the source plane. The result are shown in Figure 4.6 (for clarity, only first 0.5ns is shown). It can be seen that they overlap completely. The corresponding frequency-domain relative errors of the incident waves, obtained by the proposed 1D FDTD simulation compared with the results obtained by the reference full-wave 3D FDTD simulation, is shown in Figure 4.7. The maximum relative error in the frequency-domain is less than -200dB, which is due to computer rounding-off errors.

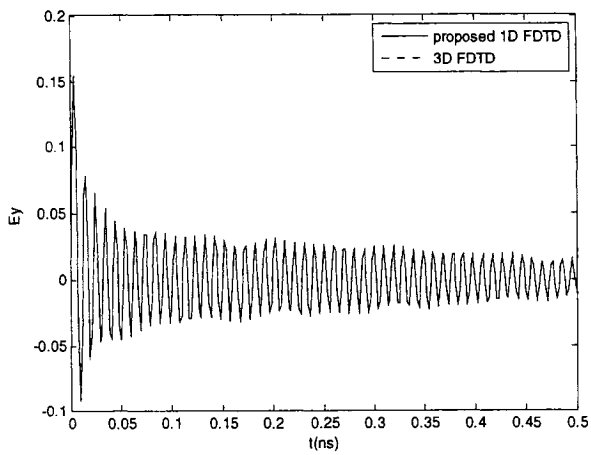

Figure 4.6 The E_y values of the first 0.5 ns recorded at a point $1\Delta z$ away from the source.

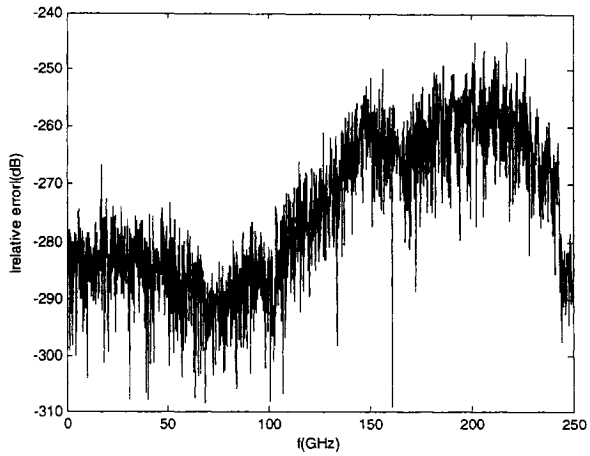

Figure 4.7 The relative errors of E_y at a point $1\Delta z$ away from the source obtained by the proposed 1D FDTD.

Table 4-1 shows the computational expenditures used for a waveguide of length 206.8cm, which was the waveguide length used in all the numerical examples. It is long enough to ensure the reflection from the far end would not reach the interface of 1D and 3D regions during the simulation time. As can be seen, the memory used by the proposed 1D method is about 0.6% of that used by the 3D FDTD, while CPU time is about 0.23%. The proposed method, therefore, saves significant amounts of memory and CPU time usage.

Table 4-1 The memory and CPU time used by the proposed 1D method and the referenced 3D FDTD method

	The reference 3D FDTD	The Proposed 1D FDTD
Memory	2334KB	14KB
CPU time	4271s	9.9s

For the second application, we used the proposed method as the absorbing boundaries to terminate the rectangular waveguides at both ends. We then measured the effectiveness of the absorption. The source was placed $2\Delta z$ away from the absorbing boundary and the E_y was recorded at a point $1\Delta z$ away for the computation of the reflection coefficient. Such placements of the source and recording points allow us to measure the absorption of evanescent modes by the absorbing boundary. The reflection

coefficient Γ caused by the 1D FDTD termination was calculated using the following formula:

$$|\Gamma| = 20\log\left|\frac{E_y - E_y^{ref}}{E_y^{ref}}\right| \text{ (dB)} \qquad (4.26)$$

where E_y^{ref} is the incident wave and obtained with a separate reference simulation where a long waveguide had been computed with the conventional full-wave 3D FDTD method.

Figure 4.8 illustrates the calculated reflection coefficient when only the single dominant mode TE_{11} was excited in the rectangular waveguide, while Figure 4.9 shows the calculated reflection coefficient when only the mode TE_{84} was excited. Figure 4.10 shows the calculated reflection coefficient when multi-modes of TE_{10}, TE_{20}, TE_{30}, TE_{40}, TE_{11}, TE_{21}, TE_{31}, and TE_{41} were excited simultaneously with equal magnitude (the worst case in which multiple modes exist).

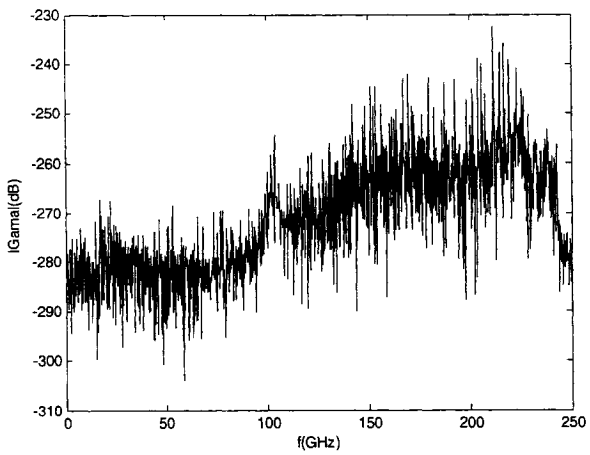

Figure 4.8 The reflection coefficient from 1D FDTD termination for TE_{11} mode.

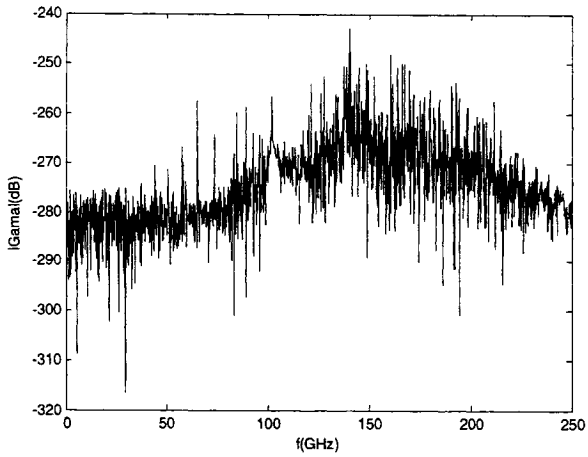

Figure 4.9 The reflection coefficient from 1D FDTD termination for TE_{84} mode.

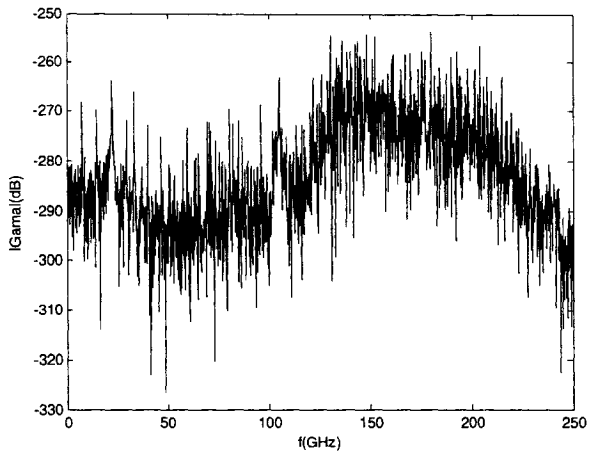

Figure 4.10 The reflection coefficient from 1D FDTD termination for multi-mode case.

It can be seen from Figure 4.8 to Figure 4.10 that the proposed 1D FDTD method provides almost perfect absorbing terminating conditions in the entire frequency spectrum from DC to 250GHz. In all the cases, the absorptions are better than -200dB even at or below the cut-off frequencies (the cut-off frequency of TE_{10} is 7.5GHz and the cut-off frequency of TE_{84} is 84.85GHz).

It should be noted that in the above numerical experiments the numbers of modes excited were chosen arbitrarily to test the performance of the proposed method. In solving a realistic structure, the number of modes to be considered can be decided in the

same manner as that employed in the mode matching techniques or in the techniques described in [74][75][77][81][73][118][119].

4.6 Discussion and Conclusion

In this chapter, a new compact 1D FDTD method for uniformly filled waveguide structures has been proposed. It has the same numerical characteristics as the conventional 3D FDTD method. Therefore, it can be used to either efficiently generate an incident wave or to effectively serve as a perfect absorbing termination for specified mode. The errors or the reflections with the proposed method were found to be extremely small, less than -200dB even at or below the cut-off frequencies. In addition, despite such a high degree of effectiveness, the programming of the proposed method is very easy and little analytical pre-processing is required.

5 FDTD-Based Modal PML

5.1 Introduction

For an unbounded structure, an absorbing boundary condition is necessary to reduce the size of the simulation domain and thus, the CPU time. PML is a very efficient and flexible absorbing boundary condition, and it can be used for full open problems or waveguide problems. The PML scheme was initially proposed by Berenger in 1994 as an electromagnetic absorbing boundary condition [50]. Since then, other variations of the PML have been developed and proven to be very effective [82]-[84]. In particular, the complex-frequency-shifted (CFS) PML was shown to be effective for arbitrary media [84]. In terminating waveguide structures, modal PMLs were proposed, which reduce 3D PML operations or 2D PML operations to 1D PML operations [85][86]. They save significant amounts of computational memory and CPU time. However, these modal PML formulae are not derived directly from conventional FDTD grids and therefore have numerical dispersion characteristics different from those of the FDTD. As a result, when connected with a FDTD grid, they do not perform as well as the original 3D PML. Based on the 1D FDTD formulae in chapter 4, a new 1D modal PML scheme is proposed in this chapter that has almost the same absorption performance as the original PML for single mode situations.

5.2 Derivation of the Proposed 1D Modal PML

For a homogeneously filled waveguide, field distributions (modal solutions) of a given mode on the cross-section do not change and can be found analytically or numerically. Using this information, a 1D FDTD scheme is obtained for modeling the waveguide in chapter 4. This idea can be similarly applied to the PML formulae.

Now, consider a waveguide with z-direction as the wave traveling direction and the CFS-PML scheme described in [84] with $S_x = 1$, $S_y = 1$, and $S_z = \kappa_z + \frac{\sigma_z}{\alpha_z + j\omega\varepsilon_0}$. Hers S_x, S_y and S_z are the stretched coordinate and α_z is a damping factor that can be optimized for better absorption performance for a specific mode. For simplicity, E_x is considered here.

The updating formula of E_x in CFS-PML is described in equation (5.1) and (5.2):

$$P_x\Big|_{i-\frac{1}{2},j,k}^{n+1} = P_x\Big|_{i-\frac{1}{2},j,k}^{n} + \frac{\Delta t}{\varepsilon \Delta y}\left(H_z\Big|_{i-\frac{1}{2},j+\frac{1}{2},k}^{n+1/2} - H_z\Big|_{i-\frac{1}{2},j-\frac{1}{2},k}^{n+1/2}\right) - \frac{\Delta t}{\varepsilon \Delta z}\left(H_y\Big|_{i-\frac{1}{2},j,k+\frac{1}{2}}^{n+1/2} - H_y\Big|_{i-\frac{1}{2},j,k-\frac{1}{2}}^{n+1/2}\right) \tag{5.1}$$

$$E_x\Big|_{i-\frac{1}{2},j,k}^{n+1} = \frac{\frac{\varepsilon_0 k_z}{\Delta t} - \frac{\alpha_z k_z + \sigma_z}{2}}{\frac{\varepsilon_0 k_z}{\Delta t} + \frac{\alpha_z k_z + \sigma_z}{2}} E_x\Big|_{i-\frac{1}{2},j,k}^{n} + \frac{\frac{\varepsilon_0}{\Delta t} + \frac{\alpha_z}{2}}{\frac{\varepsilon_0 k_z}{\Delta t} + \frac{\alpha_z k_z + \sigma_z}{2}} P_x\Big|_{i-\frac{1}{2},j,k}^{n+1} - \frac{\frac{\varepsilon_0}{\Delta t} - \frac{\alpha_z}{2}}{\frac{\varepsilon_0 k_z}{\Delta t} + \frac{\alpha_z k_z + \sigma_z}{2}} P_x\Big|_{i-\frac{1}{2},j,k}^{n} \tag{5.2}$$

where P_x is an auxiliary or intermediate variable.

Comparing (5.1) with (4.1), it can be readily seen that the same 1D formula in (4.3) can be applied to (5.1) in the same manner. This results the 1D modal CFS-PML equation for E_x:

$$P_x\Big|_{i-\frac{1}{2},j,k}^{n+1} = P_x\Big|_{i-\frac{1}{2},j,k}^{n} + \frac{\Delta t}{\varepsilon \Delta y}(\alpha_{zy}|_{i-\frac{1}{2},j-\frac{1}{2}} - 1)H_z\Big|_{i-\frac{1}{2},j-\frac{1}{2},k}^{n+\frac{1}{2}} - \frac{\Delta t}{\varepsilon \Delta z}\left(H_y\Big|_{i-\frac{1}{2},j,k+\frac{1}{2}}^{n+1/2} - H_y\Big|_{i-\frac{1}{2},j,k-\frac{1}{2}}^{n+1/2}\right) \tag{5.3}$$

$$E_x\Big|_{i-\frac{1}{2},j,k}^{n+1} = \frac{\frac{\varepsilon_0 k_z}{\Delta t} - \frac{\alpha_z k_z + \sigma_z}{2}}{\frac{\varepsilon_0 k_z}{\Delta t} + \frac{\alpha_z k_z + \sigma_z}{2}} E_x\Big|_{i-\frac{1}{2},j,k}^{n} + \frac{\frac{\varepsilon_0}{\Delta t} + \frac{\alpha_z}{2}}{\frac{\varepsilon_0 k_z}{\Delta t} + \frac{\alpha_z k_z + \sigma_z}{2}} P_x\Big|_{i-\frac{1}{2},j,k}^{n+1} - \frac{\frac{\varepsilon_0}{\Delta t} - \frac{\alpha_z}{2}}{\frac{\varepsilon_0 k_z}{\Delta t} + \frac{\alpha_z k_z + \sigma_z}{2}} P_x\Big|_{i-\frac{1}{2},j,k}^{n} \tag{5.4}$$

where the definition α_z is the same as (4.9).

The PML in a waveguide acts like a waveguide filled with a lossy medium. The medium is uniform on the cross section of the waveguide and therefore it does not change the cross-sectional field patterns of a mode. In other words, the cross-sectional field distribution pattern in the PML region is the same as that in the waveguide for a given mode.

The equations for other field components can be found in a similar manner and are listed in appendix B. They form the new 1D modal PML. Since it is derived directly from

the FDTD grid, it should have numerical characteristics similar to the original FDTD grid. It should also perform at least the same level as the original 3D PML for a single mode. Numerical results presented in the next section serve to validate these claims.

Note that like other modal PMLs, the proposed modal PML can be applied to one mode only. In a multimode situation, the interesting modes can be extracted using the method described in chapter 4 and then terminated with the modal PML associated with it.

5.3 Numerical Examples

To validate the proposed 1D modal PML, a rectangular waveguide was considered. The waveguide had a rectangular cross section with a width of a=0.04m in the x-direction, a height of b=0.02m in the y-direction, and the wave propagation direction was in the z-direction. The mesh sizes for FDTD simulation were Δx=0.001m , Δy=0.001m , and Δz=0.001m. The time step was taken as $\Delta t=\Delta t_{\max}=1.9245ps$ where $\Delta t_{\max}$ was the CFL time step limit of the FDTD formulae. The total number of the iterations was 8192. One end of the waveguide was terminated with a 10-layer PML and another end was connected to a very long waveguide. The conductivity profile for the PML was $\sigma_z(z)=\sigma_{zm}(1-z/d)^4$, $\kappa_z(z)=1$, and $\alpha_z(z)=\alpha_{zm}(1-z/d)^4$ for $0\le z\le d$ (d was the total length of the PML). The source plane was placed 2 Δzs away from the PML. E_y was recorded at a point 1 Δz from the PML. The source in the time-domain was the Dirac impulse function $\delta(n)$. $\alpha_{zm}=2\pi\varepsilon_0 f_c$ with f_c being the cut-off frequency of the considered mode.

Two modes, TE_{10} and TE_{11}, were excited in the waveguide, respectively. Two separate simulations were run: one with the proposed 1D modal CFS-PML and the other with the original 3D CFS-PML. The relative differences between the E_ys of the two simulations are shown in Figure 5.1 and Figure 5.2. Figure 5.1 is for the TE_{10} mode, while Figure 5.2 is for the TE_{11} mode.

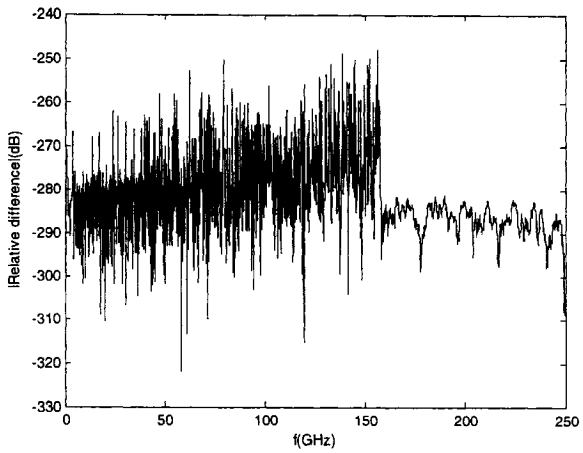

Figure 5.1 The difference between the E_y obtained by the proposed 1D modal CFS-PML and that obtained by the original 3D CFS-PML for TE_{10} mode.

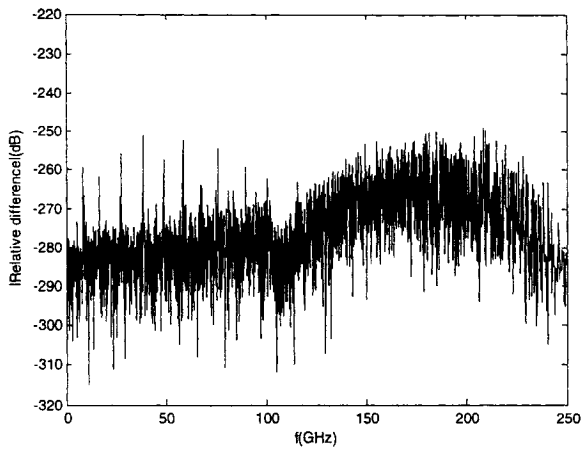

Figure 5.2 The difference between the E_y s obtained by the proposed 1D modal CFS-PML and that obtained by the original 3D CFS-PML for TE_{11}.

As can be seen from Figure 5.1 and Figure 5.2, the differences between the proposed 1D PML and the 3D PML are extremely small, less than -220dB across the whole frequency spectrum, including those frequencies at and below cutoff. We therefore conclude that the proposed 1D modal PML has numerical properties very close to those of the original 3D PML of FDTD grid.

To assess the absorption performance of the proposed modal PML in a general multimode situation, inductive fins were inserted into the waveguide (see Figure 5.3).

The TE_{10} mode was excited with a modulated Gaussian pulse $\sin(2\pi f_0 t)e^{-(t-t_0)^2/T^2}$ in the center of the structure. Parameter T was equal to $150\Delta t$ and t_0 to $600\Delta t$. The 10-layer CFS-PML was $5\Delta z$s away from the closest fins. E_y field was recorded at a point $1\Delta z$ before the PML and $2\Delta x$ away from the side wall. In this case, the presence of the fins caused the E_y field to consist of many higher order modes. For conventional CFS-PML, f_c is the cut-off frequency of the TE_{10} mode; for 1D modal CFS-PML, f_c is the cut-off frequency of each mode considered. In this example, the modes considered in the 1D modal CFS-PML include TE_{10} to TE_{90}.

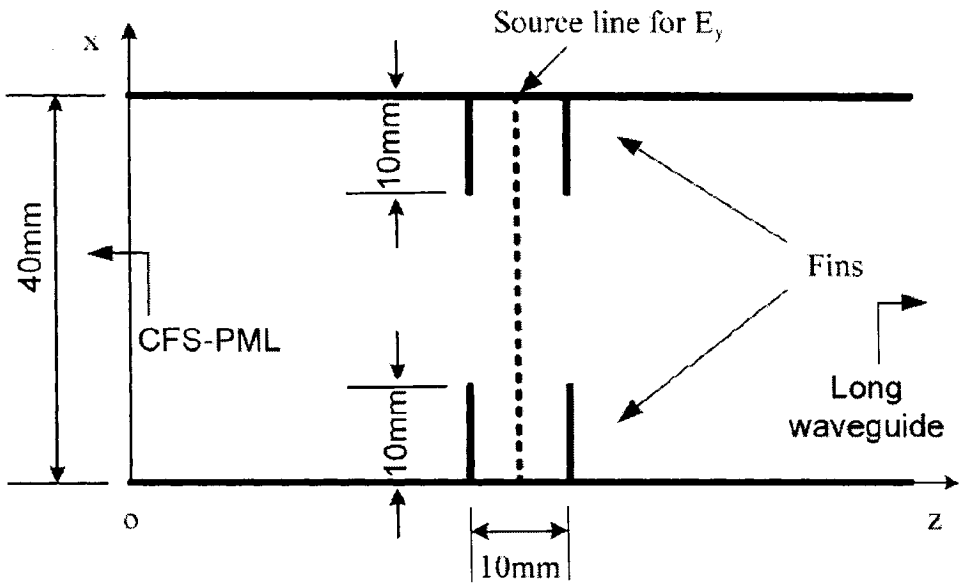

Figure 5.3 The waveguide structure with two strips under study.

Again, two separate simulations were run: one with the proposed 1D modal PML and another with the original 3D CFS-PML. Figure 5.4 shows the reflected E_ys obtained with the proposed 1D modal PML and with the original 3D CFS-PML. Figure 5.5 shows the corresponding reflection coefficients in the frequency-domain with the total number of the iterations in the time-domain being 4096.

As can be seen from Figure 5.4 and Figure 5.5, the 1D CFS-PML method actually performs better than the original 3D PML with smaller numerical reflections.

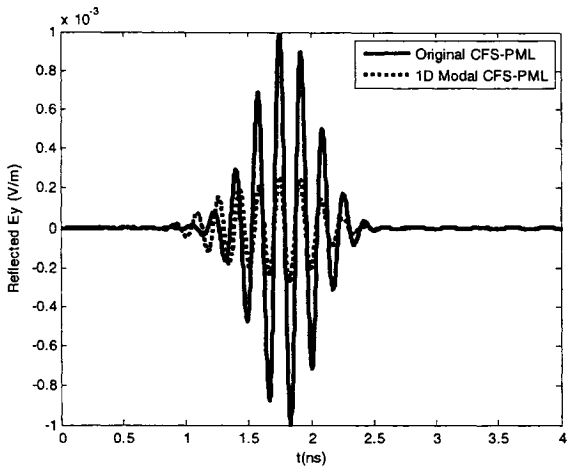

Figure 5.4 The reflected E_y obtained by the proposed 1D CFS-PML for the first 9 modes and the original CFS-PML.

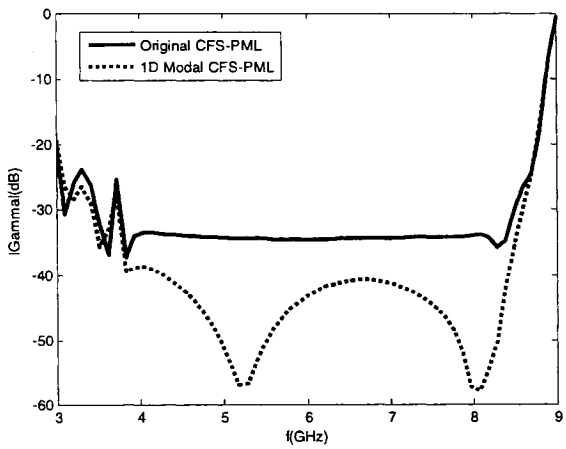

Figure 5.5 The computed reflection coefficients by the PML in the corresponding frequency-domain.

5.4 Discussion and Conclusion

In this chapter, a new efficient FDTD-based 1D modal PML method was proposed. It was derived directly from the original FDTD formulae and therefore has numerical characteristics very close to those of the original 3D PML of FDTD. Numerical results show that:

a) The relative differences between the results of the proposed method and the original PMLs are extremely small (less than -220dB) for specified modes.

b) The proposed method performs at least as well as the original PMLs, if not better.

6 A New Subgridding Method for 2D FDTD

6.1 Introduction

For complex problems with a large solution domain and fine geometry, FDTD simulations still require a large amount of memory and a long CPU time. One of the principal reasons is that fine geometry requires small mesh sizes to resolve the fields around them. In order to solve the problem, many subgridding schemes have been developed for the FDTD method [87]-[98]. Fine meshes are employed only in the regions that contain fine geometry while coarse meshes are used as much as possible. Schemes are then developed to interface the fine mesh regions and the coarse mesh regions. However, these subgridding schemes suffer from two problems: A) long-term or late-time instability and B) uncontrollable reflections from the interfaces. In certain cases, long-term stability is achieved but at the cost of high complexity of the subgridding algorithms [89][90][92][96]. The schemes presented in [94][97] are simple and of low reflections, but they do not guarantee long term stability.

In this chapter, a simple and stable subgridding scheme with low reflection is proposed for 2D FDTD simulations. It is not only very simple with controllable low reflections but also proven to be stable.

The chapter is organized as follows. First, we present the proposed simple and stable subgridding scheme and discuss how low reflections are achieved. Two numerical examples are then computed to demonstrate the validity and effectiveness of the proposed schemes. Finally, discussions and conclusions concerning this method are presented.

6.2 Derivation of the Stable Subgridding Scheme

In a linear and lossless medium, the spatially discretized Maxwell's equations can be expressed as follows:

$$\mu\Big|_{i,j+\frac{1}{2},k+\frac{1}{2}} \frac{\partial H_x\Big|_{i,j+\frac{1}{2},k+\frac{1}{2}}}{\partial t} = \frac{E_y\Big|_{i,j+\frac{1}{2},k+1} - E_y\Big|_{i,j+\frac{1}{2},k}}{\Delta z} - \frac{E_z\Big|_{i,j+1,k+\frac{1}{2}} - E_z\Big|_{i,j,k+\frac{1}{2}}}{\Delta y} \tag{6.1}$$

$$\mu\Big|_{i+\frac{1}{2},j,k+\frac{1}{2}} \frac{\partial H_y\Big|_{i+\frac{1}{2},j,k+\frac{1}{2}}}{\partial t} = \frac{E_z\Big|_{i+1,j,k+\frac{1}{2}} - E_z\Big|_{i,j,k+\frac{1}{2}}}{\Delta x} - \frac{E_x\Big|_{i+\frac{1}{2},j,k+1} - E_x\Big|_{i+\frac{1}{2},j,k}}{\Delta z} \tag{6.2}$$

$$\mu\Big|_{i+\frac{1}{2},j+\frac{1}{2},k} \frac{\partial H_z\Big|_{i+\frac{1}{2},j+\frac{1}{2},k}}{\partial t} = \frac{E_x\Big|_{i+\frac{1}{2},j+1,k} - E_x\Big|_{i+\frac{1}{2},j,k}}{\Delta y} - \frac{E_y\Big|_{i+1,j+\frac{1}{2},k} - E_y\Big|_{i,j+\frac{1}{2},k}}{\Delta x} \tag{6.3}$$

$$\varepsilon\Big|_{i+\frac{1}{2},j,k} \frac{\partial E_x\Big|_{i+\frac{1}{2},j,k}}{\partial t} = \frac{H_z\Big|_{i+\frac{1}{2},j+\frac{1}{2},k} - H_z\Big|_{i+\frac{1}{2},j-\frac{1}{2},k}}{\Delta y} - \frac{H_y\Big|_{i+\frac{1}{2},j,k+\frac{1}{2}} - H_y\Big|_{i+\frac{1}{2},j,k-\frac{1}{2}}}{\Delta z} - J_x\Big|_{i+\frac{1}{2},j,k} \tag{6.4}$$

$$\varepsilon\Big|_{i,j+\frac{1}{2},k} \frac{\partial E_y\Big|_{i,j+\frac{1}{2},k}}{\partial t} = \frac{H_x\Big|_{i,j+\frac{1}{2},k+\frac{1}{2}} - H_x\Big|_{i,j+\frac{1}{2},k-\frac{1}{2}}}{\Delta z} - \frac{H_z\Big|_{i+\frac{1}{2},j+\frac{1}{2},k} - H_z\Big|_{i-\frac{1}{2},j+\frac{1}{2},k}}{\Delta x} - J_y\Big|_{i,j+\frac{1}{2},k} \tag{6.5}$$

$$\varepsilon\Big|_{i,j,k+\frac{1}{2}} \frac{\partial E_z\Big|_{i,j,k+\frac{1}{2}}}{\partial t} = \frac{H_y\Big|_{i+\frac{1}{2},j,k+\frac{1}{2}} - H_y\Big|_{i-\frac{1}{2},j,k+\frac{1}{2}}}{\Delta x} - \frac{H_x\Big|_{i,j+\frac{1}{2},k+\frac{1}{2}} - H_x\Big|_{i,j-\frac{1}{2},k+\frac{1}{2}}}{\Delta y} - J_z\Big|_{i,j,k+\frac{1}{2}} \tag{6.6}$$

Equations (6.1)-(6.6) can be rewritten as:

$$\Delta y \Delta z \frac{\partial B_x\Big|_{i,j+\frac{1}{2},k+\frac{1}{2}}}{\partial t} = \Delta y (E_y\Big|_{i,j+\frac{1}{2},k+1} - E_y\Big|_{i,j+\frac{1}{2},k}) - \Delta z (E_z\Big|_{i,j+1,k+\frac{1}{2}} - E_z\Big|_{i,j,k+\frac{1}{2}}) \tag{6.7}$$

$$\Delta z \Delta x \frac{\partial B_y\Big|_{i+\frac{1}{2},j,k+\frac{1}{2}}}{\partial t} = \Delta z (E_z\Big|_{i+1,j,k+\frac{1}{2}} - E_z\Big|_{i,j,k+\frac{1}{2}}) - \Delta x (E_x\Big|_{i+\frac{1}{2},j,k+1} - E_x\Big|_{i+\frac{1}{2},j,k}) \tag{6.8}$$

$$\Delta x\Delta y\frac{\partial B_z\Big|_{i+\frac{1}{2},j+\frac{1}{2},k}}{\partial t}=\Delta x(E_x\Big|_{i+\frac{1}{2},j+1,k}-E_x\Big|_{i+\frac{1}{2},j,k})-\Delta y(E_y\Big|_{i+1,j+\frac{1}{2},k}-E_y\Big|_{i,j+\frac{1}{2},k}) \tag{6.9}$$

$$\Delta y\Delta z\frac{\partial D_x\Big|_{i+\frac{1}{2},j,k}}{\partial t}-\Delta y\Delta z J_x\Big|_{i+\frac{1}{2},j,k}= \Delta z(H_z\Big|_{i+\frac{1}{2},j+\frac{1}{2},k}-H_z\Big|_{i+\frac{1}{2},j-\frac{1}{2},k})-\Delta y(H_y\Big|_{i+\frac{1}{2},j,k+\frac{1}{2}}-H_y\Big|_{i+\frac{1}{2},j,k-\frac{1}{2}}) \tag{6.10}$$

$$\Delta z\Delta x\frac{\partial D_y\Big|_{i,j+\frac{1}{2},k}}{\partial t}-\Delta z\Delta x J_y\Big|_{i,j+\frac{1}{2},k}= \Delta x(H_x\Big|_{i,j+\frac{1}{2},k+\frac{1}{2}}-H_x\Big|_{i,j+\frac{1}{2},k-\frac{1}{2}})-\Delta z(H_z\Big|_{i+\frac{1}{2},j+\frac{1}{2},k}-H_z\Big|_{i-\frac{1}{2},j+\frac{1}{2},k}) \tag{6.11}$$

$$\Delta x\Delta y\frac{\partial D_z\Big|_{i,j,k+\frac{1}{2}}}{\partial t}-\Delta x\Delta y J_z\Big|_{i,j,k+\frac{1}{2}}= \Delta y(H_y\Big|_{i+\frac{1}{2},j,k+\frac{1}{2}}-H_y\Big|_{i-\frac{1}{2},j,k+\frac{1}{2}})-\Delta x(H_x\Big|_{i,j+\frac{1}{2},k+\frac{1}{2}}-H_x\Big|_{i,j-\frac{1}{2},k+\frac{1}{2}}) \tag{6.12}$$

where

$$B_x\Big|_{i,j+\frac{1}{2},k+\frac{1}{2}}=\mu\Big|_{i,j+\frac{1}{2},k+\frac{1}{2}}H_x\Big|_{i,j+\frac{1}{2},k+\frac{1}{2}} \tag{6.13}$$

$$B_y\Big|_{i+\frac{1}{2},j,k+\frac{1}{2}}=\mu\Big|_{i+\frac{1}{2},j,k+\frac{1}{2}}H_y\Big|_{i+\frac{1}{2},j,k+\frac{1}{2}} \tag{6.14}$$

$$B_z\Big|_{i+\frac{1}{2},j+\frac{1}{2},k}=\mu\Big|_{i+\frac{1}{2},j+\frac{1}{2},k}H_z\Big|_{i+\frac{1}{2},j+\frac{1}{2},k} \tag{6.15}$$

$$D_x\Big|_{i+\frac{1}{2},j,k}=\varepsilon\Big|_{i+\frac{1}{2},j,k}E_x\Big|_{i+\frac{1}{2},j,k} \tag{6.16}$$

$$D_y\Big|_{i,j+\frac{1}{2},k}=\varepsilon\Big|_{i,j+\frac{1}{2},k}E_y\Big|_{i,j+\frac{1}{2},k} \tag{6.17}$$

$$D_z\Big|_{i,j,k+\frac{1}{2}}=\varepsilon\Big|_{i,j,k+\frac{1}{2}}E_z\Big|_{i,j,k+\frac{1}{2}} \tag{6.18}$$

Equations (6.7)-(6.18) can be rewritten as:

$$(e_z\Big|_{i,j+1,k+\frac{1}{2}} - e_z\Big|_{i,j,k+\frac{1}{2}}) - (e_y\Big|_{i,j+\frac{1}{2},k+1} - e_y\Big|_{i,j+\frac{1}{2},k}) = -\frac{\partial b_x\Big|_{i,j+\frac{1}{2},k+\frac{1}{2}}}{\partial t} \tag{6.19}$$

$$(\tilde{e}_x\Big|_{i+\frac{1}{2},j,k+1} - \tilde{e}_x\Big|_{i+\frac{1}{2},j,k}) - (\tilde{e}_z\Big|_{i+1,j,k+\frac{1}{2}} - \tilde{e}_z\Big|_{i,j,k+\frac{1}{2}}) = -\frac{\partial \tilde{b}_y\Big|_{i+\frac{1}{2},j,k+\frac{1}{2}}}{\partial t} \tag{6.20}$$

$$(e_y\Big|_{i+1,j+\frac{1}{2},k} - e_y\Big|_{i,j+\frac{1}{2},k}) - (e_x\Big|_{i+\frac{1}{2},j+1,k} - e_x\Big|_{i+\frac{1}{2},j,k}) = -\frac{\partial \tilde{b}_z\Big|_{i+\frac{1}{2},j+\frac{1}{2},k}}{\partial t} \tag{6.21}$$

$$(\tilde{h}_z\Big|_{i+\frac{1}{2},j+\frac{1}{2},k} - \tilde{h}_z\Big|_{i+\frac{1}{2},j-\frac{1}{2},k}) - (\tilde{h}_y\Big|_{i+\frac{1}{2},j,k+\frac{1}{2}} - \tilde{h}_y\Big|_{i+\frac{1}{2},j,k-\frac{1}{2}}) = \frac{\partial \tilde{d}_x\Big|_{i+\frac{1}{2},j,k}}{\partial t} - \tilde{j}_x\Big|_{i+\frac{1}{2},j,k} \tag{6.22}$$

$$(\tilde{h}_x\Big|_{i,j+\frac{1}{2},k+\frac{1}{2}} - \tilde{h}_x\Big|_{i,j+\frac{1}{2},k-\frac{1}{2}}) - (\tilde{h}_z\Big|_{i+\frac{1}{2},j+\frac{1}{2},k} - \tilde{h}_z\Big|_{i-\frac{1}{2},j+\frac{1}{2},k}) = \frac{\partial \tilde{d}_y\Big|_{i,j+\frac{1}{2},k}}{\partial t} - \tilde{j}_y\Big|_{i,j+\frac{1}{2},k} \tag{6.23}$$

$$(\tilde{h}_y\Big|_{i+\frac{1}{2},j,k+\frac{1}{2}} - \tilde{h}_y\Big|_{i-\frac{1}{2},j,k+\frac{1}{2}}) - (\tilde{h}_x\Big|_{i,j+\frac{1}{2},k+\frac{1}{2}} - \tilde{h}_x\Big|_{i,j-\frac{1}{2},k+\frac{1}{2}}) = \frac{\partial \tilde{d}_z}{\partial t}\Big|_{i,j,k+\frac{1}{2}} - \tilde{j}_z\Big|_{i,j,k+\frac{1}{2}} \tag{6.24}$$

$$\tilde{b}_x\Big|_{i,j+\frac{1}{2},k+\frac{1}{2}} = \frac{\Delta y \Delta z}{\Delta x}\mu\Big|_{i,j+\frac{1}{2},k+\frac{1}{2}} \tilde{h}_x\Big|_{i,j+\frac{1}{2},k+\frac{1}{2}} \tag{6.25}$$

$$\tilde{b}_y\Big|_{i+\frac{1}{2},j,k+\frac{1}{2}} = \frac{\Delta z \Delta x}{\Delta y}\mu\Big|_{i+\frac{1}{2},j,k+\frac{1}{2}} \tilde{h}_y\Big|_{i+\frac{1}{2},j,k+\frac{1}{2}} \tag{6.26}$$

$$\tilde{b}_z\Big|_{i+\frac{1}{2},j+\frac{1}{2},k} = \frac{\Delta x \Delta y}{\Delta z}\mu\Big|_{i+\frac{1}{2},j+\frac{1}{2},k} \tilde{h}_z\Big|_{i+\frac{1}{2},j+\frac{1}{2},k} \tag{6.27}$$

$$\tilde{d}_x\Big|_{i+\frac{1}{2},j,k} = \frac{\Delta y \Delta z}{\Delta x}\varepsilon\Big|_{i+\frac{1}{2},j,k} \tilde{e}_x\Big|_{i+\frac{1}{2},j,k} \tag{6.28}$$

$$\tilde{d}_y\Big|_{i,j+\frac{1}{2},k} = \frac{\Delta z \Delta x}{\Delta y}\varepsilon\Big|_{i,j+\frac{1}{2},k} \tilde{e}_y\Big|_{i,j+\frac{1}{2},k} \tag{6.29}$$

$$\tilde{d}_z\Big|_{i,j,k+\frac{1}{2}} = \frac{\Delta x \Delta y}{\Delta z}\varepsilon\Big|_{i,j,k+\frac{1}{2}} \tilde{e}_z\Big|_{i,j,k+\frac{1}{2}} \tag{6.30}$$

where

$$\tilde{b}_x\Big|_{i,j+\frac{1}{2},k+\frac{1}{2}} = \Delta y \Delta z B_x\Big|_{i,j+\frac{1}{2},k+\frac{1}{2}} \tag{6.31}$$

$$\tilde{b}_y\Big|_{i+\frac{1}{2},j,k+\frac{1}{2}} = \Delta z \Delta x B_y\Big|_{i+\frac{1}{2},j,k+\frac{1}{2}} \tag{6.32}$$

$$\tilde{b}_z\Big|_{i+\frac{1}{2},j+\frac{1}{2},k} = \Delta x \Delta y B_z\Big|_{i+\frac{1}{2},j+\frac{1}{2},k} \tag{6.33}$$

$$\tilde{d}_x\Big|_{i+\frac{1}{2},j,k} = \Delta y \Delta z D_x\Big|_{i+\frac{1}{2},j,k} \tag{6.34}$$

$$\tilde{d}_y\Big|_{i,j+\frac{1}{2},k} = \Delta z \Delta x D_y\Big|_{i,j+\frac{1}{2},k} \tag{6.35}$$

$$\tilde{d}_z\Big|_{i,j,k+\frac{1}{2}} = \Delta x \Delta y D_z\Big|_{i,j,k+\frac{1}{2}} \tag{6.36}$$

$$\tilde{j}_x\Big|_{i+\frac{1}{2},j,k} = \Delta y \Delta z J_x\Big|_{i+\frac{1}{2},j,k} \tag{6.37}$$

$$\tilde{j}_y\Big|_{i,j+\frac{1}{2},k} = \Delta z \Delta x J_y\Big|_{i,j+\frac{1}{2},k} \tag{6.38}$$

$$\tilde{j}_z\Big|_{i,j,k+\frac{1}{2}} = \Delta x \Delta y J_z\Big|_{i,j,k+\frac{1}{2}} \tag{6.39}$$

$$\tilde{e}_x\Big|_{i+\frac{1}{2},j,k} = \Delta x E_x\Big|_{i+\frac{1}{2},j,k} \tag{6.40}$$

$$\tilde{e}_y\Big|_{i,j+\frac{1}{2},k} = \Delta y E_y\Big|_{i,j+\frac{1}{2},k} \tag{6.41}$$

$$\tilde{e}_z\Big|_{i,j,k+\frac{1}{2}} = \Delta z E_z\Big|_{i,j,k+\frac{1}{2}} \tag{6.42}$$

$$\tilde{h}_x\Big|_{i,j+\frac{1}{2},k+\frac{1}{2}} = \Delta x H_x\Big|_{i,j+\frac{1}{2},k+\frac{1}{2}} \tag{6.43}$$

$$\tilde{h}_y\Big|_{i+\frac{1}{2},j,k+\frac{1}{2}} = \Delta y H_y\Big|_{i+\frac{1}{2},j,k+\frac{1}{2}} \tag{6.44}$$

$$\tilde{h}_z\Big|_{i+\frac{1}{2},j+\frac{1}{2},k} = \Delta z H_z\Big|_{i+\frac{1}{2},j+\frac{1}{2},k} \tag{6.45}$$

Here $\tilde{e}$ is denoted as an electric voltage along the edge of the mesh and $\tilde{b}$ is the magnetic flux through a mesh cell facet. The definitions of $\tilde{h}$ and $\tilde{d}$ are the same as $\tilde{e}$ and $\tilde{b}$ except they refer to magnetic voltage and electric flux. $\tilde{j}$ is the current through a mesh cell facet.

Equations (6.19)-(6.44) can be written as a matrix form:

$$\begin{aligned} C\bar{e} &= -\frac{\partial \bar{b}}{\partial t} \\ \tilde{C}\bar{h} &= \frac{\partial \bar{d}}{\partial t} + \bar{j} \\ \bar{d} &= D_\varepsilon \bar{e} \\ \bar{b} &= D_\mu \bar{h} \end{aligned} \tag{6.46}$$

where $\bar{e}$ is a vector containing all electric voltages, $\bar{h}$ is a vector containing all magnetic voltages, $\bar{d}$ is a vector containing all electric fluxes, $\bar{b}$ is a vector containing all magnetic fluxes, $\bar{j}$ is a vector containing all the currents through mesh cell facets. The matrices C and $\tilde{C}$ contain the signs for the summation of the field quantities. The diagonal matrices D_ε and D_μ contain material properties and mesh dimensions.

Equation (6.46) can also be obtained by discretizing the following integral form of the Maxwell's equations directly, especially for non-uniform meshes:

$$\frac{\partial}{\partial t}\iint_S \bar{B}\cdot d\bar{S} = -\oint_C \bar{E}\cdot d\bar{l} \tag{6.47}$$

$$\frac{\partial}{\partial t}\iint_S \bar{D}\cdot d\bar{S} = \oint_C \bar{H}\cdot d\bar{l} - \iint_S \bar{J}\cdot d\bar{S} \tag{6.48}$$

It is shown in [120] that the following equation is a sufficient condition to ensure the stability of (6.46):

$$C = \tilde{C}^{\mathrm{T}} \tag{6.49}$$

This stability condition can only ensure that the spatially dicretized system is stable. When the temporal discretization is also applied, an additional stability condition is needed.

The above concept is now applied to the construction of a new 2D FDTD subgridding scheme. For a subgridding structure with a ratio of 3:1 shown in Figure 6.1, by discretizing (6.47) directly and using equation (6.49) (with the help of Maple), the following simple subgridding formulations are obtained:

$$H_z^{n+\frac{1}{2}}(2,1) = H_z^{n-\frac{1}{2}}(2,1) + \frac{\Delta t}{\mu \Delta Y}[E_x^n(2,1) - E_x^n(2,0)] - \frac{\Delta t}{\mu \Delta X}[E_y^n(2,1) - E_y^n(1,1)] \tag{6.50}$$

$$H_z^{n+\frac{1}{2}}(1,2) = H_z^{n-\frac{1}{2}}(1,2) + \frac{\Delta t}{\mu \Delta Y}[E_x^n(1,2) - E_x^n(1,1)] - \frac{\Delta t}{\mu \Delta X}[E_y^n(1,2) - E_y^n(0,2)] \tag{6.51}$$

$$h_z^{n+\frac{1}{2}}(1,1) = h_z^{n-\frac{1}{2}}(1,1) + \frac{\Delta t}{\mu \Delta y}[e_x^n(1,1) - E_x^n(2,1)] - \frac{\Delta t}{\mu \Delta x}[e_y^n(1,1) - E_y^n(1,2)] \tag{6.52}$$

$$h_z^{n+\frac{1}{2}}(2,1) = h_z^{n-\frac{1}{2}}(2,1) + \frac{\Delta t}{\mu \Delta y}[e_x^n(2,1) - E_x^n(2,1)] - \frac{\Delta t}{\mu \Delta x}[e_y^n(2,1) - e_y^n(1,1)] \tag{6.53}$$

$$h_z^{n+\frac{1}{2}}(1,2) = h_z^{n-\frac{1}{2}}(1,2) + \frac{\Delta t}{\mu \Delta y}[e_x^n(1,2) - e_x^n(1,1)] - \frac{\Delta t}{\mu \Delta x}[e_y^n(1,2) - E_y^n(1,2)] \tag{6.54}$$

$$E_x^{n+1}(2,1) = E_x^n(2,1) + \frac{\Delta t}{\varepsilon \Delta y}\left[\frac{h_z^{n+\frac{1}{2}}(1,1) + h_z^{n+\frac{1}{2}}(2,1) + h_z^{n+\frac{1}{2}}(3,1)}{3} - H_z^{n+\frac{1}{2}}(2,1)\right] \tag{6.55}$$

$$E_y^{n+1}(1,2) = E_y^n(1,2) - \frac{\Delta t}{\varepsilon \Delta x}\left[\frac{h_z^{n+\frac{1}{2}}(1,1) + h_z^{n+\frac{1}{2}}(1,2) + h_z^{n+\frac{1}{2}}(1,3)}{3} - H_z^{n+\frac{1}{2}}(1,2)\right] \tag{6.56}$$

where E_x, E_y, and H_z are field components in coarse meshes, e_x, e_y, and h_z are field components in subgridded meshes, $\Delta X = 3\Delta x$, and $\Delta Y = 3\Delta y$.

Although the subgridding formulations as derived above are stable when the CFL stability condition for fine meshes is satisfied, numerical experiments have shown that the reflection from the interface between the coarse meshes and the fine meshes is too

large for general applications. In order to reduce the reflection from the interface while retain the simplicity and stability, a parameter α is introduced as follows:

$$H_z^{n+\frac{1}{2}}(2,1) = H_z^{n-\frac{1}{2}}(2,1) + \frac{\Delta t}{\mu \Delta Y}[\alpha E_x^n(2,1) - E_x^n(2,0)] - \frac{\Delta t}{\mu \Delta X}[E_y^n(2,1) - E_y^n(1,1)] \tag{6.57}$$

$$H_z^{n+\frac{1}{2}}(1,2) = H_z^{n-\frac{1}{2}}(1,2) + \frac{\Delta t}{\mu \Delta y}[E_x^n(1,2) - E_x^n(1,1)] - \frac{\Delta t}{\mu \Delta x}[\alpha E_y^n(1,2) - E_y^n(0,2)] \tag{6.58}$$

$$h_z^{n+\frac{1}{2}}(1,1) = h_z^{n-\frac{1}{2}}(1,1) + \frac{\Delta t}{\mu \Delta y}[e_x^n(1,1) - \alpha E_x^n(2,1)] - \frac{\Delta t}{\mu \Delta x}[e_y^n(1,1) - \alpha E_y^n(1,2)] \tag{6.59}$$

$$h_z^{n+\frac{1}{2}}(2,1) = h_z^{n-\frac{1}{2}}(2,1) + \frac{\Delta t}{\mu \Delta y}[e_x^n(2,1) - \alpha E_x^n(2,1)] - \frac{\Delta t}{\mu \Delta x}[e_y^n(2,1) - e_y^n(1,1)] \tag{6.60}$$

$$h_z^{n+\frac{1}{2}}(1,2) = h_z^{n-\frac{1}{2}}(1,2) + \frac{\Delta t}{\mu \Delta y}[e_x^n(1,2) - e_x^n(1,1)] - \frac{\Delta t}{\mu \Delta x}[e_y^n(1,2) - \alpha E_y^n(1,2)] \tag{6.61}$$

$$E_x^{n+1}(2,1) = E_x^n(2,1) + \frac{\Delta t}{\varepsilon \Delta y}\alpha[\frac{h_z^{n+\frac{1}{2}}(1,1) + h_z^{n+\frac{1}{2}}(2,1) + h_z^{n+\frac{1}{2}}(3,1)}{3} - H_z^{n+\frac{1}{2}}(2,1)] \tag{6.62}$$

$$E_y^{n+1}(1,2) = E_y^n(1,2) - \frac{\Delta t}{\varepsilon \Delta x}\alpha[\frac{h_z^{n+\frac{1}{2}}(1,1) + h_z^{n+\frac{1}{2}}(1,2) + h_z^{n+\frac{1}{2}}(1,3)}{3} - H_z^{n+\frac{1}{2}}(1,2)] \tag{6.63}$$

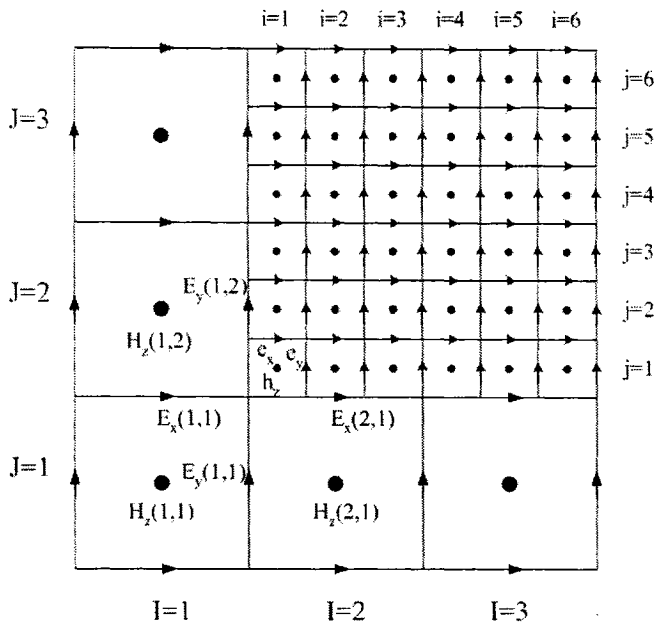

Figure 6.1 A subgridding structure with a mesh ratio of 3:1 in a FDTD lattice.

It can be verified using the Maple that the new subgridding formulations (6.57)-(6.63) still satisfy the stability condition (6.49). If the time step size Δt is determined by the CFL stability condition of fine meshes, the time-domain marching should be stable. This has been verified by numerical examples. Therefore, the focus now is to minimize the reflections due to the subgridding. The trial-and-error technique is used to obtain α by minimizing the reflection from the interface based on the geometry shown in Figure 6.2. Table 6-1 gives the optimized values of α we found for subgridding ratios 3:1, 5:1 and 7:1.

Table 6-1 The values of α for subgridding ratios K=3:1, 5:1, and 7:1.

subgridding ratio K	The value of α
3:1	0.718
5:1	0.5875
7:1	0.509

It should be noted that only a single α was introduced for the reflection minimization. More parameters may be introduced in (6.57)-(6.63) with increased complexity of the optimization process.

6.3 Numerical Example

To verify the proposed method, we first apply the proposed method to a perfect parallel plate waveguide for the TM mode that propagates in the x direction (see Figure 6.2). The width between two plates is 10mm.

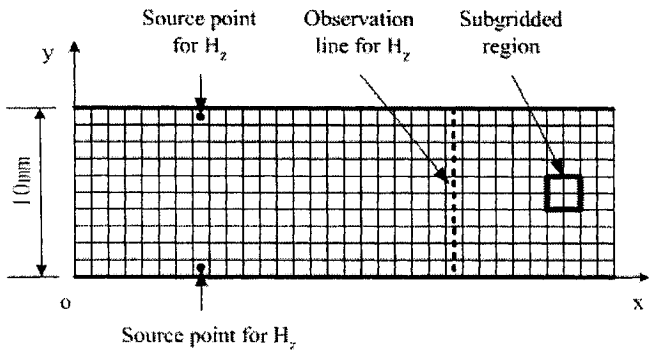

Figure 6.2 The parallel plate waveguide with width of 10mm and coarse mesh size of Δx=1mm and Δy=1mm.

The coarse mesh size is Δx=1mm and Δy=1mm. $2\times2=4$ coarse meshes in the center are then replaced by a subgridded fine mesh of $\Delta x=\frac{1}{K}$ mm and $\Delta y=\frac{1}{K}$ mm. K is the subgridding ratio. The time step for both the coarse mesh and the fine mesh is the same, and $\Delta t=\Delta t_{CFL}$ Δt_{CFL} is the maximum time step determined for the fine mesh region based on the CFL stability condition. The source is a Gaussian pulse in time-domain. In order to contruct propagating mode before the subgridded fine region, the source points are located in two symmetric points just beside the two plates and are 20 mesh sizes away from the subgridded fine region. The observation points are a line 5 mesh sizes away from the fine region. The coarse mesh size is equal to $\frac{\lambda}{20}$ at the maximum frequency considered (15GHz in this case); the maximum reflections produced by the subgridded fine meshes are recorded and shown in Figure 6.3. As can be seen, the reflections are below -63dB for the three given subgridding ratios, $K=3:1,5:1,7:1$. This is a strong indication that the proposed method is effective.

The second example computed is a 2D resonator of 6mm×5mm with a fin of length 2mm in the middle (see Figure 6.4). The coarse mesh size is Δx=1mm and Δy=1mm. $2\times2=4$ coarse mesh around the end of the fin are replaced by a subgridded mesh of $\Delta x=\frac{1}{K}$ mm

and $\Delta y=\frac{1}{K}$ mm. The time step for both coarse mesh region and fine mesh region is the same, $\Delta t=\Delta t_{CFL}$ and Δt_{CFL} is the maximum time step determined for the subgridded fine mesh region based on the CFL stability condition. The point source used in the FDTD simulation equals 1 at n=1 and equals 0 when n>1 in time-domain. Table 6-2 shows the relative errors of the computed resonant frequency of the first mode in comparisons with the results of the subgridding method presented in [94]. It can be seen from Table 6-2 that the proposed method gives almost the same results compared with the low reflection subgridding method.

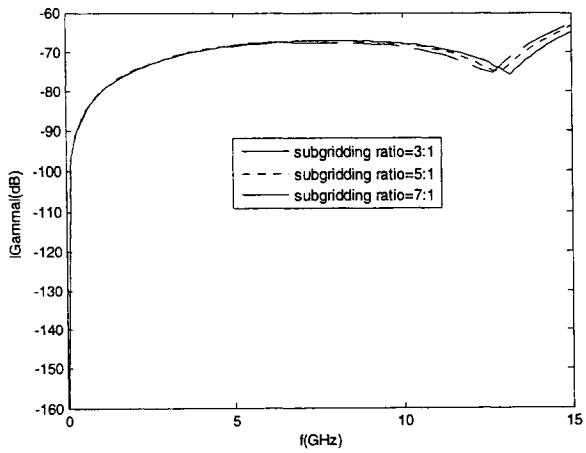

Figure 6.3 The reflection coefficient from the subgridded meshes in the center corresponding to the parallel plate waveguide in Figure 6.2.

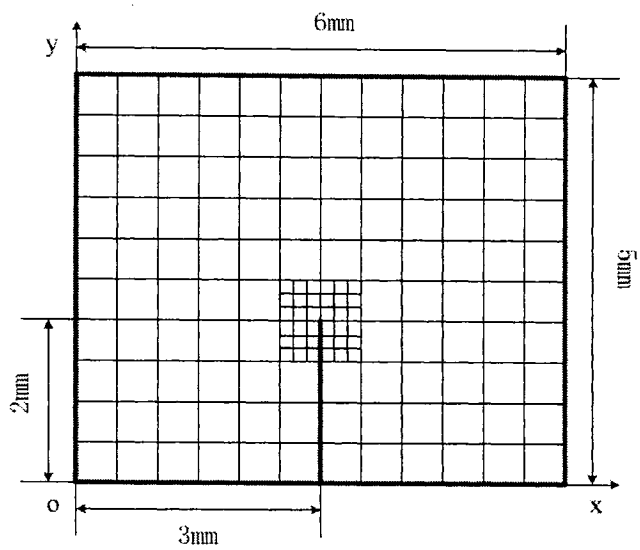

Figure 6.4 The rectangular resonator of 6mm×5mm with a fin of length 2mm in the middle.

It can also be found that the relative error of the computed resonant frequency decreases as the subgridding ratio increases. However, this decrease will level off when the subgridding ratio increases beyond a certain value. This is due to the fact that there are two types of errors in the subgridding scheme: the error due to the interface between the coarse mesh and fine mesh and the error due to the approximation errors of the FDTD method in computing fine geometric structures. When the error due to the FDTD approximation is prominent, increase in the subgridding ratio can reduce the overall error. When the error due to the interface is prominent, increase in the subgridding ratio will have no effect in reducing the overall error.

To check the long time stability, we have tried different positions of the fin and different sizes of the subgridded meshes around the end of the fin with iterations larger than 500,000. In all cases, the method is found to be stable. This has verified the stability of the proposed method numerically.

Table 6-2 The relative errors of the computed resonant frequency of the fin structure.

subgridding ratio K	Errors of the method in this chapter	Errors of the method in [94]	The total time step numbers used
3:1	-2.05%	-2.05%	1×8192
5:1	-1.26%	-1.26%	2×8192
7:1	-0.47%	-0.47%	2×8192

6.4 Conclusion

In this chapter, a simple and stable 2D FDTD subgridding scheme is proposed. The term stable doesn't mean the method is absolutely stable for any time step size Δt. It just means it is stable when the time step size Δt is determined by the CFL stability condition of the fine mesh. This scheme adapts the stability condition proposed in [120] and introduces a controlling parameter that minimizes the reflections due to the subgridding. Numerical experiments were performed to confirm the stability and effectiveness of the proposed subgridding scheme. However, further study is required to study the sensitivity of α to different structures. Because of its low reflection and stability, this new 2D subgridding scheme is a very good option for the optimization of 2D photonic crystal structures and H-plane filters.

7 Extraction of Causal Time-Domain Parameters Using Iterative Methods

7.1 Introduction

Recent interest in the time-domain modeling methods has been largely motivated by the demands for broadband electronic systems and high-speed digital circuits. When FDTD is used to analyze circuits including active devices, the most convenient way is to solve the time-domain lump-element circuit model of the active device directly. However, the time-domain lump-element circuit model of an active device is often unavailable and only the frequency-domain network parameters are available. The frequency-domain parameters need to be converted to time-domain parameters and the parameters in the time-domain have to be causal in order to be compatible with the FDTD simulator.

Under normal circumstances, network parameters are given or measured only in the frequency-domain and over a limited frequency range. For instance, most manufacturers provide the S-parameters for a FET transistor over only a limited frequency range under certain biasing conditions. To convert these frequency-domain parameters to their time-domain counterparts, transformation techniques such as the inverse Fourier Transform can be applied. However, direct application of these transformation techniques usually leads to non-causal time-domain parameters. For instance, the S-parameters of NE425S01 were given by manufactures over the frequency range of 0.5GHz – 18GHz [121]. One can supposedly obtain the frequency-domain Y-parameters from the given frequency-domain S-parameters [122] and then apply the inverse Fourier transform directly to obtain the time-domain Y-parameters. Figure 7.1 shows the time-domain $y_{11}(t)$ obtained as such for NE425S01. As can be seen, $y_{11}(t)$ has some significant values at $t<0$ and therefore is non-causal. In other words, the simple inverse Fourier transform is not adequate. Therefore, schemes need to be developed that can extract the causal time-domain parameters from the band-limited frequency-domain parameters.

It should be noted that the proposed methods do not guarantee the obtained frequency-domain parameters outside the given frequency range are close to actual

values; however, it is not of concern to a user.

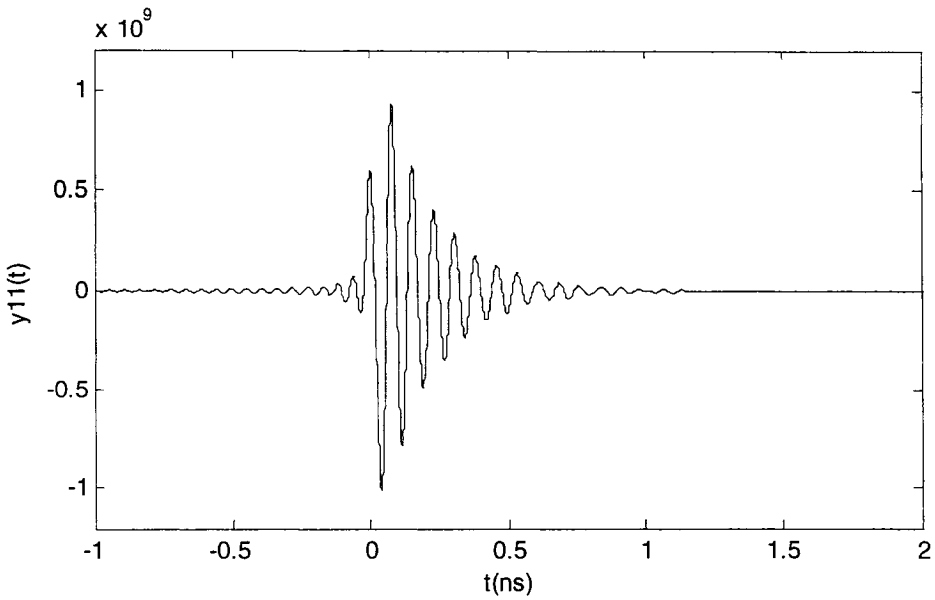

Figure 7.1 The time-domain $y_{11}(t)$ obtained with the direct inverse Fourier transform of the frequency-domain Y-parameters.

Perry et al. [123] and Chen [124] studied such phenomena and proposed the use of the Hilbert transform to tackle the problem. The method proposed by Perry *et. al.* achieves the causality by maintaining the magnitudes of the original parameters but modifying their phases for the minimum-phase systems [123]. The technique proposed by Chen has difficulties in handling the singularity of the Hilbert transformation integrals [124]. The errors were found to be somewhat large because of the simple direct extrapolation.

To obtain causal time-domain parameters from the band-limited frequency-domain parameters with good accuracy in the given frequency range, two iterative techniques to extract causal time-domain parameters are explored. They are conceptually simple and easy to implement. The extracted time-domain parameters not only are causal but also contain the same frequency-domain information as the original parameters over the given limited frequency range in both magnitude and phase. Comprehensive numerical studies on the effectiveness and validity of the proposed approach are presented.

7.2 The Error Feedback Based FFT Method

Suppose that $Y_{ori}(f) = Y_{ori\_r}(f) + jY_{ori\_i}(f)$ is the given frequency parameter that is known over a finite frequency range of interest. We propose the following procedure to obtain its causal time-domain counterpart:

Step 1: Let the values of the target frequency-domain Y-parameters, denoted as $Y_T(f) = Y_{T\_r}(f) + jY_{T\_i}(f)$, be equal to $Y_{ori}(f)$ within the given frequency range and equal to zero outside the given frequency range. Transform $Y_T(f)$ to its time-domain counterpart, denoted as $y(t)$, with a straightforward inverse fast Fourier transform (IFFT). $y(t)$ is usually non-causal.

Step 2: Force the causality into the obtained $y(t)$ by simply setting all the values to zero for $t < 0$. That is, let $y(t) = 0$ for $t < 0$.

Step 3: Fourier Transform the time-domain parameters obtained in Step 2 back into frequency-domain and obtain the corresponding frequency-domain parameter, denoted as $Y_{\text{mod}}(f) = Y_{\text{mod}\_r}(f) + jY_{\text{mod}\_i}(f)$. Compute differences or errors between $Y_{\text{mod}}(f)$ and the original $Y_{ori}(f)$ over the frequency range of interest. The difference is defined as

$$\Delta Y(f) = Y_{\text{mod}}(f) - Y_{ori}(f) \tag{7.1}$$

The error functions are defined as

$$error1 = \frac{\max(\Delta Y_r(f))}{\max(|Y_{orir}(f)|)} \tag{7.2}$$

$$error2 = \frac{\max(\Delta Y_i(f))}{\max(|Y_{orii}(f)|)} \tag{7.3}$$

$$error = \max(error1, error2) \tag{7.4}$$

Here max means the maximum value within the frequency range of

interest. If *error* is acceptably small, the time-domain parameters obtained in Step 2 are the causal time-domain parameters that we can accept and the computations terminate here; otherwise, go to the next step.

Step 4: Modify the target frequency-domain Y-parameters $Y_T(f) = Y_{T\_r}(f) + jY_{T\_i}(f)$ in the frequency range of interest as follows:

$$Y_T(f) = Y_T(f) - \Delta Y(f) \tag{7.5}$$

$$\Delta Y(f) = \Delta Y_r(f) + j(\alpha \Delta Y_i(f)) \tag{7.6}$$

where α is a coefficient used to balance the convergence speed between the real part and imaginary part. α is selected empirically in the following manner: the initial α is set to be 1; in the subsequent iterations, it is given by

$$\alpha = \alpha + (error2 - error1) \tag{7.7}$$

Extrapolate the target frequency-domain Y-parameters $Y_T(f) = Y_{T\_r}(f) + jY_{T\_i}(f)$ outside the frequency range of interest with the following formulas:

$$Y_T(f_n) = Y_T(f_n) - \Delta Y(f_n) \tag{7.8}$$

$n = m+1, \ldots, N$. f_n is the FFT frequency point. n is the index in the FFT. The first frequency point f_m is the border frequency point inside and outside of the frequency range of interest. N is the FFT index of the highest frequency point used in FFT. $\Delta Y(f_n)$ is obtained with the following recursive formulas:

$$\Delta Y(f_n) = 0.9 * \Delta Y(f_{n-1}), \qquad m+1 \le n \le N \tag{7.9}$$

The factor 0.9 is used to smooth the change of the parameter values outside the given frequency range. It is selected empirically.

Step 5: Take the inverse Fourier Transform of the frequency-domain parameters obtained in Step 4 and go back to Step 2.

In the procedure described above, the error $\Delta Y(f)$ is introduced into the iterative loop. Therefore, we call the method the error feedback based method. The flow chart in Figure 7.2 illustrates the iterative procedure.

Our numerical experience shows that the above iterations normally lead to the convergence. However, if the known parameters are not the frequency-domain parameters of causal parameters, the iterations may not converge. To deal with the problem, like in any other iterative methods, a prescribed number can be introduced into the iterations such that the computation will be terminated once the number of iterations exceeds the prescribed number. In the numerical examples later, the prescribed number is set to be 500 with errors in (7.4) set to be less than 1%.

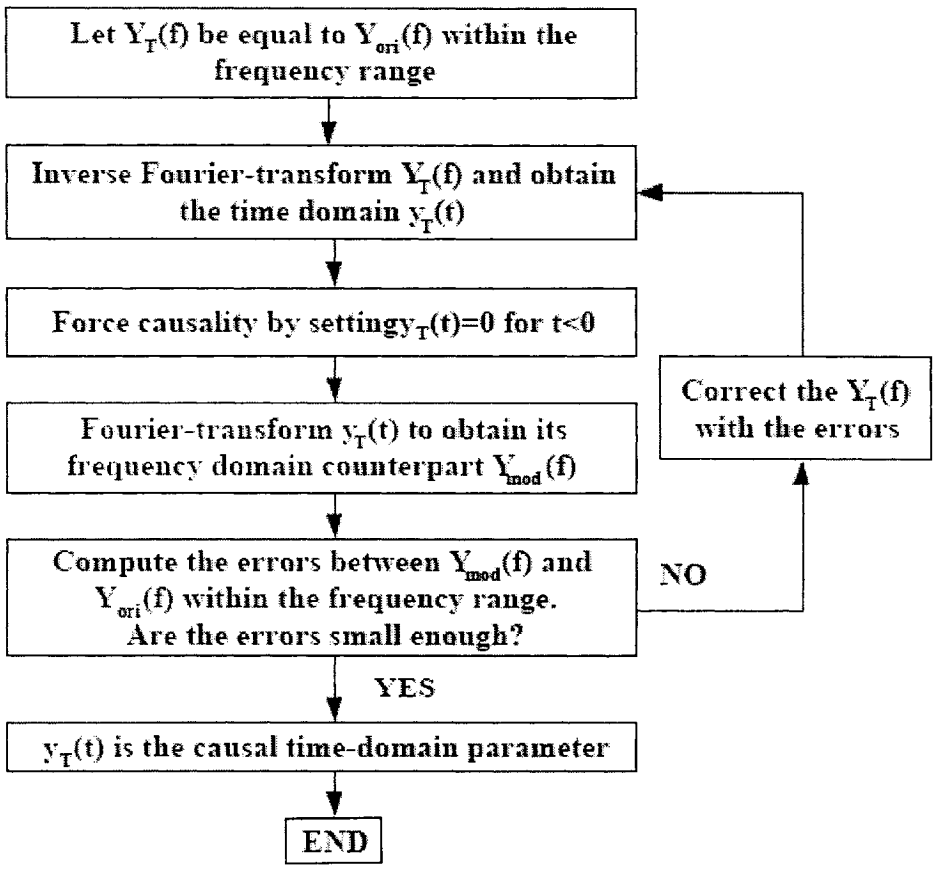

Figure 7.2 The flow chart of the error feed-back based FFT method.

7.3 The Hilbert Transform Based FFT Method

Hilbert transform can also be used with FFT to form another iterative method for extracting the causal time-domain parameters. For a real causal signal $y(t)$, let $Y(f)$ be its Fourier transform or the frequency-domain counterpart:

$$Y(f) = F\{y(t)\} \tag{7.10}$$

where $F\{\}$ represents the Fourier transform. Then the real part of $Y(f)$ and the imaginary part of $Y(f)$ should satisfy the following Hilbert transform relation [125]:

$$Y_r(f) = \frac{1}{\pi}\int_{-\infty}^{\infty}\frac{Y_i(f')}{f-f'}df' = \frac{1}{\pi f}\otimes Y_i(f) \tag{7.11}$$

$$Y_i(f) = -\frac{1}{\pi}\int_{-\infty}^{\infty}\frac{Y_r(f')}{f-f'}df' = -\frac{1}{\pi f}\otimes Y_r(f) \tag{7.12}$$

where $Y_r(f) = real(Y(f))$, $Y_i(f) = imag(Y(f))$ and $Y(f) = Y_r(f) + jY_i(f)$. $\otimes$ represents the convolution in the frequency-domain.

The inverse Fourier transform of $-\frac{j}{\pi f}$ is a sign function:

$$\text{sgn}(t) = \begin{cases} 1 & t > 0 \\ -1 & t < 0 \end{cases} \tag{7.13}$$

or simply,

$$-\frac{j}{\pi f} = F\{\text{sgn}(t)\} \tag{7.14}$$

Consequently, the Hilbert transform (7.11) and (7.12) can be rewritten as:

$$Y_r(f) = F\{F^{-1}\{\frac{-j}{\pi f}\otimes jY_i(f)\}\} \tag{7.15}$$

$$jY_i(f) = F\{F^{-1}\{\frac{-j}{\pi f}\otimes Y_r(f)\}\} \tag{7.16}$$

or,

$$Y_r(f) = F\{\text{sgn}(t)F^{-1}\{jY_i(f)\}\} \tag{7.17}$$

$$jY_i(f) = F\{\text{sgn}(t)F^{-1}\{Y_r(f)\}\} \tag{7.18}$$

With the application of FFT, equation (7.17) and (7.18) can be expressed as

$$Y_r(f) = FFT\{\text{sgn}(t)IFFT\{jY_i(f)\}\} \tag{7.19}$$

$$jY_i(f) = FFT\{\text{sgn}(t)IFFT\{Y_r(f)\}\} \tag{7.20}$$

The above relations are used as the basis for the iteration method; therefore, the method is named the Hilbert transform-based FFT method.

In the following paragraphs, the procedure for the Hilbert transform-based FFT method is described. To do so, let $Y_{ori\_r}(f)$ and $Y_{ori\_i}(f)$ be denoted again as the real and imaginary parts of the original frequency-domain $Y_{ori}(f) = Y_{ori\_r}(f) + jY_{ori\_i}(f)$ that is known over a finite frequency range of interest. The procedure involves five steps:

Step 1: Set $Y_r(f)$ to be equal to $Y_{ori\_r}(f)$ within the given frequency range and equal to zero outside the range. Use equation (7.20) to compute the imaginary part $Y_i(f)$ of the frequency-domain Y parameter

Step 2: Force $Y_i(f)$ to be equal to $Y_{ori\_i}(f)$ within the frequency range of interest. For the values outside the range, an extrapolation technique similar to that used in the previously discussed error feedback FFT method is applied. That is, $Y_i(f)$ outside the interest frequency range are updated with the recursive formula:

$$Y_i(f_n) = Y_i(f_n) - \Delta Y_i(f_n) \tag{7.21}$$

where $n = m+1, \ldots, N$. f_n is a FFT frequency point that lies outside the frequency range of interest. n is the FFT index. The first frequency point f_m is the border frequency point of the frequency range of interest. N is the FFT index of the highest frequency point used in FFT. $\Delta Y_i(f_n)$ is updated with the following recursive formulas:

$$\Delta Y_i(f_n) = 0.9 * (Y_i(f_n) - Y_i(f_{n-1})) \tag{7.22}$$

Note that $Y_i(f_n)$ in the right-hand side of (7.21) and (7.22) is the value obtained in the previous iteration. The factor 0.9 is used to smooth the change of the parameter values outside the given frequency range. It is selected empirically.

Step 3: Compute the causal time-domain parameter $y(t)$ and check the errors of its frequency-domain counterpart:

A) Store the values of $Y_r(f)$ in $Y_{r\_old}(f)$ as temporary values and use equation (7.19) to compute the new values $Y_{r\_new}(f)$.

B) Set $Y_r(f) = (Y_{r\_old}(f) + Y_{r\_new}(f))/2$ and take the inverse Fourier Transform of $Y(f) = Y_r(f) + jY_i(f)$ to obtain the corresponding time-domain parameter $y(t)$.

C) Force the causality into the obtained $y(t)$ by setting all the values to zero for $t < 0$ and then transform it back into the frequency-domain and obtain the corresponding frequency-domain parameter that becomes the new $Y(f) = Y_r(f) + jY_i(f)$.

D) Compute differences or errors between the frequency-domain parameter $Y(f)$ and the originally specified or given frequency-domain parameters $Y_{ori}(f)$ within the frequency range of interest. If the differences or errors are acceptably small, the time-domain parameters $y(t)$ are the causal time-domain parameters we can accept and the computations terminate here; otherwise, go to the next step.

Step 4: Force $Y_r(f)$ to be equal to $Y_{ori\_r}(f)$ within the frequency range of interest. To update the values outside the range, an extrapolation technique similar to that used in Step 2 is applied. That is, $Y_r(f)$ outside the interest frequency range are updated with the recursive formula:

$$Y_r(f_n) = Y_r(f_n) - \Delta Y_r(f_n) \tag{7.23}$$

where $n = m+1, \ldots, N$. f_n is a FFT frequency point that lies outside the frequency range of interest at the FFT index of n. The first frequency point f_m is the border frequency point of the frequency range of interest. N is the FFT index of the highest frequency point used in FFT. $\Delta Y_r(f_n)$ is obtained with the following recursive formulas:

$$\Delta Y_r(f_n) = 0.9 * (Y_r(f_n) - Y_r(f_{n-1})) \tag{7.24}$$

Note that $Y_r(f_n)$ in the right-hand side of (7.23) and (7.24) is the value obtained in the previous iteration. The factor 0.9 is used to smooth the change of the parameter values outside the given frequency range. It is selected empirically.

Step 5: Use equation (7.20) to compute the new $Y_i(f)$ and go to Step 2.

The factor 0.9 in step 2 and step 4 is used to smooth the change of the parameter values outside the given frequency range. It is a trial and empirical selection.

The error functions must be defined in Step 3 to assess the differences between the computed frequency-domain Y parameter and the prior-known or -specified frequency Y parameter within the frequency range of interest. In our case, we take following error functions, with the note that the other error functions can be used depending on a user's preference:

$$error1 = \frac{\max(|Y_r(f) - Y_{ori\_r}(f)|)}{\max(|Y_{ori\_r}(f)|)} \tag{7.25}$$

$$error2 = \frac{\max(|Y_i(f) - Y_{ori\_i}(f)|)}{\max(|Y_{ori\_i}(f)|)} \tag{7.26}$$

$$error = \max(error1, error2) \tag{7.27}$$

The iterative procedure above is illustrated by the flow chart in Figure 7.3. As

described above for the error feedback method, the above iterations should be halted if the computations cannot converge after the number of iterations becomes too large or exceeds a prescribed number. In our computations described in the following section, the pre-set number is 500 and the error in (7.27) is set to be less than 1%.

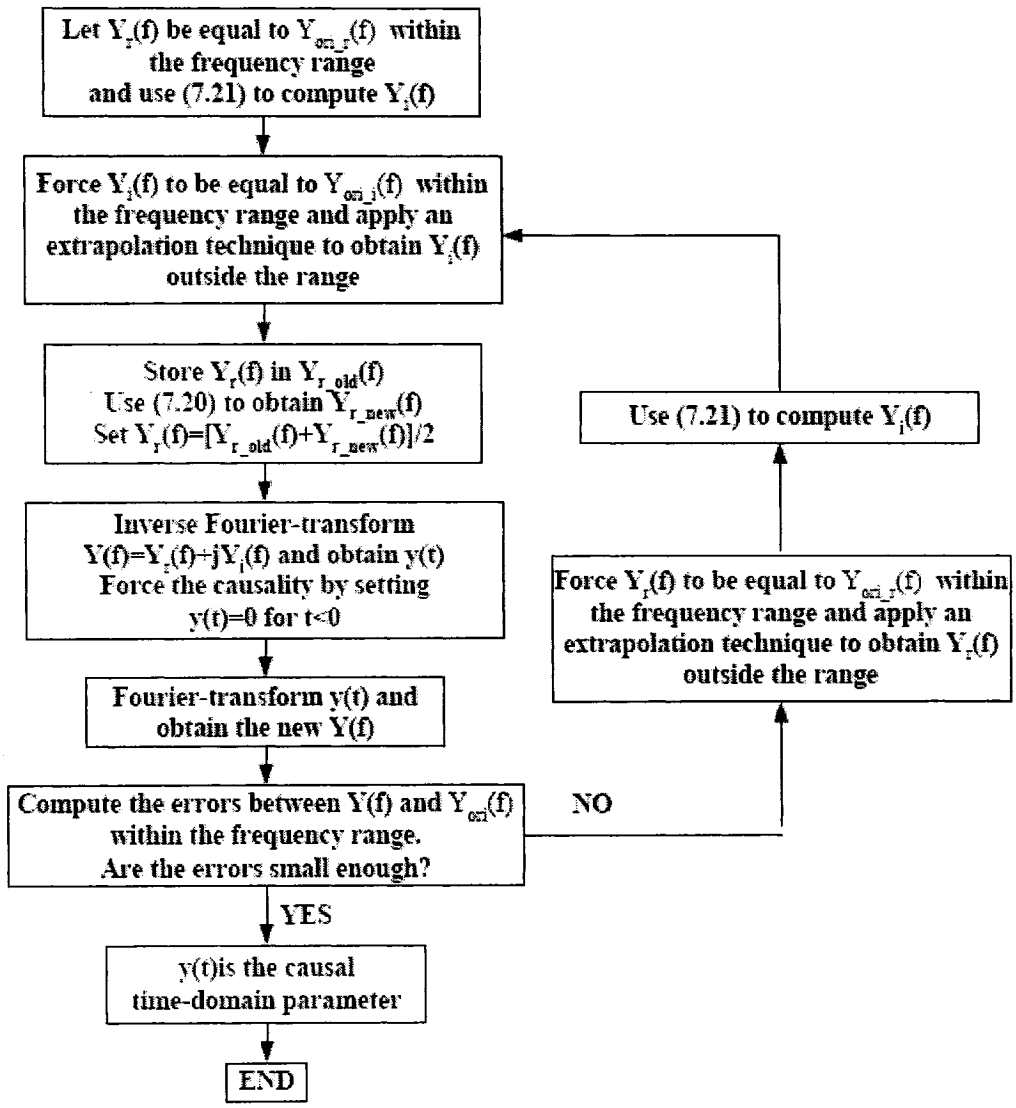

Figure 7.3 The flow chart of the Hilbert transform based FFT method.

7.4 Numerical Validation

To validate the two proposed methods, we first apply them to two theoretically known cases: a temporal triangular pulse and a temporal rectangular pulse with their spectra only partially known. Once the methods are proven valid, they are applied to a real FET amplifier.

A) Triangular pulse

The triangular pulse considered is expressed as follows:

$$y(t) = \begin{cases} 1 - \dfrac{|t-T|}{T} & |t| \le T \\ 0 & otherwise \end{cases} \tag{7.28}$$

where T = 0.1(ns) is the duration of the pulse in time. By taking the Fourier transform, a complete spectrum of the triangular pulse is obtained as

$$Y(f) = (Te^{-j2\pi fT})\frac{\sin^2(Tf)}{(Tf)^2} \tag{7.29}$$

The pulse has a finite duration in the time-domain but extends to infinity in frequency-domain.

Suppose now that $Y(f)$ is only given or known over 0Hz –6GHz. That is, we now have

$$Y(f) = \begin{cases} Te^{-j2\pi fT}\dfrac{\sin^2(Tf)}{(Tf)^2} & 0 \le f \le 6GHz \\ unknown & f > 6GHz \end{cases} \tag{7.30}$$

To extract the pulse in the time-domain with the above limited information, the simplest approach is to directly take the inverse Fourier transform of $Y(f)$ with assumption of $Y(f)$ being zero beyond 6GHz. The resulting time-domain signal is found to be not causal. To ensure the causality, one can simply cut off the time-domain values for t<0 (i.e. set the values for t<0 to be zero). We call the approach the *direct cut-off method*. The causal time-domain signal obtained with the direct cut-off method can be converted to the frequency-domain to check its spectrum. The results are shown in Figure 7.4, which demonstrates that there is a big difference between the computed spectrum

and the original value within the frequency range of 0-6GHz. The maximum relative error is nearly 100%.

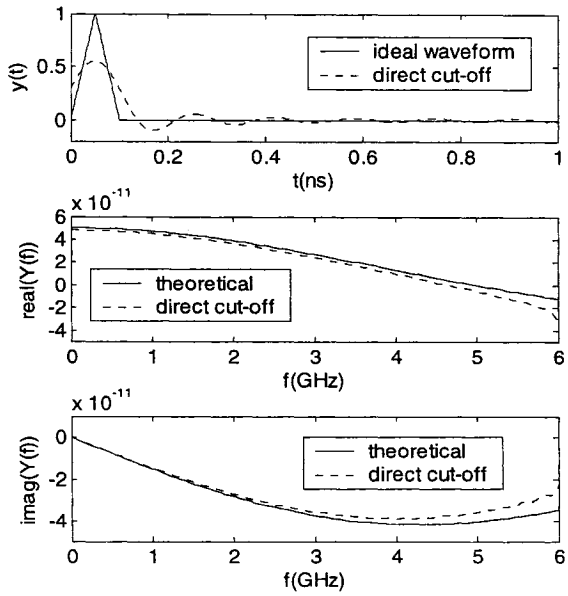

Figure 7.4 The time-domain pulse and its Fourier transform obtained with the direct cut-off method.

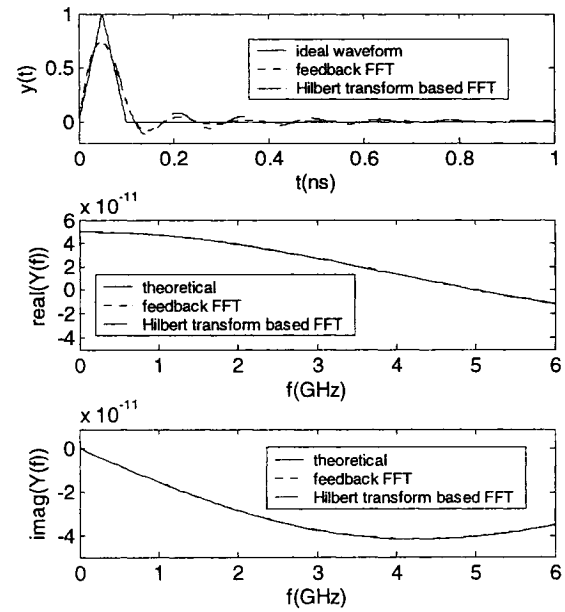

Figure 7.5 The time-domain waveforms and its spectra extracted with the proposed two iterative methods when the known frequency range is from 0 to 6GHz for the triangular pulse.

Now the two methods proposed in this chapter are applied. Figure 7.5 shows the results. Because the extracted time-domain signals are fully causal, their values for negative time are equal to zero and are not plotted in the figures for space limitation.

As can be seen, there is big difference between the extracted time-domain pulse and the original triangular pulse. The reason is that the proposed methods only warrant the frequency-domain parameters are close to the actual values within the given frequency range but not outside the given frequency range. The differences in the frequency-domain within the range of 0 to 6GHz are less than 1%.

B) Rectangular pulse

The second example of a rectangular pulse is defined as

$$y(t)=\begin{cases}1 & 0\le t\le T\\ 0 & otherwise\end{cases} \tag{7.31}$$

where T = 0.1(ns) is the duration of the pulse. Fourier transform of the rectangular pulse gives

$$Y(f)=Te^{-j\pi Tf}\frac{\sin(Tf)}{Tf} \tag{7.32}$$

Now suppose that $Y(f)$ is known only from 0 to 6GHz, application of the *direct cut-off approach* as described in the last section leads to the results shown in Figure 7.6.

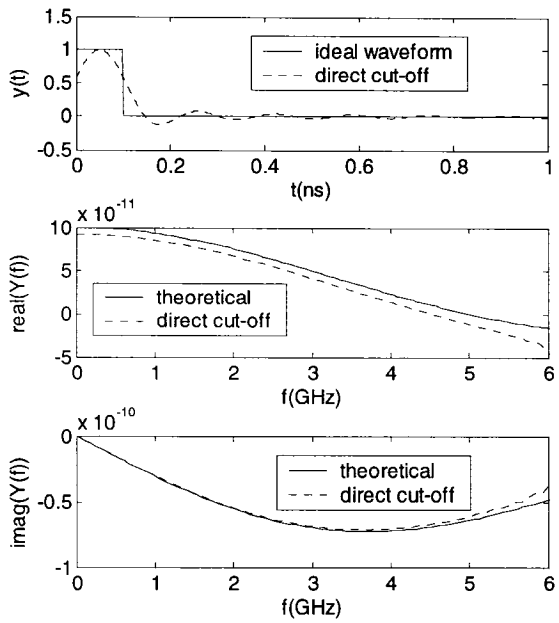

Figure 7.6 The time-domain waveform and its spectra extracted with the direct cut-off approach.

It can be seen from Figure 7.6 that the difference between the computed spectrum and the original value is large, especially the real part. However, the results from the proposed methods are much closer to the original values within the concerned frequency range of 0 to 6GHz. They are shown in Figure 7.7.

From the two examples relating to triangular and rectangular pulses, we can see that although the extracted time-domain pulses are different from the original shapes, the corresponding frequency spectra are very close to the original values within the concerned frequency range. Therefore, the extracted time-domain pulses shown in Figure 7.6 and Figure 7.7 can be used to adequately represent the original triangular and rectangular pulses in terms of the frequency range of interest.

In summarizing the above results, we can conclude that the proposed iterative methods are effective and useful in extracting time-domain signals from the given frequency-domain information in a *limited* frequency range of interest. The time-domain signals extracted as such are causal and can be used to represent the original pulses in light of the frequency range of interest.

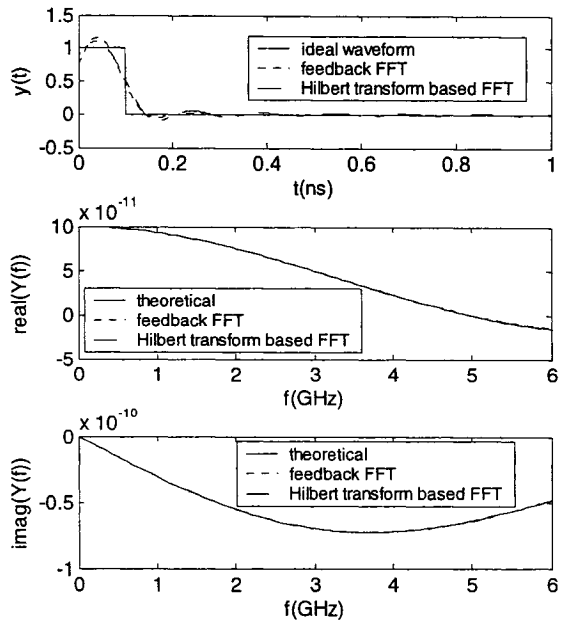

Figure 7.7 The time-domain waveforms and their spectra extracted with the two proposed iterative method methods when the known frequency range of interest is from 0Hz –6GHz for the rectangular pulse.

In the following section, we apply the proposed iterative methods to a linear FET amplifier.

C) FET amplifier

The FET amplifier used NE425S01 as its active device [121]. As indicated before, the S-parameters of the active device are given by the manufacturer only over the frequency range of 0.5GHz to 18GHz. They can be easily converted to the Y-parameters in the frequency-domain. Since the given frequency data is quite sparse and not suitable for FFT directly, the spline interpolation was applied.

Now the proposed methods are applied to extract the causal time-domain parameters of the device. Figure 7.8 and Figure 7.9 show that the extracted time-domain parameters are causal. The spectra of the extracted time-domain parameters and their comparisons with the original parameters are shown in Figure 7.10. The parameters extracted with the two methods are similar in general shapes in the time-domain but different in details. For example, $y_{11}(t)$ extracted with the Hilbert transform based FFT iterative method has one more small ripple at the initial time than the $y_{11}(t)$ extracted with the error feedback FFT

method. These differences can be attributed to the fact that the different values of $Y_{11}(f)$ outside the frequency range with the two methods.

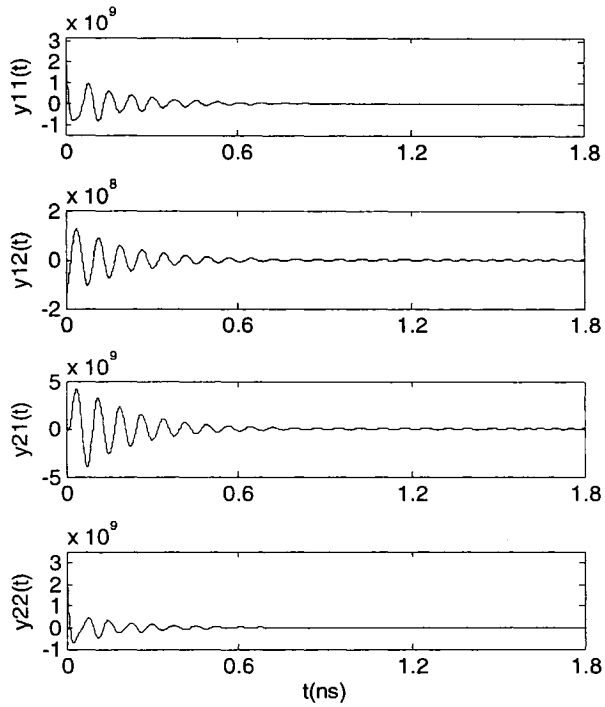

Figure 7.8 The time-domain Y-parameters extracted with the error feedback FFT method for the FET used in the amplifier.

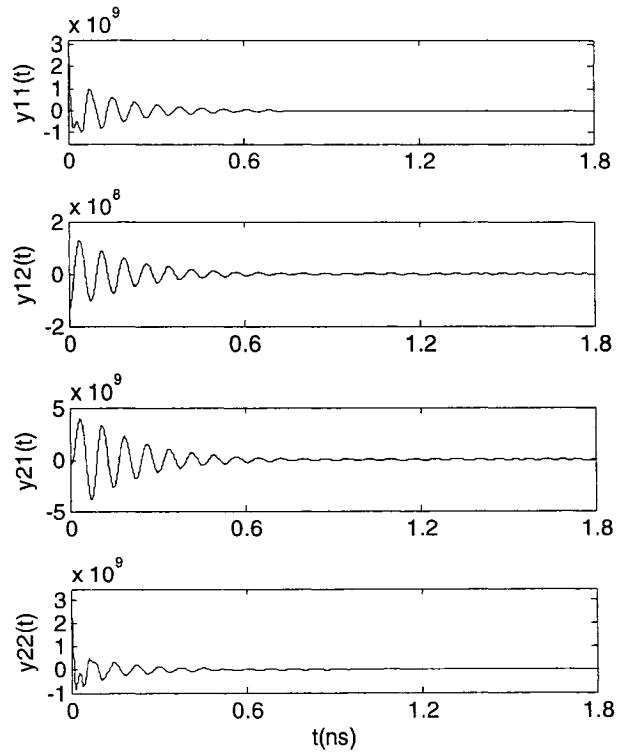

Figure 7.9 The time-domain Y-parameters extracted with the Hilbert transform based FFT method for the FET used in the amplifier.

Figure 7.11 shows the results of the S-parameters converted from the Y-parameters. As can be seen, the S-parameters extracted from the direct cut-off approach are vastly different from the original data but the results from the proposed methods are very close to the original data within the frequency range of interest with their time-domain counterparts being causal and compatible with the FDTD modeling.

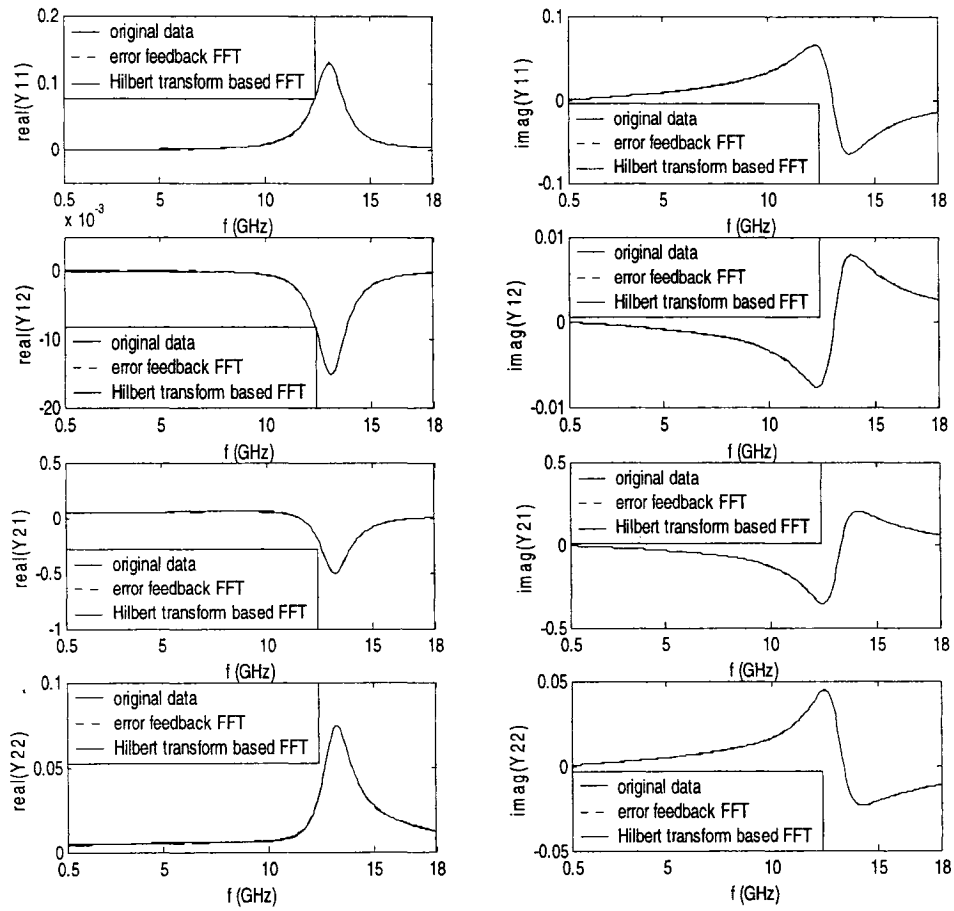

Figure 7.10 The Y-parameters in frequency-domain after using the iteration methods.

After the causal time-domain Y-parameters of the FET are obtained, they are included into an in-house time-domain simulator that is based on the modified central difference method (MCD) [126] for modeling the overall amplifier. Figure 7.12 shows the layout of the amplifier. The characteristic impedances of main transmission line TL1 and open-circuited stub line TL2 are both 50Ω. The phase velocities on TL1 and TL 2 are both 2.12535×10^{8} (m/s). The length of TL1 is 6.4(mm) and the length of TL2 is 3.6(mm).

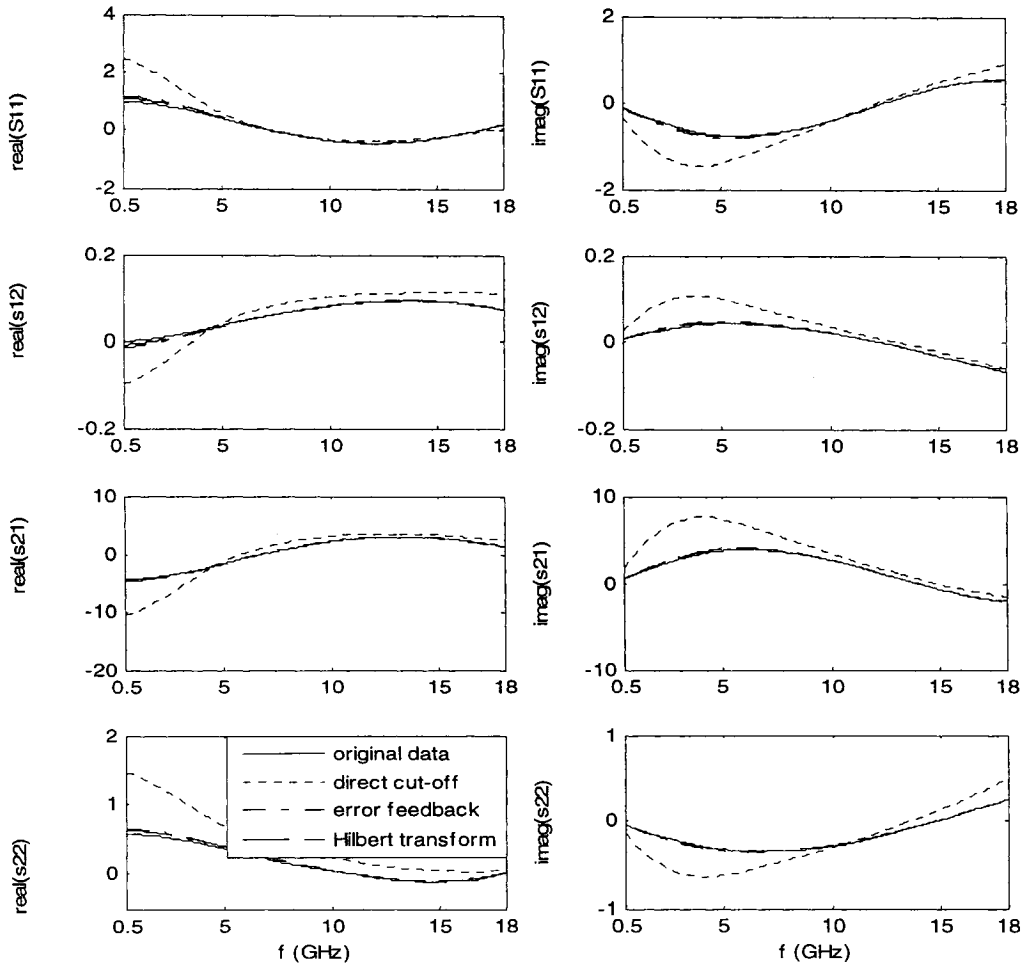

Figure 7.11 The S-parameters after using the iteration methods and direct cut-off.

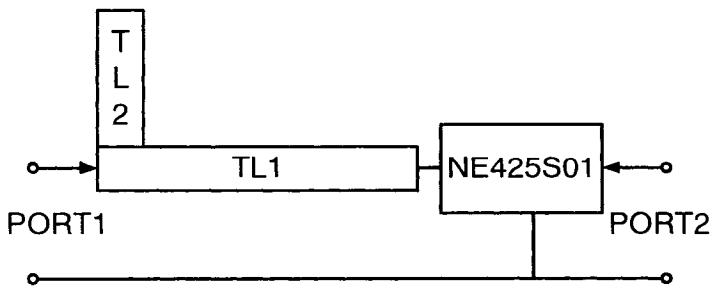

Figure 7.12 The Layout of the FET amplifier circuit.

Figure 7.13 is the computed overall S21 of the whole amplifier circuit. For reference, the Agilent Advanced System Design (a frequency-domain simulator) was also employed to simulate the circuit. The results are also plotted in Figure 7.13. As can be seen, the results from MCD that employs the extracted causal time-domain Y-parameters are very close to the results from ADS.

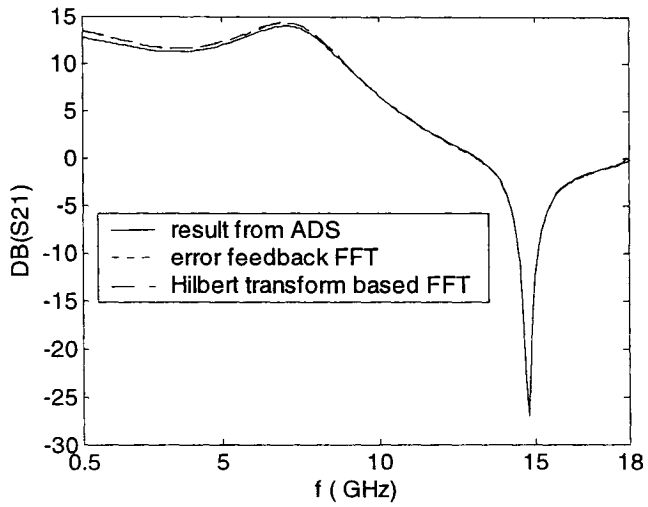

Figure 7.13 The computed S21 of the amplifier in Figure 7.10 from different methods.

7.5 Discussion and Conclusion

In this chapter, two iterative approaches were proposed for extracting causal time-domain parameters from their frequency-domain counterparts that are known only over a frequency range of interest. Both methods are shown to be effective and useful with a good degree of accuracy of less than 1%. The time-domain parameters extracted as such can be included in a time-domain simulator that has a stringent requirement for time causality.

It should be noted that the method described in this chapter can only be applied to small signal linear parameters. Extension to large signal nonlinear situations is the subject of future research.

8 Extraction of Causal Time-Domain Parameters Using Rational Function Approximation

8.1 Introduction

Network parameters of a lump-element device are usually given in a limited frequency band of interest, or an operation frequency range. To include them in time-domain simulations, they need to be converted to their causal time-domain counterparts. In chapter 7, two iterative methods were discussed. However, the resulting time-domain parameters are in numerical data format. The convolution with them in the time-domain is very time consuming for long simulations. In [127], various rational function fitting techniques except the vector fitting (VF) were discussed. In [128], the vector fitting was developed with the aim of better curve fitting of frequency-domain data, but only considered passive structures in frequency-domain.

In this chapter, we propose the use of the rational fitting technique to extract the causal time-domain parameters of a lumped device, in particular an active device, from their known band-limited frequency-domain counterparts. One of the major advantages of this approach is that the resulting time-domain parameters can be expressed in the form of exponential functions. The convolution with these exponential functions can then be performed in a recursive fashion without requiring a complete past history of the time-domain parameters. The CPU time for each time-marching step is constant, and the CPU time and memory can therefore be significantly reduced, especially for a simulation with a large number of iterations.

In the following sections, the proposed rational fitting technique is described and the recursive convolution is shown. Finally, a numerical example is presented to demonstrate its validity and effectiveness.

8.2 Causal Time-Domain Extraction With The Rational Fitting Technology

The objective in this section is to find rational functions in the frequency-domain that match the original parameters within the frequency range of interest. Suppose that

$Y(s)\big|_{s=j\omega}$ is an admittance parameter known at frequency points $\omega_n (n=1,2,...,NF)$ over a specified frequency range of interest. A rational function $\tilde{Y}$ is used to approximate Y. It should differ little or not at all from the original parameter $Y(s)\big|_{s=j\omega}$ on the known frequency points.

The rational function can then be expressed as [127]:

$$Y(s) \approx \tilde{Y}(s) = \frac{N(s)}{D(s)} \tag{8.1}$$

$$N(s) = a_0 + a_1 s + a_2 s^2 + ... + a_N s^N \tag{8.2}$$

$$D(s) = b_0 + b_1 s + b_2 s^2 + ... + b_N s^N \tag{8.3}$$

where $s = j\omega = j2\pi f$. a_i, $_{i=0,1,2,...,N}$ and b_i, $_{i=0,1,2,...,N}$ are the coefficients to be determined; N is the order of approximation and $(N+1)$ is not bigger than the number NF.

To find the coefficients a_i and b_i, one may force $\tilde{Y}(s)$ to be equal to the original parameter $Y(s)\big|_{s=j\omega}$ at the given or known NF frequency points f_n. That is,

$$\tilde{Y}(s)\big|_{s=s_n} = Y(s)\big|_{s=s_n} \tag{8.4}$$

or

$$Y(s)\big|_{s=s_n} \bullet D(s)\big|_{s=s_n} - N(s)\big|_{s=s_n} = 0, \tag{8.5}$$

with $s_n = j\omega_n = j2\pi f_n$ and $n=1,2,..., NF$.

Equation (8.5) contains NF complex equations, or equivalently, $2NF$ real equations. However, equation (8.5) is homogeneous. An additional condition is needed to make (8.5) inhomogeneous so the solutions will not be trivial. To do so, we can set $b_N = 1$ [127]. As long as $(N+1) < NF$ is set, the remaining $(2N+1)$ coefficients can then be solved by using the least squares technique.

After the coefficients are found, the rational function is determined. To obtain the corresponding time-domain expression, the poles of the rational function need to be decided. Many software packages can be used. In our case, MATLAB was employed. Once all the poles are found, $\tilde{Y}(s)$ can be rewritten as:

$$\tilde{Y}(s) = \sum_{n=1}^{N} \frac{R_n}{s - \gamma_n} + k_0 \tag{8.6}$$

where γ_n is the pole and R_n is the residue of $\tilde{Y}(s)$ at $s = \gamma_n$.

In order to ensure the stability of the time-domain counterpart of $\tilde{Y}(s)$ and to express it in an exponential form, any poles that are in the right half s-plane need to be removed or flipped to the left half plane, followed by a refitting of the residues.

Although the above procedure appears theoretically feasible, there are two drawbacks in practice: first, the process may suffer from numerical problems such as ill-conditioning of the system matrix for high-order approximations, and secondly, multiplication with the denominator in (8.5) may result in a frequency-domain weighting that induces large errors or limits the method to a low-order approximation when the frequency range is wide. To overcome these problems, the vector fitting proposed in [128] is then applied. The procedure is summarized below.

Suppose $\bar{a}_n$, $_{n=1,2,...,M}$ are the poles in the left half s-plane after the poles of (8.6) in the right half s-plane are discarded. The resulting $\tilde{Y}(s)$ becomes:

$$\tilde{Y}(s) \approx \sum_{n=1}^{M} \frac{R'_n}{s - \bar{a}_n} + k_0 \tag{8.7}$$

where R'_n is the residue of $\tilde{Y}(s)$ at $s = \bar{a}_n$.

Let $\bar{a}_n$, $_{n=1,2,...,M}$ be the starting poles. Then the following three steps are taken:

Step #1: an unknown auxiliary function $\sigma(s)$ is introduced and $\sigma(s)$ and $\sigma(s)Y(s)$ are approximated with rational functions with the poles $\bar{a}_n$, $_{n=1,2,...,M}$:

$$\sigma(s)Y(s) \approx \sum_{n=1}^{M} \frac{c_n}{s - \bar{a}_n} + d = d \frac{\prod_{n=1}^{M} (s - z_n)}{\prod_{n=1}^{M} (s - \bar{a}_n)} \tag{8.8}$$

$$\sigma(s) = \sum_{n=1}^{M} \frac{\tilde{c}_n}{s - \bar{a}_n} + 1 = \frac{\prod_{n=1}^{M} (s - \tilde{z}_n)}{\prod_{n=1}^{M} (s - \bar{a}_n)} \tag{8.9}$$

where c_n, $\tilde{c}_n$, and d are the unknown coefficients to be found. z_n and $\tilde{z}_n$ are the zeros of

$\sigma(s)Y(s)$ and $\sigma(s)$, respectively. They can be found once c_n, $\tilde{c}_n$, and d are determined.

Equation (8.9) is then multiplied with the original $Y(s)$ and the resulting equation is set equal to (8.8):

$$\sum_{n=1}^{M}\frac{c_n}{s-\bar{a}_n}+d\approx[\sum_{n=1}^{M}\frac{\tilde{c}_n}{s-\bar{a}_n}+1]Y(s) \tag{8.10}$$

Equation (8.10) is enforced at the known frequency points and solved for c_n, $\tilde{c}_n$ and d with the least squares techniques.

Step #2: (8.8) is divided with (8.9) :

$$Y(s)\approx d\frac{\prod_{n=1}^{M}(s-z_n)}{\prod_{n=1}^{M}(s-\tilde{z}_n)} \tag{8.11}$$

Equation (8.11) shows that the poles of $Y(s)$ are equal to the zeros of $\sigma(s)$ in (8.9), which can be calculated from the solution of (8.10) by solving an eigenvalue problem [128].

Step #3: If $Y(s)\big|_{s=j\omega}$ obtained in (8.11) is not sufficiently close to the original parameters within the frequency range of interest, $\bar{a}_n$ is replaced with $\tilde{z}_n$ and another iteration can be started by going back to Step #1.

The final approximating function can be rewritten in the following form:

$$Y(s)\approx\tilde{Y}(s)=\sum_{i=1}^{M}\frac{r_i}{s-p_i}+\alpha \tag{8.12}$$

where r_i is the residue at pole p_i. α is a constant.

Using the inverse Laplace transform [129], the time-domain form of (8.12) can be expressed as:

$$y(t)\approx\tilde{y}(t)=\alpha\delta(t)+u(t)\sum_{i=1}^{M}r_i e^{p_i t} \tag{8.13}$$

where $\delta(t)$ is the Dirac Delta function and $u(t)$ is the unit step function that ensures the causality. $\tilde{y}(t)$ is the causal time-domain representation of the original parameter $Y(s)\big|_{s=j\omega}$.

Since (8.13) is in exponential form in the time-domain, its convolution in time-domain can be computed very efficiently in a recursive fashion [130][131]. More specifically, a current $i(t)$ can be found as:

$$\begin{aligned} i(t)|_{t=k\Delta t} &= [y(t) \otimes v(t)]|_{t=k\Delta t} \\ &\approx [\tilde{y}(t) \otimes v(t)]|_{t=k\Delta t} \\ &= \alpha v(t)|_{t=k\Delta t} + \sum_{i=1}^{M} r_i \psi_i(t)|_{t=k\Delta t} \end{aligned} \tag{8.14}$$

where $v(t)$ is a voltage , $\otimes$ is the convolution in time-domain, Δt is the time step used in a time-domain simulator and k is the iteration number, and

$$\begin{aligned} \psi_i(t)|_{t=k\Delta t} &= [e^{p_i t} \otimes v(t)]|_{t=k\Delta t} \\ &= e^{p_i \Delta t} \psi_i(t)|_{t=(k-1)\Delta t} \\ &\quad + \int_{(k-1)\Delta t}^{k\Delta t} e^{p_i (k\Delta t - \tau)} v(\tau) d\tau \end{aligned} \tag{8.15}$$

By using the trapezoidal rule, the integration in the above equation can be numerically evaluated as:

$$\begin{aligned} &\int_{(k-1)\Delta t}^{k\Delta t} e^{p_i (k\Delta t - \tau)} v(\tau) d\tau \\ &\approx \frac{\Delta t}{2} [e^{p_i \Delta t} v(t)|_{t=(k-1)\Delta t} + v(t)|_{t=k\Delta t}] \end{aligned} \tag{8.16}$$

The above recursive convolution takes a total of $3 \cdot M \cdot k$ additions and $(4M+1) \cdot k$ multiplications to reach the *k-th* time step (i.e. the computation time for each time step is constant), while the numerical convolution involving a whole past history of a parameter needs $0.5 \cdot k \cdot (k-1)$ additions and $0.5 \cdot k \cdot (k+3)$ multiplications (i.e. the computation time for each time step increases with the iteration number). In other words, the computation time with the recursive convolution is proportional to the number of iteration, while the regular convolution is proportional to the square of the number of iterations. That is, for a simulation with a large number of iterations, the computation time with the recursive convolution will be much smaller than that with the regular convolution.

8.3 Numerical Validation

In order to verify the efficiency of the proposed method, it is tested with the same amplifier shown in Figure 7.12 in chapter 7. As in chapter 7, the frequency-domain Y parameters of the FET transistor need to be converted into causal time-domain Y parameters. In this case, N in (8.1) is taken to be 12 for Y11(f), Y12(f), Y21(f), and Y22(f). The number of frequency points provided by the manufacturer is NF =21. The computed poles for the rational approximations of Y11(f), Y12(f), Y21(f), and Y22(f), before the application of the vector fitting as expressed by (8.7), are shown in Table 8-1. The poles, residues, and the constant term α, after application of the vector fitting as shown in (8.12), are listed in Table 8-2 and Table 8-3.

The frequency-domain differences between the Y-parameters obtained with the proposed method and the original data are less than 1.3% within the frequency range of interest. The difference or error is defined by:

$$error1 = \frac{\max(|Y_r(f) - Y_{ori\_r}(f)|)}{\max(|Y_{ori\_r}(f)|)} \tag{8.17}$$

$$error2 = \frac{\max(|Y_i(f) - Y_{ori\_i}(f)|)}{\max(|Y_{ori\_i}(f)|)} \tag{8.18}$$

$$error = \max(error1, error2) \tag{8.19}$$

where max means the maximum value within the frequency range of interest. $Y_{ori\_r}(f)$ and $Y_{ori\_i}(f)$ are the real part and imaginary part of the original frequency-domain data. $Y_r(f)$ and $Y_i(f)$ are the real part and imaginary part of the rational approximation data.

Figure 8.1 shows the causal time-domain Y-parameters obtained with the proposed technique ($\alpha\delta(t)$ term is not plotted for clarity), while Figure 8.2 shows their frequency-domain correspondents that includes the $\alpha\delta(t)$ term. For comparison, the original data are also plotted on the same figure. For further validations, the corresponding S-parameters are also compared in Figure 8.3

As can be seen, the parameters obtained with the proposed method are basically overlapping the manufacturer's data, while the results obtained with the direct cut-off

method show significant differences within the frequency range of 0.5GHz to 18GHz. Therefore, we conclude that the causal time-domain responses represented in an exponential form by (8.13) are valid and can be used to model the FET in the time-domain, with little frequency-domain information inaccuracy.

Once the causal representation of the Y-parameters of the FET are obtained with the proposed method, they can be put into a FDTD based simulator for modeling the overall amplifier as shown in Figure 7.12. In our case, the modified central difference method (MCD) [126] was employed in constructing the simulator. Figure 8.4 is the computed overall S21 of the amplifier. For reference, the Agilent Advanced System Design was employed to simulate the circuit. The results are also plotted in Figure 8.4. As can be seen, the two curves are very.

Table 8-1 The initial poles (Hz) of Y11, Y12, Y21, and Y22 as in (8.7)

$Y_{11}(f)$	$Y_{12}(f)$	$Y_{21}(f)$	$Y_{22}(f)$
-1.6390e+08 ±j1.0627e+11	-2.1594e+08 ±j1.0652e+11	-2.2991e+06 ±j1.1302e+11	-9.7073e+07 ±j1.0656e+11
-2.6371e+08 ±j9.6443e+10	-2.8411e+08 ±j9.7359e+10	-1.7657e+06 ±j1.0639e+11	-1.5727e+08 ±j9.7509e+10
-7.8294e+08 ±j8.5994e+10	-6.4923e+08 ±j8.6824e+10	-9.5890e+07 ±j9.6994e+10	-5.8508e+08 ±j8.6887e+10
-2.3385e+08 ±j7.8650e+10	-3.4879e+08 ±j7.9242e+10	-5.5625e+08 ±j8.6497e+10	-3.4192e+08 ±j7.9307e+10
	-8.9298e+07 ±j6.5207e+10	-3.3949e+08 ±j7.9156e+10	
		-6.9017e+06 ±j6.5179e+10	

Table 8-2 The final poles and residuals of Y11, Y12, Y21, and Y22 as in (8.12)

Y11(f)		Y12(f)	
Poles (Hz)	Residues (Hz)	Poles (Hz)	Residues (Hz)
-3.9005e+10	7.2486e+07	-4.6629e+09 ±j6.3163e+10	1.9162e+05 ±j4.8670e+05
-2.7216e+11	-8.8473e+09	-1.2964e+10 ±j6.9695e+10	1.6009e+06 ∓j2.2171e+06
-6.1162e+09 ±j 6.2023e+10	-5.1316e+06 ∓j3.0844e+06	-2.2396e+09 ±j7.4970e+10	1.6074e+05 ±j 4.1186e+04
-6.5318e+09 ±j 7.4647e+10	-3.8004e+06 ±j2.9213e+06	-5.1509e+09 ±j8.2227e+10	-7.9590e+07 ∓2.1019e+06
-5.1854e+09 ±j 8.2233e+10	6.7926e+08 ∓j4.1983e+07	-6.4961e+09 ±j1.3625e+11	-4.1183e+06 ∓j1.1193e+07
Y21(f)		Y22(f)	
Poles (Hz)	Residues (Hz)	Poles (Hz)	Residues (Hz)
-3.4487e+09 ±j4.2532e+10	6.7096e+06 ∓j1.3006e+06	-2.5779e+10 ±j4.5645e+10	4.9684e+06 ±j5.2463e+07
-7.3245e+09 ±j6.3089e+10	3.7669e+07 ∓j8.6430e+06	-1.0385e+10 ±j6.7829e+10	-8.8947e+06 ±j4.6101e+05
-1.3942e+09 ±j6.9142e+10	4.9240e+06 ±j2.3011e+04	-5.2475e+09 ±j8.2188e+10	3.2774e+08 ±j1.3077e+08
-1.8947e+10 ±j7.5759e+10	1.5974e+08 ±j1.7481e+08	-6.6450e+09 ±j1.1915e+11	-2.4210e+07 ±j2.1270e+07
-5.1568e+09 ±j8.2266e+10	-2.8295e+09 ∓j8.0159e+08		
-6.9454e+10 ±j1.0174e+11	2.0019e+09 ∓j1.3756e+09		

Table 8-3 The constant term of Y11, Y12, Y21, and Y22 as in (8.12)

	Y11(f)	Y12(f)	Y21(f)	Y22(f)
α	2.6856e-002	-1.3213e-004	8.8978e-003	1.2232e-002

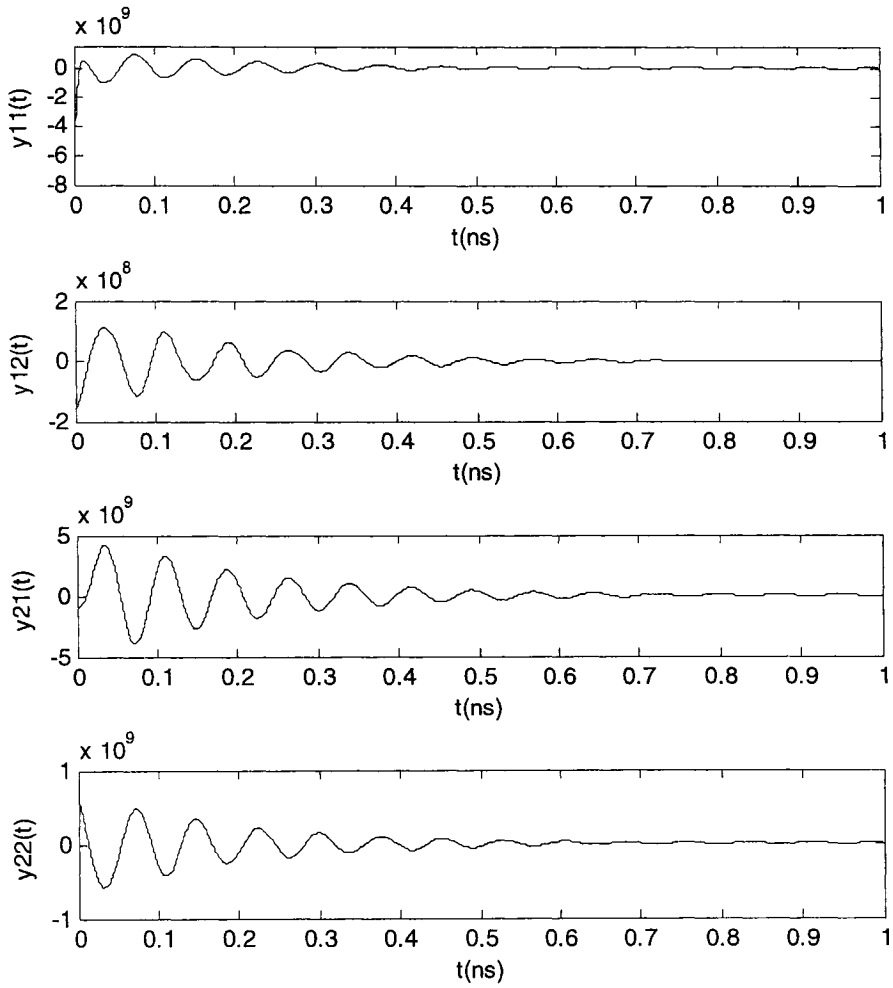

Figure 8.1 The Y-parameters in the time-domain corresponding to Table 8-2 and (8.13) but without the $\alpha\delta(t)$ term.

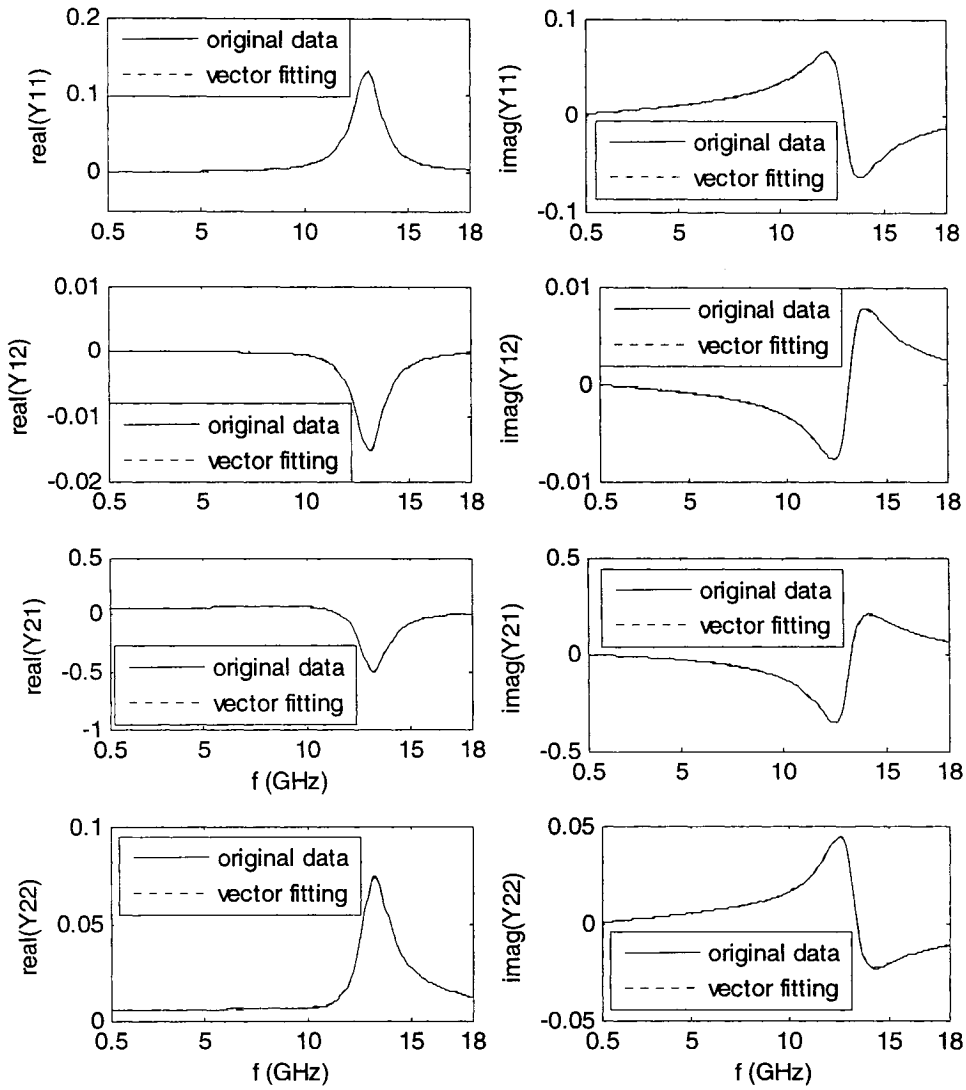

Figure 8.2 The Y-parameters in the frequency-domain obtained with the proposed.

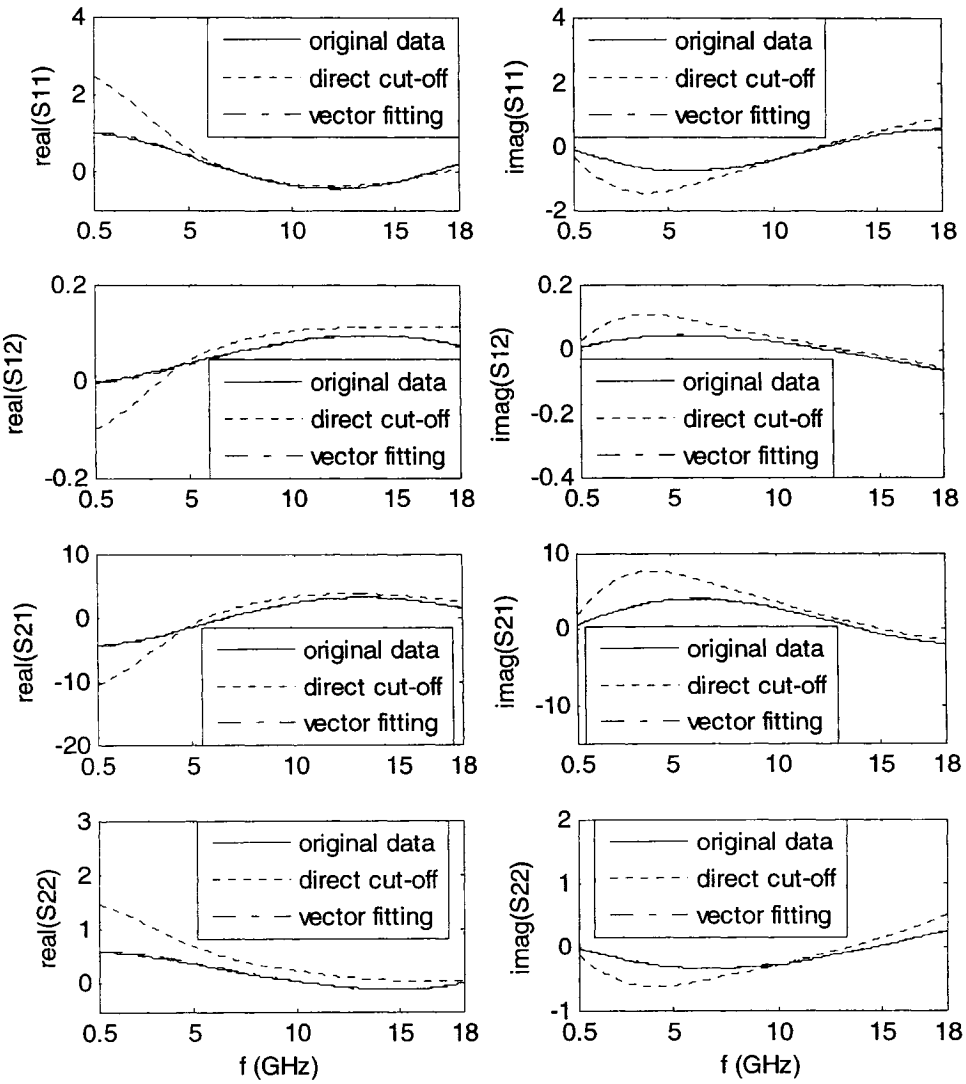

Figure 8.3 S-parameters in the frequency-domain obtained with the proposed method and direct cut-off.

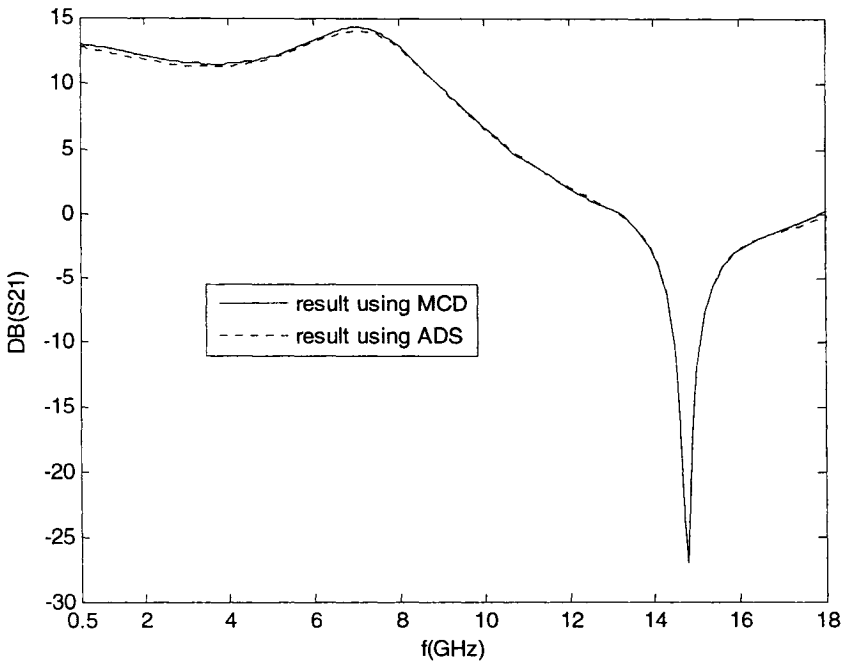

Figure 8.4 The overall S21 of the amplifier.

To show the advantage of the proposed method in convolution, Figure 8.5 demonstrates the computation time versus the number of iterations using recursive convolution formulas. For comparison, the CPU time using non-recursive convolutions is also plotted. As can be seen, the total computation time with recursive convolution using (8.14) and (8.15) is proportional to the number of iterations (i.e., the CPU time for every time-marching step of the MCD computation is the same). However, the computation time with non-recursive convolution is proportional to the square of the number of time-marching steps (i.e., the CPU time for an MCD time-marching step is increased as the number of time-marching steps increases). In other words, as the number of time-marching steps becomes larger and larger, the computation with non-recursive convolutions becomes slower and slower and will eventually come to stand-still. When the number of MCD time-marching steps reaches the order of 10^5, the saving in CPU time with the recursive convolutions is approximately thirty times.

Nevertheless, from observing Figure 8.5, one can see that there is a threshold of the number of time-marching steps when the recursive convolution starts to use less computation time than the non-recursive convolutions. This is because at the beginning,

non-recursive convolutions only involve a short history of data while the recursive convolutions always involve M terms (see (8.14)). In this case, the threshold number is approximately 1500.

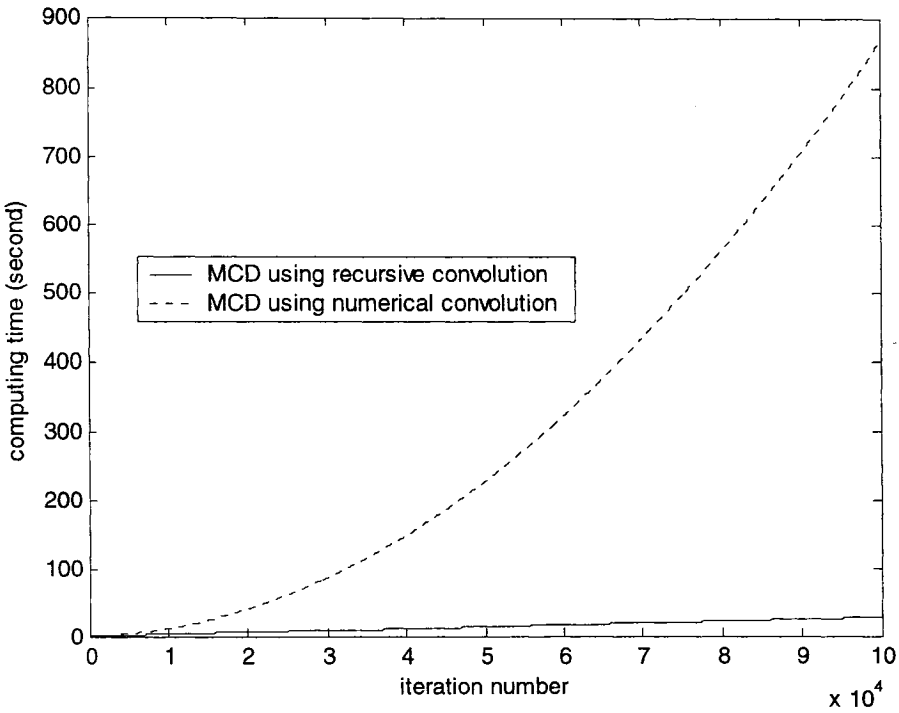

Figure 8.5 The computation time versus the number of iterations for the amplifier.

8.4 Conclusion

In this chapter, a method using rational approximation was proposed for extracting casual time-domain network parameters. It results in a time-domain parameter in an exponential form, which leads to an efficient recursive time-domain convolution computation. The saving in the CPU time in comparison with the non-recursive convolutions can be tens, hundreds and even thousands of times, depending on the number of time-marching steps. Numerical examples have been provided to numerically verify the effectiveness and accuracy of the proposed method.

It should be noted that the method described in this chapter can only be applied to small signal linear parameters. Extension to large signal nonlinear situations is the subject of future research.

9 Conclusion and Future Work

9.1 Summary

The FDTD method is one of the most flexible and powerful numerical time-domain techniques to be widely used to simulate complex electromagnetic systems and RF/microwave circuits, including passive structures and active devices. The focus of this work can be divided into two parts: the first relates to bringing about some improvements to the FDTD method and the second relates to time-domain modeling of active device.

In order to improve the efficiency of the FDTD method, four methods were proposed. First, in chapter 3 a new compact 2D FDTD method was proposed, which can reduce a 3D waveguide problem into a 2D problem that is uniform in one of the transverse directions. Second, a compact 1D FDTD method was proposed in chapter 4 that can be used as incident wave generators and modal absorbing boundary conditions in uniformly filled waveguides. Third, a new 1D modal PML was proposed in chapter 5 that utilizes the proposed 1D FDTD formula to reduce the 3D PML into a 1D modal PML. Finally, a new 2D FDTD subgridding method was proposed in chapter 6 that is not only stable and simple, but also has low reflections.

When the FDTD method is used to analyze RF/microwave circuits with element active devices, it needs to convert the frequency-domain parameters into time-domain parameters because the network parameters of many element active devices are given by the manufactures or measured in frequency-domain and are band-limited. In order to extract the causal time-domain parameters from the band-limited frequency-domain parameters, three methods were proposed.

First two iterative methods based on FFT were proposed in chapter 7: one uses the negative feedback and another uses the Hilbert transform technique. Then, the rational function fitting technique was used to obtain a time-domain model from the band-limited frequency-domain in chapter 8. The time-domain model obtained from the iterative methods is in numerical data format, while the time-domain model extracted from the rational function fitting is in exponential function form.

When the extracted time-domain model are used in the time-domain simulator, for example, FDTD, there exists time-consuming numerical convolution with these extracted time-domain parameters. Because the convolution with the exponential function can be realized very efficiently by a recursive form, the time-domain model extracted from rational function fitting is more useful. However, the rational function fitting technique has some limitation on applicable functions, the shape of target function must be suitable for the rational function approximation; while the iterative methods do not have this limitation.

9.2 Future Work

There are some aspects for methods proposed in this thesis that are worthy of further research:

a) For the compact 2D FDTD method, only a few simple examples were used. The next step can use this method in the optimum design of waveguide devices. A comprehensive analytical study of its stability condition and numerical dispersion relationship is also needed.

b) For the compact 1D FDTD method and the 1D modal PML, hybrid absorbing boundary conditions can be obtained by using the proposed 1D methods to absorb a few of the lower order modes and the traditional PML to absorb the other higher order modes.

c) For the 2D FDTD subgridding method, further study on the extension to 3D FDTD and on the sensitivity of α on different structures is needed.

d) The three methods in chapter 7 and 8 can only be used for time-domain modeling of active devices in small signal situations. However, active devices can also work in a large signal mode such as a transistor in a power amplifier or mixer. Further study is needed to extend these methods to time-domain large signal modeling.

References:

[1] Harrington, R. F., *Field Computation by Moment Methods*, The Macmillan Co., New York, 1968.

[2] Amitay, N. and Galindo, V., "On Energy Conservation and the Method of Moments in Scattering Problems," *IEEE Trans. Antennas and Propagat.*, vol. 17, pp. 747–751, Nov. 1969.

[3] Rahmat-Samii, Y. and Mittra, R., "Integral equation solution and RCS computation of a thin rectangular plate," *IEEE Trans. Antennas Propagat.*, vol. 22, pp. 608-610, July 1974.

[4] Davis, W. A. and Mittra, R., "A new approach to the thin scatterer problem using the hybrid equations," *IEEE Trans. Antennas and Propagat.,* vol. 25, pp.402-406, May 1977.

[5] Newman, E. H. and Pozar, D. M., "Electromagnetic Modeling of Composite Wire and Surface Geometries," *IEEE Trans. Antennas and Propagat.*, vol. 26, pp. 784–789, Nov. 1978.

[6] Sarkar, T. K., "A Note on the Choice Weighting Functions in the Method of Moments," IEEE Trans. Antennas and Propagat., vol. 33, pp. 436-441, April 1985.

[7] Ney, M. M., "Method of Moments as Applied to Electromagnetic Problems," *IEEE Trans. Microwave Theory Tech.,* vol. 33, pp. 972-980, Oct. 1985.

[8] Newman, E. H., "TM and TE Scattering by a Dielectric/Ferrite Cylinder in the Presence of a Half-plane," IEEE Trans. Antennas Propagat., vol. 34, pp. 804-813, June 1986.

[9] Leviatan, Y., Hudis, E. and Einziger, P. D., "A Method of Moments Analysis of Electromagnetic Coupling Through Slots Using a Guassian Beam Expansion," IEEE Trans. Antennas Propagat., vol. 37, pp. 1537-1544, Dec. 1989.

[10] Goggans, P. M. and Shumpert, T. H., "CFIE MM Solution for TE and TM Incidence on a 2-D Conducting Boday with Dielectric Filled Cavity," IEEE Trans. Antennas Propagat., vol. 38, pp. 1645-1649, Oct. 1990.

[11] Peters, M. E. and Newman, E. H., "Method of Moments Analysis of Anisotropic

Artificial Media Composed of Dieletric Wire Objects," IEEE Trans. Microwave Theory Tech., vol. 43, pp. 2023-2027, Sept. 1995.

[12] Khalil, A. I., Yakovlev, A. B. and Steer, M. B., "Efficient Method-of-Moments Formulation for the Modeling of Planar Conductive Layers in a Shielded Guided-Wave Structure," IEEE Trans. Microwave Theory Tech., vol. 47, pp. 1730-1736, Sept. 1999.

[13] Li, J. and Li, L., "Electromagnetic Scattering by a Mixture of Conducting and Dielectric Objects: Analysis Using Method of Moments," IEEE Trans. Microwave Theory Tech., vol. 53, pp. 514-520, Mar. 2004.

[14] Yuceer, M., Mautz, J. R. and Arvas, E., "Method of Moments Solution for the Radar Cross Section of a Chiral Body of Revolution," IEEE Trans. Antennas Propagat., vol. 53, pp. 1163-1167, Mar. 2005.

[15] Ubeda, E. and Rius, J. M., "Novel Monopolar MFIE MoM-Discretization for the Scattering Analysis of Small Objects," IEEE Trans. Antennas Propagat., vol. 54, pp. 50-57, Jan. 2006.

[16] Rao, S., Wilton, D. and Glisson, A., "Electromagnetic scattering by surfaces of arbitrary shape," IEEE Trans. Antennas Propagat., vol. 30, No. 3, pp. 409-418, May 1982.

[17] Weimin, S. and Balanis, C. A., "MFIE analysis and design of ridged waveguides," IEEE Trans. Microwave Theory Tech., vol. 41, No. 11, pp. 1965-1971, Nov. 1993.

[18] Huddleston, P., Medgyesi-Mitschang, L. and Putnam, J., "Combined field integral equation formulation for scattering by dielectrically coated conducting bodies," IEEE Trans. Antennas Propagat., vol. 34, No. 4, pp. 510-520, April 1986.

[19] Hubing, T. H., Survey of Numerical Electromagnetic Modeling Techniques, Report Number TR91-001.3, University of Missouri-Rolla, EMC Laboratory, 1991.

[20] Winslow, A. M., "Magnetic field calculations in an irregular triangular mesh," Lawrence Radiation Laboratory, Livermore, California, UCRL-7784-T, Rev. 1, 1965.

[21] Silvester, P., "A General High-Order Finite-Element Analysis Program Waveguide," IEEE Trans. Microwave Theory Tech., vol. 17, No. 4, pp. 204-210, Apr 1969.

[22] Chari, M. V. K., Bedrosian, G., D'Angelo, J. and Konrad, A., "Finite element applications in electrical engineering," IEEE Transactions on Magnetics, vol. 29, No. 2, pp. 1306-1314, Mar 1993.

[23] Daly, P., "Hybrid-Mode Analysis of Microstrip by Finite-Element Methods," IEEE Trans. Microwave Theory Tech., vol. 19, No. 1, pp. 19-25, Jan. 1971.

[24] Hara, M., Wada, T., Fukasawa, T. and Kikuchi, F., "A three dimensional analysis of RF electromagnetic fields by the finite element method," IEEE Transactions on Magnetics, vol. 19, No. 6, pp. 2417-2420, Nov. 1983.

[25] Hano, M., "Finite-Element Analysis of Dielectric-Loaded Waveguides," IEEE Trans. Microwave Theory Tech., vol. 32, No.10, pp. 1275-1279, Oct. 1984.

[26] Angkaew, T., Matsuhara, M. and Kumagai, N., "Finite-Element Analysis of Waveguide Modes: A Novel Approach that Eliminates Spurious Modes," IEEE Trans. Microwave Theory Tech., vol. 35, No. 2, pp. 117-123, Feb. 1987.

[27] Jin, J. M., Volakis, J. L. and Liepa, V. V., "Fictitious absorber for truncating finite element meshes in scattering," IEE Proc H Microwaves Antenna Propag. vol. 139, No. 5, pp. 472-476, Oct. 1992.

[28] Riblet, G. P., "Treatment of two-dimensional E-plane bandstop filters using the finite element method," IEE Proc H Microwaves Antenna Propag. vol. 144, No. 6, pp. 411-414, Dec. 1997.

[29] Koning, J., Rieben, R. N. and Rodriguez, G. H., "Vector finite-element modeling of the full-wave Maxwell equations to evaluate power loss in bent optical fibers," Journal of Lightwave Technology, vol. 23, No. 12, pp. 4147-4154, Dec. 2005.

[30] Giannacopoulos, D. D., Kak, K. F. and Mirican, B., "Efficient load balancing for parallel adaptive finite-element electromagnetics with vector tetrahedra," IEEE Transactions on Magnetics, vol. 42, No. 4, pp. 555-558, April 2006.

[31] Schneider, M. V., "Computation of Impedance and Attenuation of TEM-Lines by Finite Difference Methods," IEEE Trans. Microwave Theory Tech., vol. 13,

No. 6, pp. 793-800, Nov. 1965.

[32] Beaubien, M. J. and Wexler, A., "An Accurate Finite-Difference Method for Higher Order Waveguide Modes," IEEE Trans. Microwave Theory Tech., vol. 16, No. 12, pp. 1007-1017, Dec. 1968.

[33] Hornsby, J. S. and Gopinath, A., "Numerical Analysis of a Dielectric-Loaded Waveguide with a Microstrip Line-Finite-Difference Method," IEEE Trans. Microwave Theory Tech., vol. 17, No. 9, pp. 684-690, Sep. 1969.

[34] Beaubien, M. J. and Wexler, A., "Unequal-Arm Finite-Difference Operators in the Positive-Definite Successive Overrelaxation (PDSOR) Algorithm," IEEE Trans. Microwave Theory Tech., vol. 18, No. 12, pp. 1132-1149, Dec. 1970.

[35] Christ, A. and Hartnagel, H. L., "Three-Dimensional Finite-Difference Method for the Analysis of Microwave-Device Embedding," IEEE Trans. Microwave Theory Tech., vol. 35, No. 8, pp. 688-696, Aug. 1987.

[36] Kim, C. M. and Ramaswamy, R. V., "Modeling of graded-index channel waveguides using nonuniform finite difference method," Journal of Lightwave Technology, vol. 7, No. 10, pp. 1581-1589, Oct. 1989.

[37] Beilenhoff, K., Heinrich, W. and Hartnagel, H. L., "Improved finite-difference formulation in frequency domain for three-dimensional scattering problems," IEEE Trans. Microwave Theory Tech., vol. 40, No. 3, pp. 540-546, March 1992.

[38] Rewienski, M. and Mrozowski, M., "Iterative application of boundary conditions in the parallel implementation of the FDFD method," IEEE Microwave and Guided Wave Letters, vol. 10, No. 9, pp. 362-364, Sept. 2000.

[39] Zscheile, H., Schmuckles, F. J. and Heinrich, W., "Finite-difference formulation accounting for field singularities," IEEE Trans. Microwave Theory Tech., vol. 54, No. 5, pp. 2000-2010, May 2006.

[40] Lou, Z. and Jin, J. M., "Modeling and simulation of broad-band antennas using the time-domain finite element method," IEEE Trans. Antennas Propagat., vol. 53, No. 12, pp. 4099-4110, Dec. 2005.

[41] Lemdiasov, R. A., Obi, A. A. and Ludwig, R., "Time domain formulation of the method of moments for inhomogeneous conductive bodies at low frequencies," IEEE Trans. Microwave Theory Tech., vo. 54, No. 2, Part 2, pp. 706-714, Feb.

2006.

[42] Yee, K. S., "Numerical solution of initial boundary value problems involving Maxwell's equations in isotropic media," IEEE Trans. Antennas Propagat., vol. 14, No. 3, pp. 302-307, May 1966.

[43] Taflove, A. and Umashankar, K., "A hybrid moment method/finite-difference time-domain approach to electromagnetic coupling and aperture penetration into complex geometries," IEEE Trans. Antennas Propagat., vol. 30, No. 4, pp. 617-627, Jul. 1982.

[44] Choi, D. H. and Hoefer, W. J. R., "The Finite-Difference-Time-Domain Method and its Application to Eigenvalue Problems," IEEE Trans. Microwave Theory Tech., vol. 34, No. 12, pp. 1464-1470, Dec. 1986.

[45] Gwarek, W. K., "Analysis of arbitrarily shaped two-dimensional microwave circuits by finite-difference time-domain method," IEEE Trans. Microwave Theory Tech., vol 36, No. 4, pp. 738-744, April 1988.

[46] Chu, S. T. and Chaudhuri, S. K., "A finite-difference time-domain method for the design and analysis of guided-wave optical structures," Journal of Lightwave Technology, vol. 7, No. 12, pp. 2033-2038, Dec. 1989.

[47] Reineix, A. and Jecko, B., "Analysis of microstrip patch antennas using finite difference time domain method," IEEE Trans. Antennas Propagat., vol. 37, No. 11, pp. 1361-1369, Nov. 1989.

[48] Kim, I. S. and Hoefer, W. J. R., "A local mesh refinement algorithm for the time domain-finite difference method using Maxwell's curl equations," IEEE Trans. Microwave Theory Tech., vol. 38, No. 6, pp. 812-815, June 1990.

[49] Sullivan, D. M., "A frequency-dependent FDTD method for biological applications," IEEE Trans. Microwave Theory Tech., vol. 40, No. 3, pp. 532-539, March 1992.

[50] Berenger, J. P., "A perfectly matched layer for the absorption of electromagnetic waves," Journal of Computational Physics, vol. 114, pp. 185–200, 1994.

[51] Kapoor, S., "Sub-cellular technique for finite-difference time-domain method," IEEE Trans. Microwave Theory Tech., vol. 45, No. 5, Part 1, pp. 673-677, May 1997.

[52] Noda, T. and Yokoyama, S., "Thin wire representation in finite difference time domain surge simulation," IEEE Transactions on Power Delivery, vol. 17, No. 3, pp. 840-847, July 2002.

[53] Karkkainen, M. K., "FDTD surface impedance model for coated conductors," IEEE Transactions on Electromagnetic Compatibility, vol. 46, No. 2, pp. 222-233, May 2004.

[54] Kokkinos, T., Sarris, C. D. and Eleftheriades, G. V., "Periodic FDTD analysis of leaky-wave structures and applications to the analysis of negative-refractive-index leaky-wave antennas," IEEE Trans. Microwave Theory Tech., vol. 54, No. 4, Part 1, pp. 1619-1630, June 2006.

[55] Taflove, A., Computational Electrodynamics, Norwood, MA: Artech House Inc., 1995.

[56] Zheng, F., Chen, Z. and Zhang, J., "Toward the development of a three-dimensional unconditionally stable finite – difference time – domain method," IEEE Trans. Microwave Theory Tech., vol. 48, No.9, pp. 1550-1558, Sept. 2000.

[57] Namiki, T. and Ito, K., "Investigation of numerical errors of the two-dimensional ADI-FDTD method," IEEE Trans. Microwave Theory Tech., vol. 48, No. 11, Part 1, pp. 1950-1956, Nov. 2000.

[58] Krumpholz, M. and Katehi, L. P. B., "MRTD: new time-domain schemes based on multiresolution analysis," IEEE Trans. Microwave Theory Tech., vol. 44, No. 4, pp. 555-571, April 1996.

[59] Liu, Q. H., "The pseudospectral time domain (PSTD): A new algorithm for solution of Maxwell's equations," IEEE Antennas and Propagation Society International Symposium, vol. 1, pp. 122–125, July 1997.

[60] Johns, P. B. and Beurle, R. L., "Numerical solution of two-dimensional scattering problems using a transmission-line matrix," Proc. Inst. Elect. Eng., vol.118, No. 9, pp. 1203-1208, 1971.

[61] Sadiku, M. N. O. and Agba, L. C., "A simple introduction to the transmission-line modeling," IEEE Transactions on Circuits and Systems, vol. 37, No. 8, pp. 991-999, Aug. 1990.

[62] Johns, P. B., "A Symmetrical Condensed Node for the TLM Method," IEEE

Trans. Microwave Theory Tech., vol. 35, No. 4, pp. 370-377, April 1987.

[63] Chen, Z., Ney, M. M. and Hoefer, W. J. R., "Absorbing and connecting boundary conditions for the TLM method," IEEE Trans. Microwave Theory Tech., vol. 41, No. 11, pp. 2016-2024, Nov. 1993.

[64] Righi, M., Hoefer, W. J. R., Mongiardo, M. and Sorrentino, R., "Efficient TLM diakoptics for separable structures," IEEE Trans. Microwave Theory Tech., vol. 43, No. 4, pp. 854-859, Part 1-2, April 1995.

[65] Trenkic, V., Christopoulos, C. and Benson, T. M., "Development of a general symmetrical condensed node for the TLM method," IEEE Trans. Microwave Theory Tech., vol. 44, No. 12, Part 1, pp. 2129-2135, Dec. 1996.

[66] Pena, N. and Ney, M. M., "Absorbing-boundary conditions using perfectly matched-layer (PML) technique for three-dimensional TLM simulations," IEEE Trans. Microwave Theory Tech., vol. 45, No. 10, Part 1, pp. 1749-1755, Oct. 1997.

[67] Pierantoni, L., Tomassoni, C. and Rozzi, T., "A new termination condition for the application of the TLM method to discontinuity problems in closed homogeneous waveguide," IEEE Trans. Microwave Theory Tech., vol. 50, No. 11, pp. 2513-2518, Nov. 2002.

[68] So, P. P. M., Du, H. and Hoefer, W. J. R., "Modeling of metamaterials with negative refractive index using 2-D shunt and 3-D SCN TLM networks," IEEE Trans. Microwave Theory Tech., vol. 53, No. 4, Part 2, pp. 1496-1505, April 2005.

[69] Valderas, D., Legarda, J., Gutierrez, I. and Sancho, J. I., "Design of UWB folded-plate monopole antennas based on TLM," IEEE Trans. Antennas Propagat., vol. 54, No. 6, pp. 1676-1687, June 2006.

[70] Krumpholz, M. and Russer, P., "On the dispersion in TLM and FDTD," IEEE Trans. Microwave Theory Tech., vol. 42, No. 7, Part 1-2, pp. 1275-1279, July 1994.

[71] Xiao, S., Vahldieck, R. and Jin, H., "Full-wave analysis of guided wave structures using a novel 2-D FDTD," IEEE Microwave and Guided Wave Letters, vol. 2, No. 5, pp.165-167, May 1992.

[72] Xiao, S. and Vahldieck, R., "An efficient 2-D FDTD algorithm using real variables," IEEE Microwave and Guided Wave Letters, Vol. 3, No. 5, pp.127-129, May 1993.

[73] Huang, T. W., Houshmand, B. and Itoh, T., "Efficient modes extraction and numerically exact matched sources for a homogeneous waveguide cross-section in a FDTD simulation," IEEE MTT-S International Microwave Symposium Digest, Vol. 1, pp. 31-34, May, 1994.

[74] Eswarappa, C., So, P. P. M. and Hoefer, W. J. R., "New procedures for 2-D and 3-D microwave circuit analysis with the TLM method," IEEE MTT-S International Microwave Symposium Digest, vol. 2, pp. 661-664, May 1990.

[75] Moglie, F., Rozzi, T., Marcozzi, P. and Schiavoni, A., "A new termination condition for the application of FDTD techniques to discontinuity problems in close homogeneous waveguide," IEEE Microwave and Guided Wave Letters, vol. 2, No. 12, pp. 475-477, Dec,1992.

[76] Huang, T. W., Houshmand, B. and Itoh, T., "The implementation of time-domain diakoptics in the FDTD method," IEEE Trans. Microwave Theory Tech., vol. 42, No. 11, pp. 2149-2155, Nov. 1994.

[77] Righi, M., Hoefer, W. J. R., Mongiardo, M. and Sorrentino, R., "Efficient TLM diakoptics for separable structures," IEEE Trans. Microwave Theory Tech., vol. 43, No. 4, Part 1-2, pp. 854-859, April 1995.

[78] Mrozowski, M., Niedz´wiecki, M. and Suchomski, P., "A fast recursive highly dispersive absorbing boundary condition using time domain diakoptics and Laguerre polynomials," IEEE Microwave and Guided Wave Letters, vol. 5, No. 6, pp.183-185, June 1995.

[79] Alimenti, F., Mezzanotte, P., Roselli, L. and Sorrentino, R., "Modal absorption in the FDTD method: A critical review," International Journal of Numerical Modeling, vol. 10, pp. 245-264, 1997.

[80] Lord, J. A., Henderson, R. I. and Pirollo, B. P., "FDTD analysis of modes in arbitrarily shaped waveguides," IEE National Conference on Antennas and Propagation, pp.221-224, 31 March-1 April 1999.

[81] Alimenti, F., Mezzanotte, P., Roselli, L. and Sorrentino, R., "A revised

formulation of modal absorbing and matched modal source boundary conditions for the efficient FDTD analysis of waveguide structures," IEEE Trans. Microwave Theory Tech., vol. 48, No. 1, pp. 50-59, Jan. 2000.

[82] Gedney, S. D., "An anisotropic perfectly matched layer-absorbing medium for the truncation of FDTD lattices," IEEE Trans. Antennas Propagat., vol. 44, no. 12, pp. 1630-1639, Dec. 1996.

[83] Kuzuoglu, M. and Mittra, R., "Frequency dependence of the constitutive parameters of causal perfectly anisotropic absorbers," IEEE Microwave and Guided Letters, vol. 6, No. 12, pp. 447-449, Dec. 1996.

[84] Roden, J. A. and Gedney, S. D., "Convolution PML (CPML): an efficient FDTD implementation of the CFS-PML for arbitrary media," Microwave and Optical Technology Letters, John Wiley and Sons, vol. 27, No. 5, pp. 334-339, Dec. 2000.

[85] Okoniewski, M., Stuchly, M. A., Mrozowski, M. and DeMoerloose, J., "Modal PML," IEEE Microwave and Wireless Components Letters, vol. 7, No. 2, pp.33-35, Feb. 1997.

[86] Jung, K. and Kim, H., "An efficient formulation of a 1-D modal PML for waveguide structures," Microwave and Optical Technology Letters, vol. 21, No. 1, pp. 48-51, April, 1999.

[87] Kim, I. S. and Hoefer, W. J. R., " A local mesh refinement algorithm for the time domain-finite difference method using Maxwell's curl equations," IEEE Trans. Microwave Theory Tech., vol. 38, No. 6, pp. 812-815, June 1990.

[88] Zivanovic, S. S., Yee, K. S., and Mei, K. K., "A subgridding method for the time-domain finite-difference method to solve Maxwell's equations," IEEE Trans. Microwave Theory Tech., vol. 39, No. 3, pp. 471-479, March 1991.

[89] Thoma, P. and Weiland, T., "A consistent subgridding scheme for the finite difference time domain method," Int. J. Num. Modeling, Vol. 9, No. 5, pp. 359-374, 1996.

[90] Krishnaiah, K. M. and Railton, C. J., "Passive equivalent circuit of FDTD: An application to subgridding," Electronics Letters, vol. 33, No. 15, pp. 1277-1278, 1997.

[91] Okoniewski, M., Okoniewska, E. and Stuchly, M. A., "Three-dimensional subgridding algorithm for FDTD," IEEE Trans. Antennas Propagat., vol. 45, No.3, pp. 422-429, March 1997.

[92] Krishnaiah, K. M. and Railton, C. J., "A stable subgridding algorithm and its application to eigenvalue problems," IEEE Trans. Microwave Theory Tech., vol. 47, No. 5, pp. 620-628, May 1999.

[93] White, M. J., Yun, Z. and Iskander, M. F., "A new 3-D FDTD multigrid technique with dielectric traverse capabilities," IEEE Trans. Microwave Theory Tech., vol. 49, No. 3, pp. 422-430, March 2001.

[94] Kulas, L. and Mrozowski, M., "A simple high-accuracy subgridding scheme," 33rd European Microwave Conference, Munich, Germany, pp. 347-350, Oct. 2003.

[95] Podebrad, O., Clemens, M., and Weiland, T., "New flexible subgridding scheme for the finite integration technique," IEEE Transactions on Magnetics, vol. 39, No. 5, pp. 1662-1665, May 2003.

[96] Marrone, M. and Mittra, R., "A new stable hybrid three-dimensional generalized finite difference time domain algorithm for analyzing complex structures," IEEE Trans. Antennas Propagat., vol. 53, No. 5, pp.1729-1737, May 2005.

[97] Kulas, L. and Mrozowski, M., "Low-reflection subgridding," IEEE Trans. Microwave Theory Tech., vol. 53, No. 5, pp. 1587–1592, May 2005.

[98] Donderici, B. and Teixeira, F. L., "Improved FDTD subgridding algorithms via digital filtering and domain overriding," IEEE Trans. Antennas Propagat., vol. 53, No.9, pp. 2938–2951, Sept. 2005.

[99] Sui, W., Christensen, D. and Durney, C., "Extending the two-dimensional FDTD to hybrid electromagnetic systems with active and passive lumped elements," IEEE Trans. Microwave Theory Tech., vol. 40, pp. 724-730, 1992.

[100] Piket-May, M. J., Taflove, A. and Baron, J., "FD-TD modeling of digital signal propagation in 3-D circuits with passive and active loads," IEEE Trans. Microwave Theory Tech., vol. 42, pp. 1514-1523, 1994.

[101] Kuo, C., Wu, R., Houshmand, B. and Itoh, T., "Modeling of microwave active devices using the FDTD analysis based on the voltage-source approach," IEEE

Microwave and Guided Wave Letters, vol. 6, No. 5, pp. 199-201, May 1996.

[102] Zhang, J. Z. and Wang, Y. Y., "FDTD analysis of active circuit based on the s-parameters," Proceeding of 1997 Asia-Pacific Microwave Conference, vol.3, pp.1049-1052, Hong Kong, Dec. 1997.

[103] Ye, X. and Drewniak, J. L., "Incorporating two-port networks with S-parameters into FDTD," IEEE Microwave and Wireless Components Letters, vol. 11, No. 2, pp. 77-79, Feb. 2001.

[104] Luo, S. and Chen, Z., "A New 2D FDTD Method for Solving 3D Guided-wave Structures," IEEE MTT-S International Microwave Symposium, pp. 1473-1476, June 11-16, 2006.

[105] Luo, S. and Chen, Z., "Efficient one-dimensional FDTD modeling of waveguide structures," Proceeding of Frontiers in Applied Computational Electromagnetics *2006*, Victoria, BC, Canada, pp. 146-149, June 19-20, 2006.

[106] Luo, S. and Chen, Z., "An efficient modal FDTD for absorbing boundary conditions and incident wave generator in waveguide structures," has been scheduled for publication in Progress In Electromagnetics Research, vol. 68, pp. 229-246, 2007.

[107] Luo, S. and Chen, Z., "A FDTD-based Modal PML," IEEE Microwave and Wireless Components Letters, vol. 16, No. 10, pp.528-530, Oct. 2006.

[108] Luo, S. and Chen, Z., "High-performance one-dimensional modal absorbing boundary conditions for FDTD modelling of waveguide structures," The 12th International Symposium on Antenna Technology and Applied Electromagnetics, (ANTEM/URSI 2006), Montreal, QC, Canada, July 16 - 19, 2006.

[109] Luo, S. and Chen, Z., "Extracting Causal Time Domain Parameters," The 10th International Symposium on Antenna Technology and Applied Electromagnetics, (ANTEM 2004/URSI), Ottawa, ON, Canada, July 20 - 23, 2004.

[110] Luo, S. and Chen, Z., "Iterative methods for extracting causal time-domain network parameters," IEEE Trans. on Microwave Theory and Techniques, vol. 53, no. 3, pp. 969-976, Mar. 2005.

[111] Luo, S. and Chen, Z., "Extraction of causal time-domain network parameters using rational functions," IEEE Transactions on Circuits and Systems I, Vol. 52, No. 6, pp.1205-1210, June 2005.

[112] Luo, S. and Chen, Z., "Causal parameter extractions by vector fitting for use in time-domain numerical modeling," IEEE Antennas and Propagation Society International Symposium, vol. 3A, pp. 325-328, 3-8 July 2005.

[113] Arcioni, P., Bozzi, M., Bressan, M., Conciauro, G. and Perregrini, L., "Fast optimization, tolerance analysis, and yield estimation of H-/E-plane waveguide components with irregular shapes," IEEE Trans. Microwave Theory Tech., vol. 52, No. 1, pp. 319-328, Jan. 2004.

[114] Ros, J. V. M., Pacheco, P. S., González, H. E., Esbert, V. E. B., Martín, C. B., Calduch, M. T., Borrás, S. C. and Martínez, B. G., "Fast automated design of waveguide filters using aggressive space mapping with a new segmentation strategy and a hybrid optimization algorithm," IEEE Trans. Microwave Theory Tech., vol. 53, No. 4, pp. 1130-1142, April 2005.

[115] Bandler, J. W., Mohamed, A. S. and Bakr, M. H., "TLM-based modeling and design exploiting space mapping," IEEE Trans. Microwave Theory Tech., vol. 53, No. 9, pp. 2801-2811, Sept. 2005.

[116] Navarro, E. A., Gimeno, B., Cruz, J. L., "Analysis of H-plane waveguide discontinuities with an improved finite-difference time domain algorithm," IEEE Proceedings H, Microwaves, Antennas and Propagation, vol. 139, No. 2, pp.183-185, April 1992.

[117] Ishii, T. K., Microwave Engineering, New York: The Ronald Press Company, 1966.

[118] Loh, T. H. and Mias, C., "Implementation of an exact modal absorbing boundary termination condition for the application of the finite-element time-domain technique to discontinuity problems in closed homogeneous waveguides," IEEE Trans. Microwave Theory Tech., vol. 52, No. 3, pp.882-888, Mar. 2004.

[119] Lou, Z. and Jin, J. M., "An accurate waveguide port boundary condition for the time-domain finite-element method," IEEE Trans. Microwave Theory Tech., vol. 53, No. 9, pp.3014-3023, Sept. 2005.

[120] Thoma, P. and Weiland, T., "Numerical Stability of Finite Difference Time Domain Methods," IEEE Transactions on Magnetics, vol. 34, No. 5, Part 1, pp. 2740-2743, Sept. 1998.

[121] California Eastern Labs, Data sheet of low noise amplifier NE425S01 [Online]. Available: www.cel.com/pdf/datasheets/ne425s01.pdf [2007, 23 January].

[122] Pozar, D. M., Microwave Engineering, Don Mills, ON: Addison-Wesley, 1990.

[123] Perry, P. and Brazil, T., "Forcing causality on S-parameter data using the Hilbert transform," IEEE Microwave and Guided Letters, Vol. 8, No. 11, pp. 378-380, Nov. 1998.

[124] Chen, Y., "Design and Simulation of Active Integrated Antennas," M.A.Sc. Thesis, Dalhousie University, 2003.

[125] Papoulis, A., The Fourier Integral and Its Applications, New York: McGraw-Hill, 1962.

[126] Murakami, K., Hontsu, S. and Ishii, J., "Transient analysis of a class of mixed lumped and distributed constant circuits," Proceedings of ISCAS'88, pp2843-2846, June 1988.

[127] Miller, E. K., "Model-Based Parameter Estimation in Electromagnetics: part I. Background and Theoretical Development," IEEE Antennas and Propagation Magazine, vol. 40, pp. 42-52, Feb. 1998.

[128] Gustavsen, B. and Semlyen, A., "Rational Approximation of Frequency Domain Responses by Vector Fitting," IEEE Trans. on Power Delivery, vol. 14, pp. 1052-1061, July 1999.

[129] Kuhfitting, P. K. F., Introduction to the Laplace Transform, New York, NY: Plenum Press, 1978.

[130] Semlyen, A. and Dabuleanu, A., "Fast and Accurate Switching Transient Calculations on Transmission Lines with Ground Return Using Recursive Convolutions," IEEE Trans. on Power App. And Syst., vol.PAS-94, No.2, pp. 561-571, March/April 1975.

[131] Lin, S. and Kuh, E. S., "Transient Simulation of Lossy Interconnects Based on the Recursive Convolution Formulation," IEEE Trans. on Circuits and Systems-I: Fundamental Theory and Applications, vol.39, pp.879-892, Nov. 1992.

Appendix A: The Numerical Dispersion of Compact 1D FDTD for TE_{mn} mode in a Rectangular Waveguide

Suppose the rectangular waveguide has width a in x direction and height b in y direction. The field components for the TE_{mn} mode along z-direction can be written as:

$$\begin{aligned}
E_x &= E_{x0}\cos(k_x x)\sin(k_y y)e^{j(k_z z-\omega t)} \\
E_y &= E_{y0}\sin(k_x x)\cos(k_y y)e^{j(k_z z-\omega t)} \\
E_z &= 0 \\
H_x &= H_{x0}\sin(k_x x)\cos(k_y y)e^{j(k_z z-\omega t)} \\
H_y &= H_{y0}\cos(k_x x)\sin(k_y y)e^{j(k_z z-\omega t)} \\
H_z &= H_{z0}\cos(k_x x)\cos(k_y y)e^{j(k_z z-\omega t)}
\end{aligned} \tag{A.1}$$

where $k_x = \frac{m\pi}{a}$, $k_y = \frac{n\pi}{b}$, k_z is the spatial frequency in the z direction, and ω is the temporal angular frequency.

Substitution of (A.1) into (4.3) reads

$$\begin{aligned}
&E_{x0}\cos[k_x(i-\tfrac{1}{2})\Delta x]\sin(k_y j\Delta y)e^{j[k_z k\Delta z-\omega(n+1)\Delta t]} \\
&= E_{x0}\cos[k_x(i-\tfrac{1}{2})\Delta x]\sin(k_y j\Delta y)e^{j[k_z k\Delta z-\omega n\Delta t]} \\
&\quad + \frac{\Delta t}{\varepsilon\Delta y}(\alpha_{zy}|_{i-\frac{1}{2},j-\frac{1}{2}}-1)H_{z0}\cos[k_x(i-\tfrac{1}{2})\Delta x]\cos[k_y(j-\tfrac{1}{2})\Delta y]e^{j[k_z k\Delta z-\omega(n+\frac{1}{2})\Delta t]} \\
&\quad - \frac{\Delta t}{\varepsilon\Delta z}\{H_{y0}\cos[k_x(i-\tfrac{1}{2})\Delta x]\sin(k_y j\Delta y)e^{j[k_z(k+\frac{1}{2})\Delta z-\omega(n+\frac{1}{2})\Delta t]} \\
&\qquad - H_{y0}\cos[k_x(i-\tfrac{1}{2})\Delta x]\sin(k_y j\Delta y)e^{j[k_z(k-\frac{1}{2})\Delta z-\omega(n+\frac{1}{2})\Delta t]}\}
\end{aligned} \tag{A.2}$$

where

$$\alpha_{zy}|_{i-\frac{1}{2},j-\frac{1}{2}} = \frac{H_{z0}\cos[k_x(i-\frac{1}{2})\Delta x]\cos[k_y(j+\frac{1}{2})\Delta y]e^{j[k_z k\Delta z-\omega(n+\frac{1}{2})\Delta t]}}{H_{z0}\cos[k_x(i-\frac{1}{2})\Delta x]\cos[k_y(j-\frac{1}{2})\Delta y]e^{j[k_z k\Delta z-\omega(n+\frac{1}{2})\Delta t]}}$$
$$= \frac{\cos[k_y(j+\frac{1}{2})\Delta y]}{\cos[k_y(j-\frac{1}{2})\Delta y]} \qquad \text{(A.3)}$$

Division of both sides of equation (A.2) by $\cos[k_x(i-\frac{1}{2})\Delta x]e^{j[k_z k\Delta z-\omega(n+\frac{1}{2})\Delta t]}$ leads to

$$E_{x0}\sin(k_y j\Delta y)(e^{-j\omega\frac{1}{2}\Delta t} - e^{j\omega\frac{1}{2}\Delta t})$$
$$= \frac{\Delta t}{\varepsilon\Delta y}(\alpha_{zy}|_{i-\frac{1}{2},j-\frac{1}{2}} - 1)H_{z0}\cos[k_y(j-\frac{1}{2})\Delta y] \qquad \text{(A.4)}$$
$$-\frac{\Delta t}{\varepsilon\Delta z}H_{y0}\sin(k_y j\Delta y)(e^{jk_z\frac{1}{2}\Delta z} - e^{-jk_z\frac{1}{2}\Delta z})$$

By substitution of (A.3) into (A.4), (A.4) can be rewritten as:

$$E_{x0}\sin(k_y j\Delta y)(e^{-j\omega\frac{1}{2}\Delta t} - e^{j\omega\frac{1}{2}\Delta t})$$
$$= \frac{\Delta t}{\varepsilon\Delta y}\{\cos[k_y(j+\frac{1}{2})\Delta y] - \cos[k_y(j-\frac{1}{2})\Delta y]\}H_{z0} \qquad \text{(A.5)}$$
$$-\frac{\Delta t}{\varepsilon\Delta z}H_{y0}\sin(k_y j\Delta y)(e^{jk_z\frac{1}{2}\Delta z} - e^{-jk_z\frac{1}{2}\Delta z})$$

By applying the following identities:

$$e^{j\theta} = \cos(\theta) + j\sin(\theta)$$
$$\cos(A) - \cos(B) = -2\sin\frac{A+B}{2}\sin\frac{A-B}{2} \qquad \text{(A.6)}$$

Equation (A.5) can be simplified to:

$$\frac{j}{\Delta t}\sin(\frac{\omega\Delta t}{2})E_{x0} - \frac{1}{\varepsilon\Delta y}\sin(\frac{k_y\Delta y}{2})H_{z0} - \frac{j}{\varepsilon\Delta z}\sin(\frac{k_z\Delta z}{2})H_{y0} = 0 \qquad \text{(A.7)}$$

Equations (4.4)(4.8) can be treated similarly. They become:

$$\frac{j}{\Delta t}\sin(\frac{\omega\Delta t}{2})E_{y0}+\frac{j}{\varepsilon\Delta z}\sin(\frac{k_z\Delta z}{2})H_{x0}+\frac{1}{\varepsilon\Delta x}\sin(\frac{k_x\Delta x}{2})H_{z0}=0 \tag{A.8}$$

$$\frac{1}{\mu\Delta z}\sin(\frac{k_z\Delta z}{2})E_{y0}+\frac{1}{\Delta t}\sin(\frac{\omega\Delta t}{2})H_{x0}=0 \tag{A.9}$$

$$\frac{1}{\mu\Delta z}\sin(\frac{k_z\Delta z}{2})E_{x0}-\frac{1}{\Delta t}\sin(\frac{\omega\Delta t}{2})H_{y0}=0 \tag{A.10}$$

$$\frac{1}{\mu\Delta y}\sin(\frac{k_y\Delta y}{2})E_{x0}-\frac{1}{\mu\Delta x}\sin(\frac{k_x\Delta x}{2})E_{y0}+\frac{j}{\Delta t}\sin(\frac{\omega\Delta t}{2})H_{z0}=0 \tag{A.11}$$

The above equations form a system of five homogeneous equations with unknowns E_{x0}, E_{y0}, H_{x0}, H_{y0}, and H_{z0}. Because the solutions of the system must not be trivial, the determinant of its coefficient matrix should be equal to zero. This leads to:

$$\sin(\frac{\omega\Delta t}{2})=0 \tag{A.12a}$$

$$\frac{\sin^2(\frac{k_z\Delta z}{2})}{\Delta z^2}=\frac{\mu\varepsilon\sin^2(\frac{\omega\Delta t}{2})}{\Delta t^2} \tag{A.12b}$$

$$\frac{\sin^2(\frac{k_x\Delta x}{2})}{\Delta x^2}+\frac{\sin^2(\frac{k_y\Delta y}{2})}{\Delta y^2}+\frac{\sin^2(\frac{k_z\Delta z}{2})}{\Delta z^2}=\frac{\mu\varepsilon\sin^2(\frac{\omega\Delta t}{2})}{\Delta t^2} \tag{A.12c}$$

where $k_x=\frac{m\pi}{a}$ and $k_y=\frac{n\pi}{b}$.

Equation (A.12a) corresponds to $\omega=0$, and represents the static solution.

From equation (A.12b), it can be obtained that

$$\Delta t^2\sin^2(\frac{k_z\Delta z}{2})=\mu\varepsilon\Delta z^2\sin^2(\frac{\omega\Delta t}{2}) \tag{A.13}$$

From equation (A.10), it can be obtained that

$$E_{x0} = \frac{\mu \Delta z \sin(\frac{\omega \Delta t}{2})}{\Delta t \sin(\frac{k_z \Delta z}{2})} H_{y0} \tag{A.14}$$

Substitution of (A.14) into (A.7) results in:

$$j \frac{\varepsilon \mu \Delta z^2 \sin^2(\frac{\omega \Delta t}{2}) - \Delta t^2 \sin^2(\frac{k_z \Delta z}{2})}{\varepsilon \Delta z \Delta t^2 \sin(\frac{k_z \Delta z}{2})} H_{y0} - \frac{1}{\varepsilon \Delta y} \sin(\frac{k_y \Delta y}{2}) H_{z0} = 0 \tag{A.15}$$

Because of equation (A.13), the first term in equation (A.15) equals zero. This will lead to $H_{z0} = 0$, which does not agree with the assumption of TE modes.

It can be seen that equation (A.12c) approaches the analytical dispersion relationship, $\omega^2 \mu \varepsilon = k_x^2 + k_y^2 + k_z^2$, when Δx, Δy, Δz and Δt approach zero. Therefore, equation (A.12c) is the numerical dispersion relationship of the TE modes for the compact 1D FDTD.

Appendix B: The Formula of 1D Modal CFS-PML

The complete formulae of 1D modal CFS-PML scheme with $S_x = 1$, $S_y = 1$, and $S_z = \kappa_z + \frac{\sigma_z}{\alpha_z + j\omega\varepsilon_0}$ can be written as:

$$P_x\Big|_{i-\frac{1}{2},j,k}^{n+1} = P_x\Big|_{i-\frac{1}{2},j,k}^{n} + \frac{\Delta t}{\varepsilon\Delta y}(\alpha_{zy}\big|_{i-\frac{1}{2},j-\frac{1}{2}} - 1)H_z\big|_{i-\frac{1}{2},j-\frac{1}{2},k}^{n+\frac{1}{2}} - \frac{\Delta t}{\varepsilon\Delta z}(H_y\Big|_{i-\frac{1}{2},j,k+\frac{1}{2}}^{n+1/2} - H_y\Big|_{i-\frac{1}{2},j,k-\frac{1}{2}}^{n+1/2}) \tag{B.1a}$$

$$E_x\Big|_{i-\frac{1}{2},j,k}^{n+1} = \frac{\frac{\varepsilon_0 k_z}{\Delta t} - \frac{\alpha_z k_z + \sigma_z}{2}}{\frac{\varepsilon_0 k_z}{\Delta t} + \frac{\alpha_z k_z + \sigma_z}{2}} E_x\Big|_{i-\frac{1}{2},j,k}^{n} + \frac{\frac{\varepsilon_0}{\Delta t} + \frac{\alpha_z}{2}}{\frac{\varepsilon_0 k_z}{\Delta t} + \frac{\alpha_z k_z + \sigma_z}{2}} P_x\Big|_{i-\frac{1}{2},j,k}^{n+1} - \frac{\frac{\varepsilon_0}{\Delta t} - \frac{\alpha_z}{2}}{\frac{\varepsilon_0 k_z}{\Delta t} + \frac{\alpha_z k_z + \sigma_z}{2}} P_x\Big|_{i-\frac{1}{2},j,k}^{n} \tag{B.1b}$$

$$P_y\Big|_{i,j-\frac{1}{2},k}^{n+1} = P_y\Big|_{i,j-\frac{1}{2},k}^{n} + \frac{\Delta t}{\varepsilon\Delta z}(H_x\Big|_{i,j-\frac{1}{2},k+\frac{1}{2}}^{n+\frac{1}{2}} - H_x\Big|_{i,j-\frac{1}{2},k-\frac{1}{2}}^{n+\frac{1}{2}}) - \frac{\Delta t}{\varepsilon\Delta x}(\alpha_{zx}\big|_{i-\frac{1}{2},j-\frac{1}{2}} - 1)H_z\big|_{i-\frac{1}{2},j-\frac{1}{2},k}^{n+\frac{1}{2}} \tag{B.2a}$$

$$E_y\Big|_{i,j-\frac{1}{2},k}^{n+1} = \frac{\frac{\varepsilon_0 K_z}{\Delta t} - \frac{\alpha_z K_z + \sigma_z}{2}}{\frac{\varepsilon_0 K_z}{\Delta t} + \frac{\alpha_z K_z + \sigma_z}{2}} E_y\Big|_{i,j-\frac{1}{2},k}^{n} + \frac{\frac{\varepsilon_0}{\Delta t} + \frac{\alpha_x}{2}}{\frac{\varepsilon_0 K_z}{\Delta t} + \frac{\alpha_z K_z + \sigma_z}{2}} P_y\Big|_{i,j-\frac{1}{2},k}^{n+1} - \frac{\frac{\varepsilon_0}{\Delta t} - \frac{\alpha_z}{2}}{\frac{\varepsilon_0 K_z}{\Delta t} + \frac{\alpha_z K_z + \sigma_z}{2}} P_y\Big|_{i,j-\frac{1}{2},k}^{n} \tag{B.2b}$$

$$P_z\Big|_{i,j,k-\frac{1}{2}}^{n+1} = P_z\Big|_{i,j,k-\frac{1}{2}}^{n} + \frac{\Delta t}{\varepsilon\Delta x}(\alpha_{yx}\big|_{i-\frac{1}{2},j} - 1)H_y\big|_{i-\frac{1}{2},j,k-\frac{1}{2}}^{n+\frac{1}{2}} - \frac{\Delta t}{\varepsilon\Delta y}(\alpha_{xy}\big|_{i,j-\frac{1}{2}} - 1)H_x\big|_{i,j-\frac{1}{2},k-\frac{1}{2}}^{n+\frac{1}{2}} \tag{B.3a}$$

$$E_z\Big|_{i,j,k-\frac{1}{2}}^{n+1} = \frac{\frac{\varepsilon_0}{\Delta t} - \frac{\alpha_z}{2}}{\frac{\varepsilon_0}{\Delta t} + \frac{\alpha_z}{2}} E_z\Big|_{i,j,k-\frac{1}{2}}^{n}$$
$$+ \frac{\frac{\varepsilon_0 K_z}{\Delta t} + \frac{\alpha_z K_z + \sigma_z}{2}}{\frac{\varepsilon_0}{\Delta t} + \frac{\alpha_z}{2}} D_z\Big|_{i,j,k-\frac{1}{2}}^{n+1} - \frac{\frac{\varepsilon_0 K_z}{\Delta t} - \frac{\alpha_z K_z + \sigma_z}{2}}{\frac{\varepsilon_0}{\Delta t} + \frac{\alpha_z}{2}} D_z\Big|_{i,j,k-\frac{1}{2}}^{n} \tag{B.3b}$$

$$Q_x\Big|_{i,j-\frac{1}{2},k-\frac{1}{2}}^{n+\frac{1}{2}} = Q_x\Big|_{i,j-\frac{1}{2},k-\frac{1}{2}}^{n-\frac{1}{2}} + \frac{\Delta t}{\mu \Delta z}\left(E_y\Big|_{i,j-\frac{1}{2},k}^{n} - E_y\Big|_{i,j-\frac{1}{2},k-1}^{n}\right)$$
$$- \frac{\Delta t}{\mu \Delta y}\left(1 - \beta_{zy}\Big|_{i,j}\right) E_z\Big|_{i,j,k-\frac{1}{2}}^{n} \tag{B.4a}$$

$$H_x\Big|_{i,j-\frac{1}{2},k-\frac{1}{2}}^{n+\frac{1}{2}} = \frac{\frac{\varepsilon_0 K_z}{\Delta t} - \frac{\alpha_z K_z + \sigma_z}{2}}{\frac{\varepsilon_0 K_z}{\Delta t} + \frac{\alpha_z K_z + \sigma_z}{2}} H_x\Big|_{i,j-\frac{1}{2},k-\frac{1}{2}}^{n-\frac{1}{2}}$$
$$+ \frac{\frac{\varepsilon_0}{\Delta t} + \frac{\alpha_x}{2}}{\frac{\varepsilon_0 K_z}{\Delta t} + \frac{\alpha_z K_z + \sigma_z}{2}} Q_x\Big|_{i,j-\frac{1}{2},k-\frac{1}{2}}^{n+\frac{1}{2}} - \frac{\frac{\varepsilon_0}{\Delta t} - \frac{\alpha_z}{2}}{\frac{\varepsilon_0 K_z}{\Delta t} + \frac{\alpha_z K_z + \sigma_z}{2}} Q_x\Big|_{i,j-\frac{1}{2},k-\frac{1}{2}}^{n-\frac{1}{2}} \tag{B.4b}$$

$$Q_y\Big|_{i-\frac{1}{2},j,k-\frac{1}{2}}^{n+\frac{1}{2}} = Q_y\Big|_{i-\frac{1}{2},j,k-\frac{1}{2}}^{n-\frac{1}{2}} + \frac{\Delta t}{\mu \Delta x}\left(1 - \beta_{zx}\Big|_{i,j}\right) E_z\Big|_{i,j,k-\frac{1}{2}}^{n}$$
$$- \frac{\Delta t}{\mu \Delta z}\left(E_x\Big|_{i-\frac{1}{2},j,k}^{n} - E_x\Big|_{i-\frac{1}{2},j,k-1}^{n}\right) \tag{B.5a}$$

$$H_y\Big|_{i-\frac{1}{2},j,k-\frac{1}{2}}^{n+\frac{1}{2}} = \frac{\frac{\varepsilon_0 K_z}{\Delta t} - \frac{\alpha_z K_z + \sigma_z}{2}}{\frac{\varepsilon_0 K_z}{\Delta t} + \frac{\alpha_z K_z + \sigma_z}{2}} H_y\Big|_{i-\frac{1}{2},j,k-\frac{1}{2}}^{n-\frac{1}{2}}$$
$$+ \frac{\frac{\varepsilon_0}{\Delta t} + \frac{\alpha_x}{2}}{\frac{\varepsilon_0 K_z}{\Delta t} + \frac{\alpha_z K_z + \sigma_z}{2}} Q_y\Big|_{i-\frac{1}{2},j,k-\frac{1}{2}}^{n+\frac{1}{2}} - \frac{\frac{\varepsilon_0}{\Delta t} - \frac{\alpha_z}{2}}{\frac{\varepsilon_0 K_z}{\Delta t} + \frac{\alpha_z K_z + \sigma_z}{2}} Q_y\Big|_{i-\frac{1}{2},j,k-\frac{1}{2}}^{n-\frac{1}{2}} \tag{B.5b}$$

$$Q_z\Big|_{i-\frac{1}{2},j-\frac{1}{2},k}^{n+\frac{1}{2}} = Q_z\Big|_{i-\frac{1}{2},j-\frac{1}{2},k}^{n-\frac{1}{2}} + \frac{\Delta t}{\mu \Delta y}\left(1 - \beta_{xy}\Big|_{i-\frac{1}{2},j}\right) E_x\Big|_{i-\frac{1}{2},j,k}^{n}$$
$$- \frac{\Delta t}{\mu \Delta x}\left(1 - \beta_{yx}\Big|_{i,j-\frac{1}{2}}\right) E_y\Big|_{i,j-\frac{1}{2},k}^{n} \tag{B.6a}$$

$$H_z\Big|_{i-\frac{1}{2},j-\frac{1}{2},k}^{n+\frac{1}{2}} = \frac{\frac{\varepsilon_0}{\Delta t} - \frac{\alpha_z}{2}}{\frac{\varepsilon_0}{\Delta t} + \frac{\alpha_z}{2}} H_z\Big|_{i-\frac{1}{2},j-\frac{1}{2},k}^{n-\frac{1}{2}} + \frac{\frac{\varepsilon_0 K_z}{\Delta t} + \frac{\alpha_z K_z + \sigma_z}{2}}{\frac{\varepsilon_0}{\Delta t} + \frac{\alpha_z}{2}} Q_z\Big|_{i-\frac{1}{2},j-\frac{1}{2},k}^{n+\frac{1}{2}} - \frac{\frac{\varepsilon_0 K_z}{\Delta t} - \frac{\alpha_z K_z + \sigma_z}{2}}{\frac{\varepsilon_0}{\Delta t} + \frac{\alpha_z}{2}} Q_z\Big|_{i-\frac{1}{2},j-\frac{1}{2},k}^{n-\frac{1}{2}} \tag{B.6b}$$

where Coefficients α and β are defined in (4.9) - (4.16).